AD-A138 394 ELECTROMAGNETIC COUPLING BETWEEN A CONDUCTING BODY AND AN APERTURE IN AN..(U) SYRACUSE UNIV NY DEPT OF ELECTRICAL AND COMPUTER ENGINEERING.. S W HSI ET AL. 1/2

UNCLASSIFIED DEC 83 SYRU/DECE/TR-83/19 N00014-76-C-0225 F/G 20/3 NL

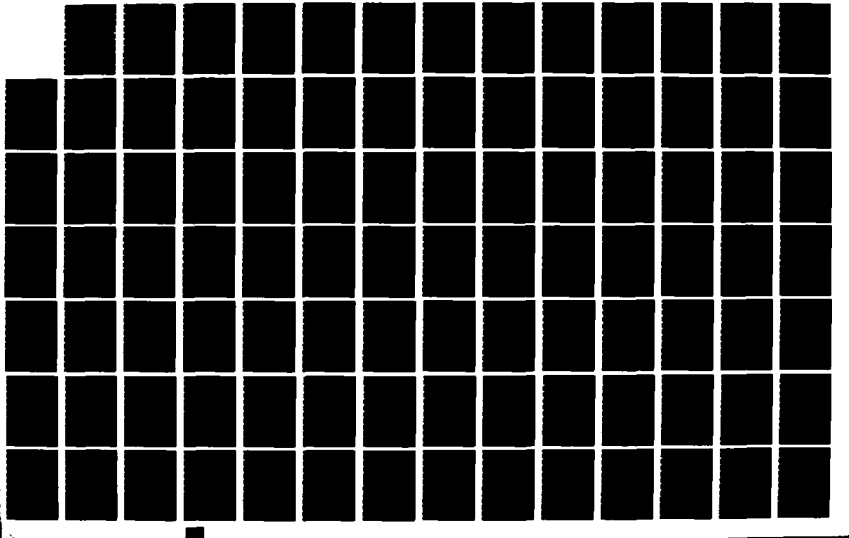

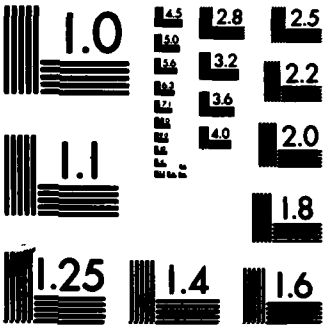

MICROCOPY RESOLUTION TEST CHART
NATIONAL BUREAU OF STANDARDS-1963-A

SYRU/DECE/TR-83/19

ELECTROMAGNETIC COUPLING BETWEEN A CONDUCTING BODY AND AN APERTURE IN AN INFINITE CONDUCTING PLANE

AD A138394

by

Sandy W. Hsi
Roger F. Harrington
Joseph R. Mautz

Department of
Electrical and Computer Engineering
Syracuse University
Syracuse, New York 13210

Technical Report No. 22
December 1983

Contract No. N00014-76-C-0225

Approved for public release; distribution unlimited

Reproduction in whole or in part permitted for any purpose of the United States Government.

Prepared for

DEPARTMENT OF THE NAVY
OFFICE OF NAVAL RESEARCH
ARLINGTON, VIRGINIA 22217

DTIC FILE COPY

DTIC ELECTE FEB 24 1984 E

84 02 23 014

SYRU/DECE/TR-83/19

ELECTROMAGNETIC COUPLING BETWEEN A CONDUCTING BODY AND AN APERTURE IN AN INFINITE CONDUCTING PLANE

by

Sandy W. Hsi
Roger F. Harrington
Joseph R. Mautz

Department of
Electrical and Computer Engineering
Syracuse University
Syracuse, New York 13210

Technical Report No. 22
December 1983

Contract No. N00014-76-C-0225

Approved for public release; distribution unlimited

Reproduction in whole or in part permitted for any purpose of the United States Government.

Prepared for

DEPARTMENT OF THE NAVY
OFFICE OF NAVAL RESEARCH
ARLINGTON, VIRGINIA 22217

Accession For
NTIS GRA&I [X]
DTIC TAB [ ]
Unannounced [ ]
Justification
By
Distribution/
Availability Codes
Dist | Avail and/or Special
A-1

UNCLASSIFIED

SECURITY CLASSIFICATION OF THIS PAGE (When Data Entered)

REPORT DOCUMENTATION PAGE		READ INSTRUCTIONS BEFORE COMPLETING FORM
1. REPORT NUMBER SYRU/DECE/TR-83/19	2. GOVT ACCESSION NO. AD-A138394	3. RECIPIENT'S CATALOG NUMBER
4. TITLE (and Subtitle) ELECTROMAGNETIC COUPLING BETWEEN A CONDUCTING BODY AND AN APERTURE IN AN INFINITE CONDUCTING PLANE		5. TYPE OF REPORT & PERIOD COVERED Technical Report No. 22 6. PERFORMING ORG. REPORT NUMBER
7. AUTHOR(s) Sandy W. Hsi Roger F. Harrington Joseph R. Mautz		8. CONTRACT OR GRANT NUMBER(s) N00014-76-C-0225
9. PERFORMING ORGANIZATION NAME AND ADDRESS Dept. of Electrical & Computer Engineering Syracuse University Syracuse, New York 13210		10. PROGRAM ELEMENT, PROJECT, TASK AREA & WORK UNIT NUMBERS
11. CONTROLLING OFFICE NAME AND ADDRESS Department of the Navy Office of Naval Research Arlington, Virginia 22217		12. REPORT DATE December 1983 13. NUMBER OF PAGES 120
14. MONITORING AGENCY NAME & ADDRESS(if different from Controlling Office)		15. SECURITY CLASS. (of this report) UNCLASSIFIED 15a. DECLASSIFICATION/DOWNGRADING SCHEDULE

16. DISTRIBUTION STATEMENT (of this Report)

Approved for public release; distribution unliited.

17. DISTRIBUTION STATEMENT (of the abstract entered in Block 20, if different from Report)

18. SUPPLEMENTARY NOTES

19. KEY WORDS (Continue on reverse side if necessary and identify by block number)

Aperture and wire	Coupling through aperture
Aperture coupling	Electromagnetic fields
Body behind aperture	Method of moments

20. ABSTRACT (Continue on reverse side if necessary and identify by block number)

In this work, the problem of electromagnetic coupling between a conducting body and an aperture in an infinite conducting plane of zero thickness is considered. The method of moments is utilized to obtain a matrix formulation for the equivalent magnetic current in the aperture and the electric current on the conducting body. The general solution is then applied to problems for which the conducting body is a wire. The aperture is arbitrarily sized and shaped. The wire is of finite length (with or without loads) or of infinite

DD FORM 1 JAN 73 1473 EDITION OF 1 NOV 65 IS OBSOLETE
S/N 0102-014-6601

UNCLASSIFIED

SECURITY CLASSIFICATION OF THIS PAGE (When Data Entered)

CONTENTS

Chapter 1

INTRODUCTION

The electromagnetic coupling between a conducting body and an aperture is an important problem. One of the studies is to investigate the response of protected objects behind an aperture-perforated metallic screen. The power transmitted through the aperture from a source on a nearby object which is behind the screen is also of interest. Situations of this nature arise in a number of applications, *e.g.*, microwave leakage through cracks in shield walls of electronic equipment and electromagnetic penetration into vehicles, aircraft, and ships. This penetration is through windows or seams of doors to cables or other metallic objects.

In the past, the problem of electromagnetic coupling to an infinitely long wire through an electrically small aperture [1] - [3] or through a narrow slot [4] has been studied. The problem of a narrow slot passing by a finite-length wire without loads [5] or with loads [6] has also been investigated.

In this work, we consider more general problems for which an aperture in an infinite conducting plane is backed by a conducting body. The aperture and the conducting body are of arbitrary size and shape. A moment method solution is developed for the equivalent magnetic current in the aperture and the electric current on the

conducting body. The solution is then applied to problems for which the conducting body is a wire of finite length (with or without loads) or of infinite length. The current distributions in the aperture and on the wire can be used to calculate the power transmitted through the aperture and other responses of the wire.

In Chapter 2, the general problem of a conducting body behind an aperture is considered. The equivalence principle [7, Sec. 3-5], boundary conditions, and moment method [8] are utilized to obtain a pair of matrix equations. These equations are used to solve for the current distributions in the aperture and on the conducting body.

In Chapter 3, we specialize the problem to an unloaded wire of finite length behind an aperture of arbitrary size and shape. Triangular patching is used to model the aperture. Pulse functions are placed on the wire. Matrices in the pair of matrix equations developed in Chapter 2 are evaluated. Numerical results are presented and compared with those in [5].

In Chapter 4, the wire considered in Chapter 3 is extended to an infinitely long wire. The expansion functions and matrices developed in Chapter 3 are modified to include the effect of the infinite length of the wire. Numerical results agree very well with the available data in [1] - [4].

In Chapter 5, the problem is generalized to that of an arbitrarily loaded wire behind an aperture. We modify the moment method solution developed in Chapter 4 to include the reflection effect from the loads of the wire. We then evaluate the power

transmitted through the aperture. The solution for a wire with matched loads is used to obtain an equivalent circuit of the aperture for the transmission line mode on an arbitrarily loaded wire. Numerical results are presented and compared with those in [4] and [6].

We summarize and conclude this study in Chapter 6. Recommendations for further work are given. Appendix A presents evaluations of some surface integrals used in Chapter 3. Fields due to outward traveling TEM (transverse electromagnetic) currents are derived in Appendix B. In Appendix C, we derive some integral formulations used in Chapter 4. An equivalent circuit of an aperture for the transmission line mode on a loaded wire is derived in Appendix D.

Figures and tables are at the end of each chapter and appendix.

Chapter 2

FORMULATION OF THE GENERAL PROBLEM

2.1. Problem Specification

The general configuration is given in Fig. 2.1. An aperture-perforated infinite conducting plane of zero thickness separates regions a and b. The size and shape of the aperture are arbitrary. In region a ($y < 0$), there are impressed sources ($\underline{J}^{ia}, \underline{M}^{ia}$). In region b ($y > 0$), there are an arbitrarily shaped and sized conducting body and impressed sources ($\underline{J}^{ib}, \underline{M}^{ib}$). The material in regions a and b is loss-free and homogeneous with permeabilities (μ_a, μ_b) and permittivities ($\varepsilon_a, \varepsilon_b$). The aperture and the conducting body are labeled A and B, respectively.

In this chapter, a moment method solution is developed to obtain the equivalent magnetic current in the aperture and the electric current on the conducting body.

2.2. Formula Derivation

We use the equivalence principle [7, Sec. 3-5] to divide the problem into two parts, as shown in Fig. 2.2. The fields in region a remain unchanged if the aperture is closed by a conducting surface and an equivalent magnetic surface current sheet $\underline{M}^a$ is placed over the aperture region where

$$\underline{M}^a = \underline{n} \times \underline{E}_A^a \qquad \text{over A} \tag{2-1}$$

$\underline{n}$ is the unit vector normal to the conducting plane and points toward region b. $\underline{E}_A^a$ is the electric field over the aperture in region a. This equivalence is shown in Fig. 2.2(a). Similarly, the fields in region b remain unchanged if the aperture is closed by a conducting surface and a magnetic current sheet $\underline{M}^b$ is placed over the aperture region where

$$\underline{M}^b = -\underline{n} \times \underline{E}_A^b \qquad \text{over A} \tag{2-2}$$

$\underline{E}_A^b$ is the electric field over A in region b. In addition, an electric current $\underline{J}$ is induced on the conducting body by $\underline{M}^b$, $\underline{J}^{ib}$, and $\underline{M}^{ib}$. This equivalence is shown in Fig. 2.2(b). Therefore, the electric and magnetic fields in region a are

$$\underline{E}^a = \underline{E}^a(\underline{M}^a) + \underline{E}^{ia} \tag{2-3}$$

$$\underline{H}^a = \underline{H}^a(\underline{M}^a) + \underline{H}^{ia} \tag{2-4}$$

Here, $(\underline{E}^a(\underline{M}^a), \underline{H}^a(\underline{M}^a))$ is the field from $\underline{M}^a$, and $(\underline{E}^{ia}, \underline{H}^{ia})$ is the short-circuit field (field existing in the presence of the complete conducting plane) from $(\underline{J}^{ia}, \underline{M}^{ia})$. Similarly, the fields in region b are

$$\underline{E}^b = \underline{E}^b(\underline{M}^b) + \underline{E}^b(\underline{J}) + \underline{E}^{ib} \tag{2-5}$$

$$\underline{H}^b = \underline{H}^b(\underline{M}^b) + \underline{H}^b(\underline{J}) + \underline{H}^{ib} \tag{2-6}$$

Here, $(\underline{E}^b(\underline{M}^b), \underline{H}^b(\underline{M}^b))$ is the field from $\underline{M}^b$, $(\underline{E}^b(\underline{J}), \underline{H}^b(\underline{J}))$ is the field from $\underline{J}$, and $(\underline{E}^{ib}, \underline{H}^{ib})$ is the short-circuit field from $(\underline{J}^{ib}, \underline{M}^{ib})$. Note that all fields are obtained with the aperture shorted.

We next appply boundary conditions to this problem. They are: (1) the tangential electric field is continuous across the aperture A, (2) the tangential magnetic field is continuous across A, and (3) the tangential electric field vanishes on the surface of the conducting body B. The first condition implies that $\underline{n} \times \underline{E}^a_A = \underline{n} \times \underline{E}^b_A$ in (2-1) and (2-2). Therefore, $\underline{M}^a = -\underline{M}^b$. From now on we use $\underline{M}$ to represent $\underline{M}^a$ and $-\underline{M}^b$. The other two conditions imply that

$$\underline{H}^a_t = \underline{H}^b_t \qquad \text{on A} \tag{2-7}$$

$$\underline{E}^b_t = \underline{0} \qquad \text{on B} \tag{2-8}$$

where t denotes the component tangent to A or B. Substitution of (2-4) - (2-6) into (2-7) and (2-8) gives

$$-\underline{H}_t^a(\underline{M}) - \underline{H}_t^b(\underline{M}) + \underline{H}_t^b(\underline{J}) = \underline{H}_t^{ia} - \underline{H}_t^{ib} \quad \text{on A} \tag{2-9}$$

$$\underline{E}_t^b(\underline{M}) - \underline{E}_t^b(\underline{J}) = \underline{E}_t^{ib} \quad \text{on B} \tag{2-10}$$

Here, the linearity of the operators is used to replace $\underline{H}_t^b(-\underline{M})$ by $-\underline{H}_t^b(\underline{M})$ and $\underline{E}_t^b(-\underline{M})$ by $-\underline{E}_t^b(\underline{M})$. Equations (2-9) and (2-10) are the equations to solve for $\underline{M}$ and $\underline{J}$.

We next use the moment method [8] to reduce (2-9) and (2-10) to matrix equations. For this, we define expansion functions $\{\underline{M}_n;$ $n=1,2,\ldots,NA\}$ over A and $\{\underline{J}_n;$ $n=1,2,\ldots,NB\}$ over B to approximate $\underline{M}$ and $\underline{J}$, respectively. That is,

$$\underline{M} = \sum_{n=1}^{NA} V_n \underline{M}_n \tag{2-11}$$

$$\underline{J} = \sum_{n=1}^{NB} I_n \underline{J}_n \tag{2-12}$$

We define testing functions $\{\hat{\underline{M}}_m;$ $m=1,2,\ldots,NA\}$ over A and $\{\hat{\underline{J}}_m;$ $m=1,2,\ldots,NB\}$ over B and a symmetric product

$$\langle \underline{F}_1 , \underline{F}_2 \rangle_S = \iint_S \underline{F}_1 \cdot \underline{F}_2 \, dS \tag{2-13}$$

where S denotes surface A or B. Now, substituting (2-11) and (2-12) into (2-9), taking the symmetric product over A with each $\hat{\underline{M}}_m$, and then using the linearity of the symmetric product, we obtain the first matrix equation. Similarly, substituting (2-11) and (2-12) into

(2-10), taking the symmetric product over B with each $\hat{J}_m$, and then using the linearity of the symmetric product, we obtain the second matrix equation. The two matrix equations are

$$[Y^a + Y^b]\,\vec{V} + [T]\,\vec{I} = \vec{I}^{ia} - \vec{I}^{ib} \tag{2-14}$$

$$[\hat{T}]\,\vec{V} + [Z]\,\vec{I} = \vec{V}^{ib} \tag{2-15}$$

Here,

$$[Y^a] = [\,\langle -\hat{M}_m\,,\ \underline{H}^a_t(\underline{M}_n)\rangle_A\,]_{NAxNA} \tag{2-16}$$

$$[Y^b] = [\,\langle -\hat{M}_m\,,\ \underline{H}^b_t(\underline{M}_n)\rangle_A\,]_{NAxNA} \tag{2-17}$$

$$[T] = [\,\langle \hat{M}_m\,,\ \underline{H}^b_t(\underline{J}_n)\rangle_A\,]_{NAxNB} \tag{2-18}$$

$$[\hat{T}] = [\,\langle \hat{J}_m\,,\ \underline{E}^b_t(\underline{M}_n)\rangle_B\,]_{NBxNA} \tag{2-19}$$

$$[Z] = [\,\langle -\hat{J}_m\,,\ \underline{E}^b_t(\underline{J}_n)\rangle_B\,]_{NBxNB} \tag{2-20}$$

$$\vec{I}^{ia} = [\,\langle \hat{M}_m\,,\ \underline{H}^{ia}_t\rangle_A\,]_{NAx1} \tag{2-21}$$

$$\vec{I}^{ib} = [\,\langle \hat{M}_m\,,\ \underline{H}^{ib}_t\rangle_A\,]_{NAx1} \tag{2-22}$$

$$\vec{V}^{ib} = [\,\langle \hat{J}_m\,,\ \underline{E}^{ib}_t\rangle_B\,]_{NBx1} \tag{2-23}$$

$$\vec{V} = [V_n]_{NAx1} \tag{2-24}$$

$$\vec{I} = [I_n]_{NBx1} \tag{2-25}$$

Thus (2-14) and (2-15) are the matrix equations to solve for the coefficients (V_n, I_n) in (2-11) and (2-12). We call $[Y^a]$ and $[Y^b]$ the admittance matrices for regions a and b, respectively. $[T]$ and $[\hat{T}]$ are the coupling matrices, $[Z]$ the impedance matrix , and $\vec{I}^{ia}$, $\vec{I}^{ib}$, and $\vec{V}^{ib}$ the source vectors. $\vec{V}$ and $\vec{I}$ are the unknown coefficient vectors to be determined.

If the sources in region a were to radiate in the homogeneous medium characterized by (μ_a, ϵ_a) and if the sources in region b were to radiate in the homogeneous medium characterized by (μ_b, ϵ_b), the fields in (2-16) - (2-20) would be given by

$$\underline{H}^l(\underline{M}_n) = -j\omega \underline{F}_n^l - \nabla \Phi_n^l \qquad l=a,b \tag{2-26}$$

$$\underline{E}^b(\underline{J}_n) = -j\omega \underline{A}_n^b - \nabla \phi_n^b \tag{2-27}$$

$$\underline{H}^b(\underline{J}_n) = \frac{1}{\mu_b} \nabla x \, \underline{A}_n^b \tag{2-28}$$

$$\underline{E}^b(\underline{M}_n) = \frac{-1}{\epsilon_b} \nabla x \, \underline{F}_n^b \tag{2-29}$$

where

$$\underline{F}_n^l = \epsilon_l \iint_A \underline{M}_n(\underline{r}') \, G(k_l, \underline{r}, \underline{r}') \, dS' \qquad l=a,b \tag{2-30}$$

$$\underline{A}_n^b = \mu_b \iint_B \underline{J}_n(\underline{r}') \, G(k_b, \underline{r}, \underline{r}') \, dS' \tag{2-31}$$

$$\phi_n^l = -\iint_A \frac{\nabla' \cdot \underline{M}_n(\underline{r}')}{j\omega\mu_l} G(k_l, \underline{r}, \underline{r}')\, dS' \qquad l=a,b \tag{2-32}$$

$$\phi_n^b = -\iint_B \frac{\nabla' \cdot \underline{J}_n(\underline{r}')}{j\omega\varepsilon_b} G(k_b, \underline{r}, \underline{r}')\, dS' \tag{2-33}$$

$$G(k_l, \underline{r}, \underline{r}') = \frac{e^{-jk_l|\underline{r}-\underline{r}'|}}{4\pi|\underline{r}-\underline{r}'|} \qquad l=a,b \tag{2-34}$$

$$k_l = \omega\sqrt{\varepsilon_l \mu_l} \qquad l=a,b \tag{2-35}$$

Here, ω is the angular frequency. All fields are evaluated in a half space with the aperture shorted.

If a Galerkin solution (i.e., $\hat{\underline{M}}_m = \underline{M}_m$, $\hat{\underline{J}}_m = \underline{J}_m$) is used, we have

$$[Y^l] = [\tilde{Y}^l] \qquad l=a,b \tag{2-36}$$

$$[Z] = [\tilde{Z}] \tag{2-37}$$

$$[\hat{T}] = -[\tilde{T}] \tag{2-38}$$

where ~ denotes the transpose of a matrix. This will save us some computations. If regions a and b are filled with the same medium characterized by (μ, ε), we can remove the conducting plane and use image theory [7, Sec. 3-4] to evaluate the matrices in (2-16) - (2-23). They become

$$[Y^a] = [Y^b] = 2\left[\, \langle -\hat{\underline{M}}_m, \underline{H}_t(\underline{M}_n)\rangle_A \,\right]_{NAxNA} \tag{2-39}$$

$$[T] = \left[\, \langle \hat{\underline{M}}_m, \underline{H}_t(\underline{J}_n, \underline{J}'_n)\rangle_A \,\right]_{NAxNB} \tag{2-40}$$

$$[\hat{T}] = 2\left[\langle \hat{J}_m , \underline{E}_t(\underline{M}_n) \rangle_B \right]_{NBxNA} \tag{2-41}$$

$$[Z] = \left[\langle -\hat{J}_m , \underline{E}_t(\underline{J}_n , \underline{J'}_n) \rangle_B \right]_{NBxNB} \tag{2-42}$$

$$\vec{I}^{ia} = 2\left[\langle \hat{M}_m , \underline{H}_t^{ioa} \rangle_A \right]_{NAx1} \tag{2-43}$$

$$\vec{I}^{ib} = 2\left[\langle \hat{M}_m , \underline{H}_t^{iob} \rangle_A \right]_{NAx1} \tag{2-44}$$

$$\vec{V}^{ib} = \left[\langle \hat{J}_m , \underline{E}_t^{iob} + \underline{E}_t^{iob'} \rangle_B \right]_{NBx1} \tag{2-45}$$

Here, $\underline{H}_t(\underline{J}_n , \underline{J'}_n)$ and $\underline{E}_t(\underline{J}_n , \underline{J'}_n)$ are the tangential fields due to $\underline{J}_n$ plus its image $\underline{J'}_n$ located in region a. $\underline{H}_t(\underline{M}_n)$ and $\underline{E}_t(\underline{M}_n)$ are the tangential fields due to $\underline{M}_n$. $\underline{H}_t^{ioa}$ is the tangential field due to $(\underline{J}^{ia}, \underline{M}^{ia})$. $\underline{H}_t^{iob}$ and $\underline{E}_t^{iob}$ are the tangential fields due to $(\underline{J}^{ib}, \underline{M}^{ib})$. $\underline{E}_t^{iob'}$ is the tangential field due to the image of $(\underline{J}^{ib}, \underline{M}^{ib})$. All the fields are evaluated in the space with the conducting plane removed. They can be calculated by using (2-26) - (2-35) with superscripts and subscripts (a,b) dropped, and $\underline{J}_n$ replaced by $(\underline{J}_n, \underline{J'}_n)$.

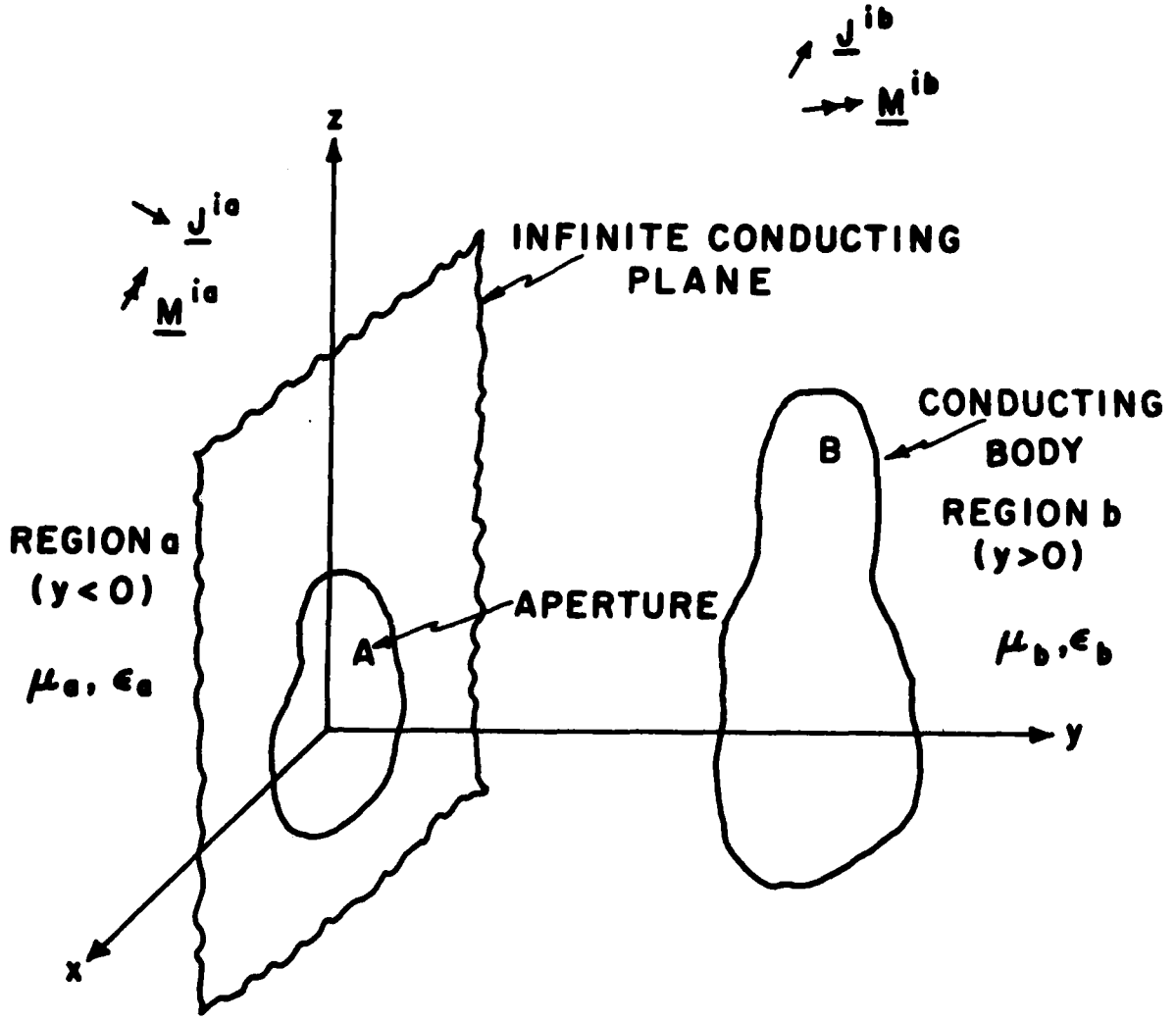

Fig. 2.1. General problem.

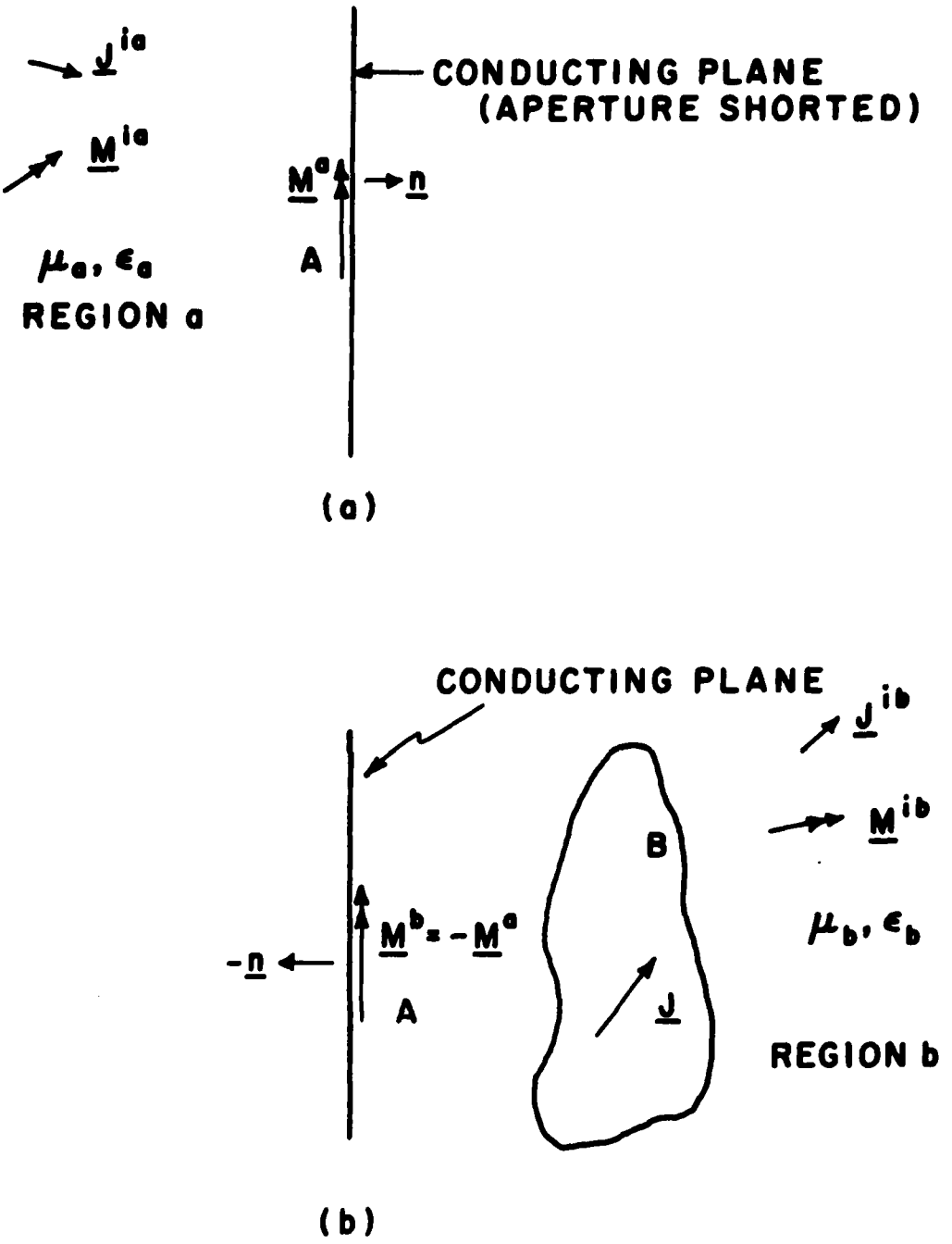

Fig. 2.2. Equivalence for the general problem. (a) Equivalence for region a. (b) Equivalence for region b.

Chapter 3

APPLICATION TO THE PROBLEM OF AN UNLOADED WIRE OF FINITE LENGTH BEHIND AN APERTURE OF ARBITRARY SIZE AND SHAPE

3.1. Problem Specification

In this chapter, the general moment method solution developed in Chapter 2 is specialized for the problem of an unloaded wire of finite length behind an aperture of arbitrary size and shape. The problem configuration is shown in Fig. 3.1. The space is filled with loss-free homogeneous medium of permeability μ and permittivity ϵ. A straight thin wire of radius r_B and length L is located at y=d and points toward the z-direction. A plane wave is incident from region a at an angle (θ_o,ϕ_o). For this excitation, we set the tangential impressed field at a point (x,0,z) in the aperture as

$$\underline{H}_t^{ioa} = (H_x^{ioa}\,\underline{u}_x + H_z^{ioa}\,\underline{u}_z) \tag{3-1}$$

where

$$H_x^{ioa} = (H_\theta^{ioa}\cos\theta_o\cos\phi_o - H_\phi^{ioa}\sin\phi_o)e^{jk(x\sin\theta_o\cos\phi_o + z\cos\theta_o)} \tag{3-2}$$

$$H_z^{ioa} = -H_\theta^{ioa}\sin\theta_o e^{jk(x\sin\theta_o\cos\phi_o + z\cos\theta_o)} \tag{3-3}$$

Here, H_{θ}^{ioa} and H_{ϕ}^{ioa} are constants, and $\underline{u}_x$ and $\underline{u}_z$ are unit vectors in the x and the z directions of the rectangular coordinate system. No impressed sources exist in region b.

An appropriate set of expansion functions and testing procedures are needed to solve for the currents in the aperture and on the wire. In this chapter and throughout the following chapters, a Galerkin solution is utilized and, for simplicity, the same medium is assumed in regions a and b. Therefore, we only need to specify the expansion functions and use (2-39) - (2-45) to evaluate the matrices.

3.2. Magnetic Current Expansion Functions in the Aperture

In this section, we model the aperture by planar triangular patching which has been used to model a surface in [9] - [13]. The advantages of the triangular patching are : (1) the ability to conform closely to an arbitrarily shaped aperture, (2) the flexibility of having greater densities on those portions of the aperture where more resolution is desired, e.g., when the edge effect is concerned, and (3) the scheme can be easily implemented on a computer. The triangular patch scheme for the aperture is explained as follows.

First, assume that a suitable triangulation is found to closely approximate the aperture region. The triangulation is defined by sets of faces (patches), edges, and nodes, such as shown in Fig. 3.2. We number the nodes and edges and specify the orientations of edges by

arrows (e.g., edge 1 is from node 3 to node 4). We next define the orientation of each face to be its normal direction, i.e., in the y-direction of Fig. 3.1. As shown in Fig. 3.3, the current reference direction across an internal (non-boundary) edge n is defined to be the direction of the cross product of the edge orientation and the face orientation. The conjoined triangles associated with edge n are denoted by T_n^+ and T_n^-, with the current reference direction from T_n^+ to T_n^-.

Next, we introduce local position vectors associated with edge n, as shown in Fig. 3.4. Any point in triangle T_n^+ can be designated by a local position vector $\underline{\hat{\rho}}_n^+$ defined with respect to the free node (node not on edge n) of T_n^+. Similarly, any point in T_n^- can be designated by $\underline{\hat{\rho}}_n^-$. Note that $\underline{\hat{\rho}}_n^+$ is defined away from the free node of T_n^+, and $\underline{\hat{\rho}}_n^-$ is toward the free node of T_n^-. $\underline{r}$ is the global position vector of a point in the aperture.

Now, we define the expansion functions in the aperture, which were originally proposed in [14]. For each internal edge n, the magnetic current expansion function is defined as

$$\underline{M}_n(\underline{r}) = \begin{cases} \dfrac{l_n \underline{\hat{\rho}}_n^+}{2A_n^+} & \underline{r} \text{ in } T_n^+ \\ \dfrac{l_n \underline{\hat{\rho}}_n^-}{2A_n^-} & \underline{r} \text{ in } T_n^- \\ 0 & \text{elsewhere} \end{cases} \tag{3-4}$$

Here, l_n is the length of edge n, and A_n^+ and A_n^- are the areas of conjoined triangles T_n^+ and T_n^-.

In the following, we discuss some properties of $\underline{M}_n$ defined in (3-4), and ensure that they are uniquely suited to be the magnetic current expansion functions in the aperture.

(1) $\underline{M}_n$ has no component normal to the boundary edges (excluding the common edge) of the conjoined triangles T_n^+ and T_n^-. Hence, no line charges exist along these boundary edges. In addition, the component of $\underline{M}_n$ normal to edge n is the constant 1 (see Fig. 3.5) and is continuous across edge n. This implies that edge n is also free of line charge.

(2) The surface magnetic charge density is defined as

$$m_n = \frac{\nabla \cdot \underline{M}_n}{-j\omega}$$

$$= \begin{cases} \dfrac{\mp l_n}{j\omega A_n^{\pm}} & \underline{r} \text{ in } T_n^{\pm} \\ 0 & \text{elsewhere} \end{cases} \qquad (3\text{-}5)$$

Therefore, the net charge in the conjoined triangles is zero.

(3) The set of functions $\underline{M}_n$ defined for all the internal edges is sufficient to represent the magnetic current anywhere in the aperture. Any current in the aperture can be well approximated by a superposition of these expansion functions. At any boundary edge of the aperture, the normal component of magnetic current must vanish, while the tangential component can be represented by a linear combination of the expansion functions associated with the two internal edges of the pertinent triangle. Therefore, we need not and should not define expansion functions for the boundary edges.

Thus, the total number of expansion functions over A, NA in (2-11), is equal to the total number of internal edges of the aperture. In addition, since the normal component of $\underline{M}_n$ across edge n is 1, V_n in (2-11) is interpreted as the normal component of the magnetic current density crossing edge n.

3.3. Electric Current Expansion Functions on the Wire

We make the following approximations for the current on the wire : (1) The current is assumed to flow only in the axial direction of the wire, (2) the current is approximated by a filament of current on the axis of the wire and depends only on the axial length variable, and (3) the boundary condition (2-10) is applied only to the axial component of the electric field at the surface of the wire. For

simplicity, the wire is equally divided into NB subsections of length $2\alpha_B$. Pulse functions are used over each subsection. The expansion functions for the current $\underline{J}$ on the wire are then defined as

$$\underline{J}_n = \underline{u}_z P(z-z_n) \quad n=1,2,\ldots,NB \quad -\frac{L}{2}+\alpha_B \leq z \leq \frac{L}{2}-\alpha_B \tag{3-6}$$

$$P(z-z_n) = \begin{cases} 1 & , z_{n-} \leq z \leq z_{n+} \\ 0 & , \text{elsewhere} \end{cases} \tag{3-7}$$

where z_{n-}, z_n, and z_{n+} are the z-coordinates of the starting point, midpoint, and termination point of the nth subsection. The subsections are enumerated from $z = -L/2 + \alpha_B$ to $L/2 - \alpha_B$. Note that by (3-6) the current is ensured to be zero at the ends of the wire.

3.4. Matrix Evaluation

(A) Evaluation of Admittance Matrix $[Y^a + Y^b]$

According to the definition, the admittance matrix $[Y^a+Y^b]$ is independent of excitations applied to the system and can be evaluated as if the wire were not present. Therefore the matrix is the same as that evaluated in [13]. We summarize the evaluation as follows.

Substituting (2-26), (2-30), (2-32), (3-4), and (3-5) into (2-39), we have

$$Y_{mn}^{a}+Y_{mn}^{b} = 4j\omega\iint_{A}\underline{M}_m\cdot\underline{F}_n\,dS + 4\iint_{A}\underline{M}_m\cdot\nabla\Phi_n\,dS$$

$$= 4j\omega\iint_{A}\underline{M}_m\cdot\underline{F}_n\,dS - 4\iint_{A}\Phi_n\nabla\cdot\underline{M}_m\,dS$$

$$= 4j\omega\left[\iint_{T_m^+}\frac{l_m\hat{\underline{\rho}}_m^{+}\cdot\underline{F}_n}{2A_m^{+}}\,dS + \iint_{T_m^-}\frac{l_m\hat{\underline{\rho}}_m^{-}\cdot\underline{F}_n}{2A_m^{-}}\,dS\right]$$

$$- 4\left[\iint_{T_m^+}\frac{l_m\Phi_n}{A_m^{+}}\,dS - \iint_{T_m^-}\frac{l_m\Phi_n}{A_m^{-}}\,dS\right]$$

$$\simeq 2j\omega\, l_m\left[\hat{\underline{\rho}}_m^{c+}\cdot\underline{F}_n(\underline{r}_m^{c+}) + \hat{\underline{\rho}}_m^{c-}\cdot\underline{F}_n(\underline{r}_m^{c-})\right]$$

$$- 4l_m\left[\Phi_n(\underline{r}_m^{c+}) - \Phi_n(\underline{r}_m^{c-})\right] \qquad (3\text{-}8)$$

where

$$\underline{F}_n(\underline{r}_m^{c\pm}) = \varepsilon\iint_{T_n^+ + T_n^-}\underline{M}_n(\underline{r}')\,G(k,\,\underline{r}_m^{c\pm},\,\underline{r}')\,dS' \qquad (3\text{-}9)$$

$$\Phi_n(\underline{r}_m^{c\pm}) = \frac{1}{\mu}\iint_{T_n^+ + T_n^-} m_n(\underline{r}')\,G(k,\,\underline{r}_m^{c\pm},\,\underline{r}')\,dS' \qquad (3\text{-}10)$$

$\hat{\underline{\rho}}_m^{c\pm}$ and $\underline{r}_m^{c\pm}$ are, respectively, the local and global position vectors of the centroids of $T_m^{\pm}$. The integrals are approximated by sampling the integrands at the centroids in (3-8).

To evaluate $\underline{F}_n(\underline{r}_m^{c\pm})$ and $\Phi_n(\underline{r}_m^{c\pm})$, we proceed face by face for each triangle. As shown in Fig. 3.6, T_p is an observation triangle and T_q a source triangle. Nodes of T_q are designated by 1, 2, and 3, and lengths of edges of T_q are l_1, l_2, and l_3. The local position vectors of a source point in T_q, $\hat{\underline{\rho}}_1$, $\hat{\underline{\rho}}_2$, and $\hat{\underline{\rho}}_3$, divide T_q into three subareas A_1, A_2, and A_3. The global position vectors of the source point and the three nodes of T_q are $\underline{r}'$, $\underline{r}_1$, $\underline{r}_2$, and $\underline{r}_3$, respectively. We now define area coordinates (ξ,η,ζ) as

$$\xi = \frac{A_2}{A_q} \tag{3-11}$$

$$\eta = \frac{A_3}{A_q} \tag{3-12}$$

$$\zeta = \frac{A_1}{A_q} = 1 - \xi - \eta \tag{3-13}$$

where A_q is the area of T_q. The relationships among the area coordinates and position vectors are

$$\hat{\underline{\rho}}_i = \pm (\underline{r}' - \underline{r}_i) \qquad i = 1, 2, 3 \tag{3-14}$$

$$\underline{r}' = \zeta \underline{r}_1 + \xi \underline{r}_2 + \eta \underline{r}_3 \tag{3-15}$$

In (3-14), the positive sign is used if the current reference direction of edge i is away from T_q, and the negative sign is used if the current reference direction is toward T_q. Note, for simplicity, superscripts $\pm$ of $\hat{\underline{\rho}}_i^{\pm}$ and $T_q^{\pm}$ are dropped.

Using the area coordinates, we can transform any surface integral over T_q into a double line integral by the following formula,

$$\iint_{T_q} f(\underline{r}')dS' = 2A_q \int_{\eta=0}^{1} \int_{\xi=0}^{1-\eta} f((1-\xi-\eta)\underline{r}_1+\xi\underline{r}_2+\eta\underline{r}_3)d\xi d\eta \qquad (3\text{-}16)$$

Therefore, the electric vector potential $\underline{F}_i^{pq}$ and magnetic scalar potential Φ_i^{pq} at the centroid $\underline{r}_p^c$ of triangle T_p due to edge i of source triangle T_q can be evaluated as follows.

By (3-4), (3-9), and (3-11) - (3-16), we have the vector potential

$$\underline{F}_i^{pq} = \varepsilon \iint_{T_q} \underline{M}_i(\underline{r}')\, G(k, \underline{r}_p^c, \underline{r}')\, dS'$$

$$= \frac{l_i \varepsilon}{2A_q} \iint_{T_q} \hat{\underline{\rho}}_i\, G(k, \underline{r}_p^c, \underline{r}')\, dS'$$

$$= \frac{\pm l_i \varepsilon}{2A_q} \iint_{T_q} [(1-\xi-\eta)\underline{r}_1+\xi\underline{r}_2+\eta\underline{r}_3-\underline{r}_i]G(k,R_p)dS'$$

$$= \pm l_i \varepsilon [(\underline{r}_2-\underline{r}_1)I_\xi^{pq}+(\underline{r}_3-\underline{r}_1)I_\eta^{pq}+(\underline{r}_1-\underline{r}_i)I^{pq}] \qquad i=1,2,3 \quad (3\text{-}17)$$

where

$$I^{pq} = \int_{\eta=0}^{1} \int_{\xi=0}^{1-\eta} G(k,R_p)d\xi d\eta \qquad (3\text{-}18)$$

$$I_{\xi}^{pq} = \int_{\eta=0}^{1} \int_{\xi=0}^{1-\eta} \xi G(k,R_p) d\xi d\eta \tag{3-19}$$

$$I_{\eta}^{pq} = \int_{\eta=0}^{1} \int_{\xi=0}^{1-\eta} \eta G(k,R_p) d\xi d\eta \tag{3-20}$$

$$G(k, R_p) = \frac{e^{-jkR_p}}{4\pi R_p} \tag{3-21}$$

$$R_p = |\underline{r}_p^c - (1 - \xi - \eta)\underline{r}_1 - \xi \underline{r}_2 - \eta \underline{r}_3| \tag{3-22}$$

Equations (3-18) - (3-20) are evaluated in Appendix A. Similarly, by (3-5) and (3-10) - (3-16), we have the scalar potential

$$\begin{aligned} \phi_i^{pq} &= \frac{1}{\mu} \iint_{T_q} m_i(\underline{r}') \, G(k, \underline{r}_p^c, \underline{r}') dS' \\ &= \frac{\mp l_i}{j\omega\mu A_q} \iint_{T_q} G(k, \underline{r}_p^c, \underline{r}') \, dS' \\ &= \frac{\mp 2}{j\omega\mu} l_i \, I^{pq} \qquad i=1,2,3 \end{aligned} \tag{3-23}$$

Again, if the current reference direction of edge i is away from T_q, the positive sign in (3-17) and the negative sign in (3-23) are used. If the direction is toward T_q, the negative sign in (3-17) and the positive sign in (3-23) are used. Note that (3-17) and (3-23) are defined only for the edge which is not a boundary edge of the aperture. If edge i is a boundary edge, $\underline{F}_i^{pq} = \Phi_i^{pq} = 0$.

Finally, $\underline{F}_n(\underline{r}_m^{c\pm})$ and $\Phi_n(\underline{r}_m^{c\pm})$ in (3-9) and (3-10) can be obtained from $\underline{F}_i^{pq}$ and Φ_i^{pq} in (3-17) and (3-23) by transferring the local index i (i = 1, 2, 3) to its corresponding global index n (n = 1, 2,..., NA). Similarly, the quantity $1_m\hat{\rho}_m^{c\pm}$ in (3-8) can be evaluated by using face to face procedure and local index. The evaluation of the admittance matrix is now complete.

(B) Evaluation of Impedance Matrix [Z]

The tangential electric field at an observation point along the surface of the wire due to the axial current $\underline{J}_n$ at (0,d,z') plus its image $\underline{J}'_n = -\underline{J}_n$ at (0,-d,z') can be obtained by (2-27), (2-31), (2-33), and (2-34). It is

$$E_z(\underline{J}_n, \underline{J}'_n) = \frac{-j\omega\mu}{4\pi}\int_B J_n(z')\left(\frac{e^{-jkR}}{R} - \frac{e^{-jkR'}}{R'}\right)dz'$$

$$+ \frac{1}{4\pi j\omega\epsilon}\frac{\partial}{\partial z}\int_B \frac{dJ_n(z')}{dz'}\left(\frac{e^{-jkR}}{R} - \frac{e^{-jkR'}}{R'}\right)dz'$$

$$n=1,2,\ldots,NB \qquad (3\text{-}24)$$

Here,

$$R = \sqrt{(z - z')^2 + r_B^2} \qquad (3\text{-}25)$$

$$R' = \sqrt{(z - z')^2 + (2d)^2} \qquad (3\text{-}26)$$

are the distances from the observation point to the source point and to the image of the source point, respectively. Substituting (3-6) and (3-24) into (2-42) and using [8, Eq. (4-20)], we obtain the impedance matrix elements

$$
\begin{aligned}
Z_{mn} = j\omega\mu\Delta l_m \Delta l_n \Big[& \underline{\psi}(z_m, z_n, r_B) - \underline{\psi}(z_m, z_n, 2d) \Big] \\
& + \frac{1}{j\omega\varepsilon}\Big[\underline{\psi}(z_{m+}, z_{n+}, r_B) - \underline{\psi}(z_{m+}, z_{n+}, 2d) \\
& - \underline{\psi}(z_{m+}, z_{n-}, r_B) + \underline{\psi}(z_{m+}, z_{n-}, 2d) \\
& - \underline{\psi}(z_{m-}, z_{n+}, r_B) + \underline{\psi}(z_{m-}, z_{n+}, 2d) \\
& + \underline{\psi}(z_{m-}, z_{n-}, r_B) - \underline{\psi}(z_{m-}, z_{n-}, 2d)\Big] \qquad m, n = 1, 2, \ldots, NB
\end{aligned}
\tag{3-27}
$$

where $\Delta l_m = \Delta l_n = 2\alpha_B$ and

$$
\underline{\psi}(z_m, z_n, \rho) = \frac{1}{4\pi\Delta l_n} \int_{z_n - \frac{\Delta l_n}{2}}^{z_n + \frac{\Delta l_n}{2}} \frac{e^{-jk\sqrt{(z_m - z')^2 + \rho^2}}}{\sqrt{(z_m - z')^2 + \rho^2}}\, dz' \tag{3-28}
$$

has been evaluated in [15].

(C) Evaluation of Coupling Matrices $[T]$ and $[\hat{T}]$

The tangential magnetic field at a point (x,0,z) in the aperture due to a z- directed current $\underline{J}_n$ on the wire at y=d plus its image $\underline{J}'_n$ is

$$\underline{H}_t(\underline{J}_n, \underline{J}'_n) = 2H_x(\underline{J}_n)\,\underline{u}_x$$

$$= \frac{2d}{\sqrt{x^2+d^2}} H_\phi(\underline{J}_n)\,\underline{u}_x \qquad (3\text{-}29)$$

Substitution of (3-4) and (3-29) into (2-40) gives

$$T_{mn} = dl_m \left[\frac{1}{A_m^+}\iint_{T_m^+} \frac{\hat{\rho}_m^+ \cdot \underline{u}_x H_\phi(\underline{J}_n)}{\sqrt{x^2+d^2}}\,dS + \frac{1}{A_m^-}\iint_{T_m^-} \frac{\hat{\rho}_m^- \cdot \underline{u}_x H_\phi(\underline{J}_n)}{\sqrt{x^2+d^2}}\,dS\right]$$

$$\simeq dl_m \left[\frac{\hat{x}_m^{c+} H_\phi(\underline{J}_n ; \underline{r}_m^{c+})}{\sqrt{(x_m^{c+})^2+d^2}} + \frac{\hat{x}_m^{c-} H_\phi(\underline{J}_n ; \underline{r}_m^{c-})}{\sqrt{(x_m^{c-})^2+d^2}}\right] \qquad (3\text{-}30)$$

Here, $\hat{x}_m^{c\pm}$ and $x_m^{c\pm}$ are the x-components of position vectors $\hat{\rho}_m^{c\pm}$ and $\underline{r}_m^{c\pm}$, respectively. $H_\phi(\underline{J}_n ; \underline{r}_m^{c\pm})$ is the ϕ-component of the magnetic field due to $\underline{J}_n$ at the centroid $\underline{r}_m^{c\pm}$.

The magnetic field $H_\phi(\underline{J}_n ; \underline{r}_m^{c\pm})$ due to $\underline{J}_n$ defined in (3-6) is

$$H_\phi(\underline{J}_n ; \underline{r}_m^{c\pm}) = -\frac{\partial A_z(\underline{J}_n)}{\mu \partial \rho}$$

$$= \frac{\sqrt{(x_m^{c\pm})^2+d^2}}{4\pi} \int_{\Delta l_n} \left(\frac{jk}{|\underline{r}_m^{c\pm} - \underline{r}'|^2} + \frac{1}{|\underline{r}_m^{c\pm} - \underline{r}'|^3} \right) e^{-jk|\underline{r}_m^{c\pm} - \underline{r}'|} dz'$$

$$\approx \frac{\Delta l_n \sqrt{(x_m^{c\pm})^2+d^2}}{4\pi} \left[\frac{jk}{(r_{mn}^{\pm})^2} + \frac{1}{(r_{mn}^{\pm})^3} \right] e^{-jkr_{mn}^{\pm}} \qquad (3\text{-}31)$$

where

$$r_{mn}^{\pm} = \sqrt{(x_m^{c\pm})^2 + d^2 + (z_m^{c\pm} - z_n)^2} \qquad (3\text{-}32)$$

is the distance between the centroid associated with edge m of the aperture and the midpoint of subsection n of the wire. $z_m^{c\pm}$ is the z-component of $\underline{r}_m^{c\pm}$. Substituting (3-31) into (3-30), we obtain

$$T_{mn} \approx \frac{dl_m \Delta l_n}{4\pi} \left\{ \hat{x}_m^{c+} \left[\frac{jk}{(r_{mn}^{+})^2} + \frac{1}{(r_{mn}^{+})^3} \right] e^{-jkr_{mn}^{+}} \right.$$

$$\left. + \hat{x}_m^{c-} \left[\frac{jk}{(r_{mn}^{-})^2} + \frac{1}{(r_{mn}^{-})^3} \right] e^{-jkr_{mn}^{-}} \right\}$$

$$m=1,2,\ldots,NA \quad n=1,2,\ldots,NB \qquad (3\text{-}33)$$

Since Galerkin's solution is used, $[\hat{T}]$ can be obtained by $[\hat{T}] = -[\tilde{T}]$.

(D) Evaluation of Source Vectors $\vec{I}^{ia}$, $\vec{I}^{ib}$, and $\vec{V}^{ib}$

Since there is no excitation from region b of Fig. 3.1, (2-44) and (2-45) give

$$\vec{I}^{ib} = \vec{V}^{ib} = 0 \tag{3-34}$$

Substitution of (3-1) - (3-4) into (2-43) gives

$$I_m^{ia} = 1_m \left[\frac{1}{A_m^+} \iint_{T_m^+} \hat{\rho}_m^+ \cdot \underline{H}_t^{ioa} \, dS + \frac{1}{A_m^-} \iint_{T_m^-} \hat{\rho}_m^- \cdot \underline{H}_t^{ioa} dS \right]$$

$$\approx 1_m \left[\hat{x}_m^{c+} H_x^{ioa}(\underline{r}_m^{c+}) + \hat{z}_m^{c+} H_z^{ioa}(\underline{r}_m^{c+}) \right.$$

$$\left. + \hat{x}_m^{c-} H_x^{ioa}(\underline{r}_m^{c-}) + \hat{z}_m^{c-} H_z^{ioa}(\underline{r}_m^{c-}) \right] \qquad m=1,2,\ldots,NA \tag{3-35}$$

Here,

$$H_x^{ioa}(\underline{r}_m^{c\pm}) = (H_\theta^{ioa} \cos\theta_o \cos\phi_o - H_\phi^{ioa} \sin\phi_o)$$

$$e^{jk(x_m^{c\pm} \sin\theta_o \cos\phi_o + z_m^{c\pm} \cos\theta_o)} \tag{3-36}$$

$$H_z^{ioa}(\underline{r}_m^{c\pm}) = - H_\theta^{ioa} \sin\theta_o \, e^{jk(x_m^{c\pm} \sin\theta_o \cos\phi_o + z_m^{c\pm} \cos\theta_o)} \tag{3-37}$$

$\hat{z}_m^{c\pm}$ and $z_m^{c\pm}$ are the z-components of $\hat{\rho}_m^{c\pm}$ and $\underline{r}_m^{c\pm}$, respectively.

By solving (2-14) and (2-15) with matrices evaluated above, we can obtain the current distributions in the aperture and on the wire.

3.5. Numerical Results

In this section, numerical results are presented for the magnetic current distribution in the aperture and the electric current distribution on the wire. Numerical results for narrow slots are available in the literature for the problem considered in this chapter. We therefore perform computations for a narrow slot backed by an unloaded wire of finite length with plane wave incidence. As we will see, our results agree very well with those in [5].

The slot has length L_a and width W_a and is centered at $(x_c,0,0)$. The wire has length L and radius r_B and is located at y=d. A plane wave is normally incident with H_x^{ioa}=1 ampere/meter. Figure 3.7 shows the triangulation used for the slot, where NA, NNODE, NEDGE, and NFACE are the numbers of unknowns, nodes, edges, and faces of the slot, respectively.

For the case of L_a/λ =0.5, W_a/λ =0.05, r_B/λ =0.001, and L/λ=0.5, Fig. 3.8 shows the comparison of our results for the total x-directed magnetic current M in the slot with those in [5]. Figure 3.9 shows the comparison of the electric current I on the wire. They both have very good agreement. Figure 3.10 shows the electric current on the wire for the case of L_a/λ =0.5, W_a/λ =0.05, x_c=0., d/λ =0.125,

r_B/λ=0.001, and L/ λ=1.0. Figure 3.11 shows the electric current on the wire for the case of L_a/λ=1.0, W_a/λ=0.05, x_c/λ=0.25, d/ λ=0.25, r_B/λ=0.001, and L/λ=1.0. Again, our results for these cases agree very well with those in [5]. Here, λ=1 meter is chosen as the wavelength in the computation. Note, the opposite sign of electric current on the wire in our results is due to the choice of a different coordinate system from that in [5].

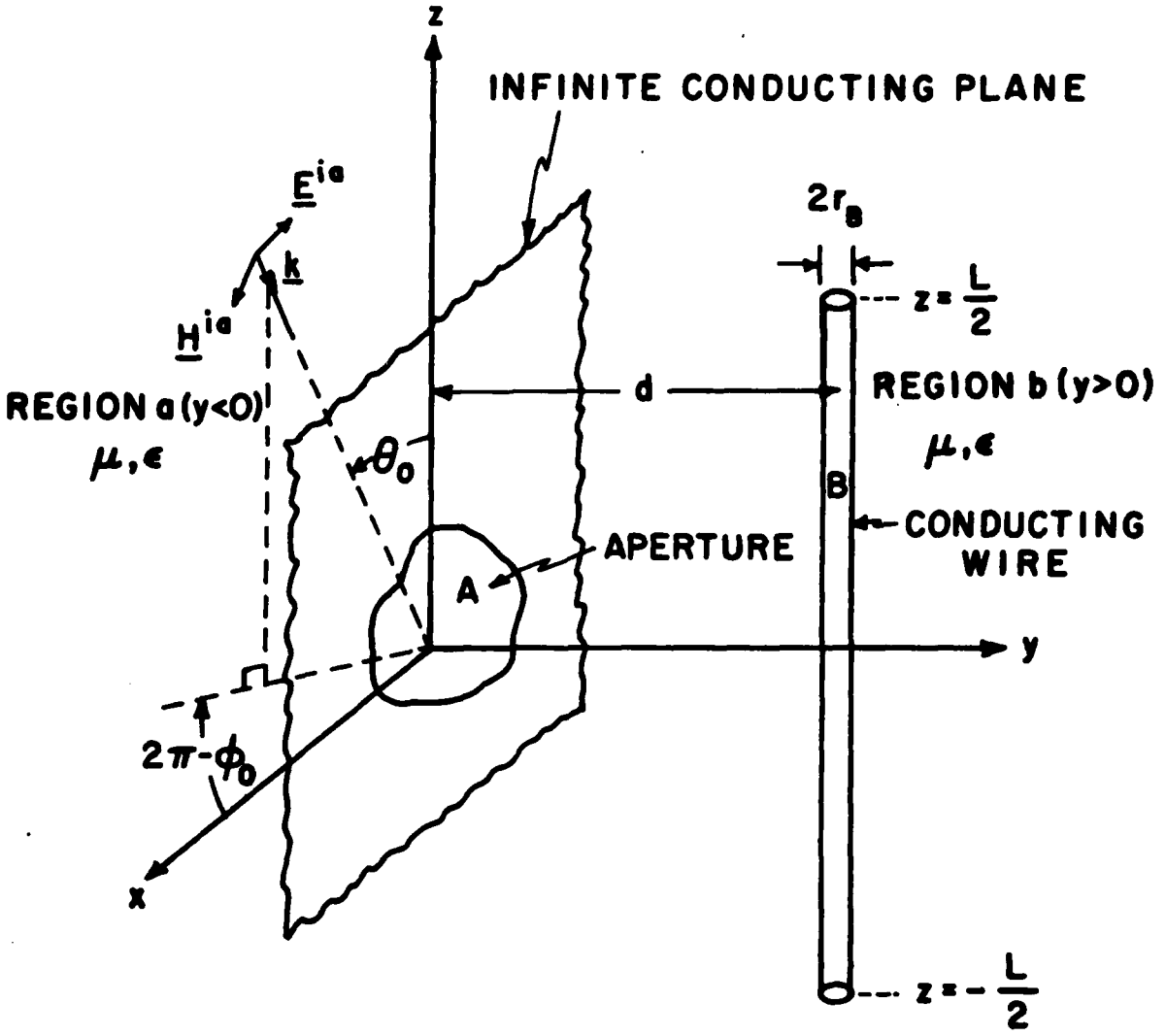

Fig. 3.1. An unloaded wire of finite length behind an aperture.

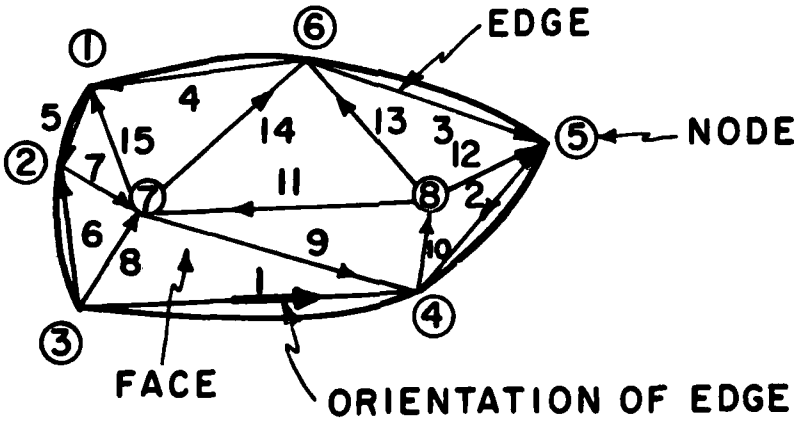

Fig. 3.2. Triangulation example.

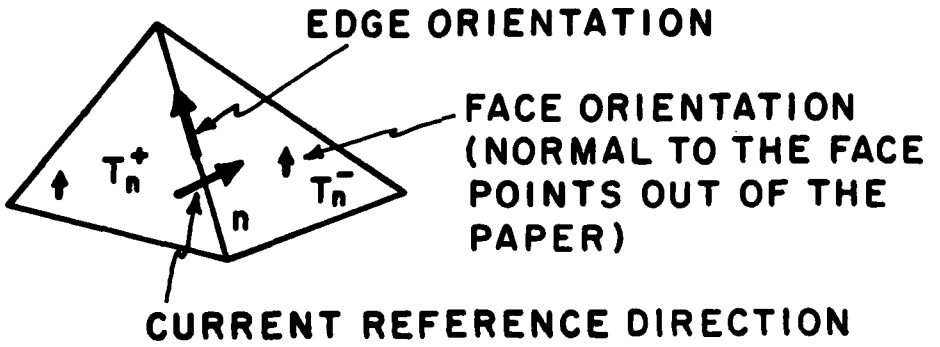

Fig. 3.3. Relationship among face orientation, edge orientation, and current reference direction across edge n.

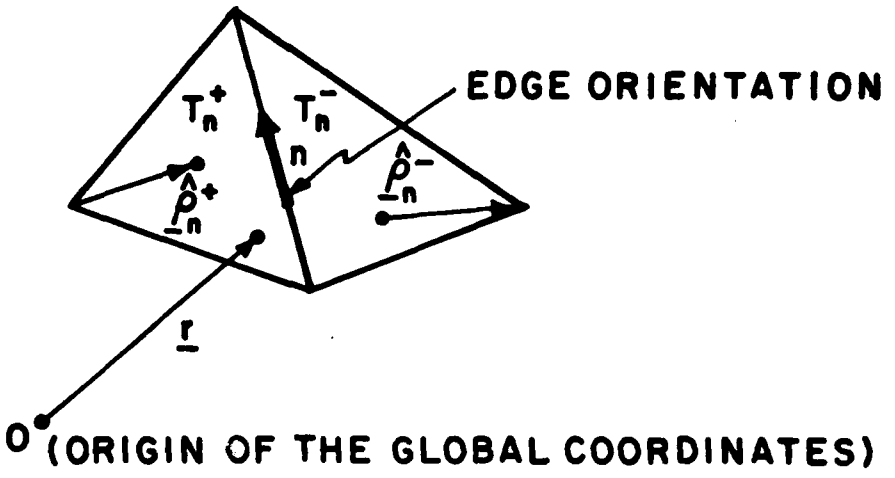

Fig. 3.4. Local position vectors $\hat{\rho}_n^+$ and $\hat{\rho}_n^-$ associated with edge n, and global position vector $\underline{r}$.

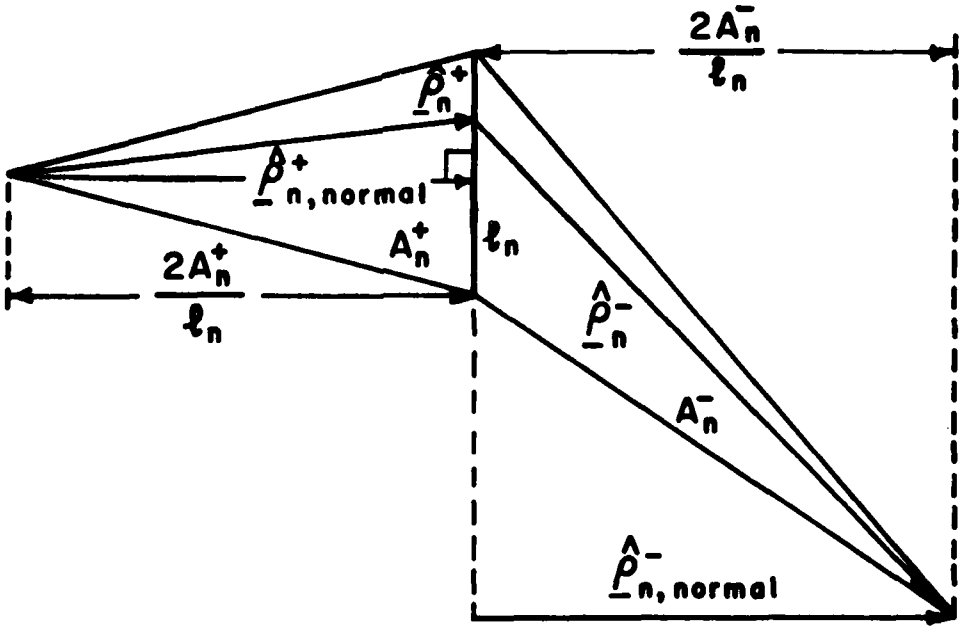

Fig. 3.5. Normal components of $\hat{\rho}_n^+$ and $\hat{\rho}_n^-$ at edge n.

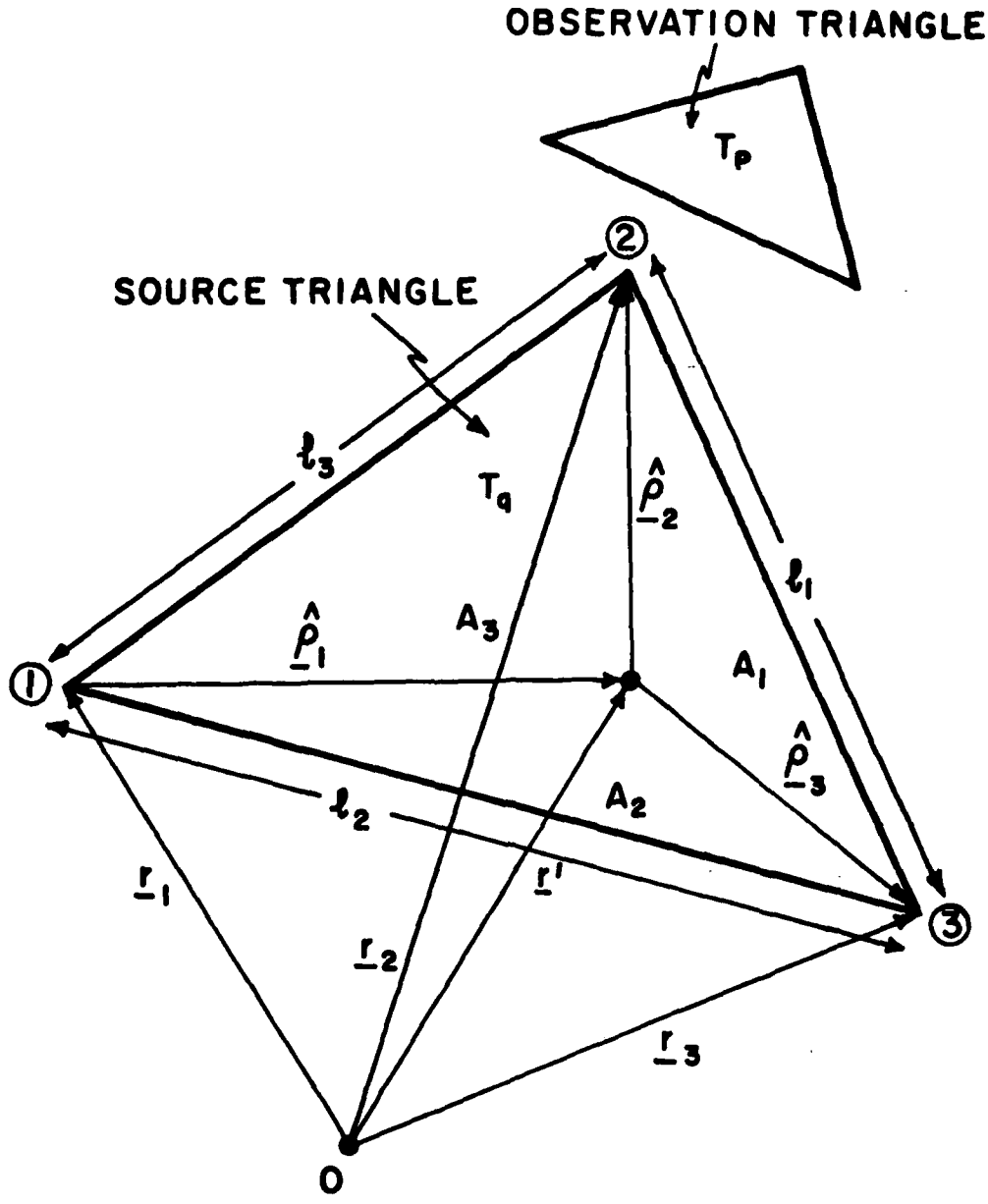

Fig. 3.6. Local and global position vectors, edges of source triangle T_q, and areas A_1, A_2, and A_3 used in defining area coordinates.

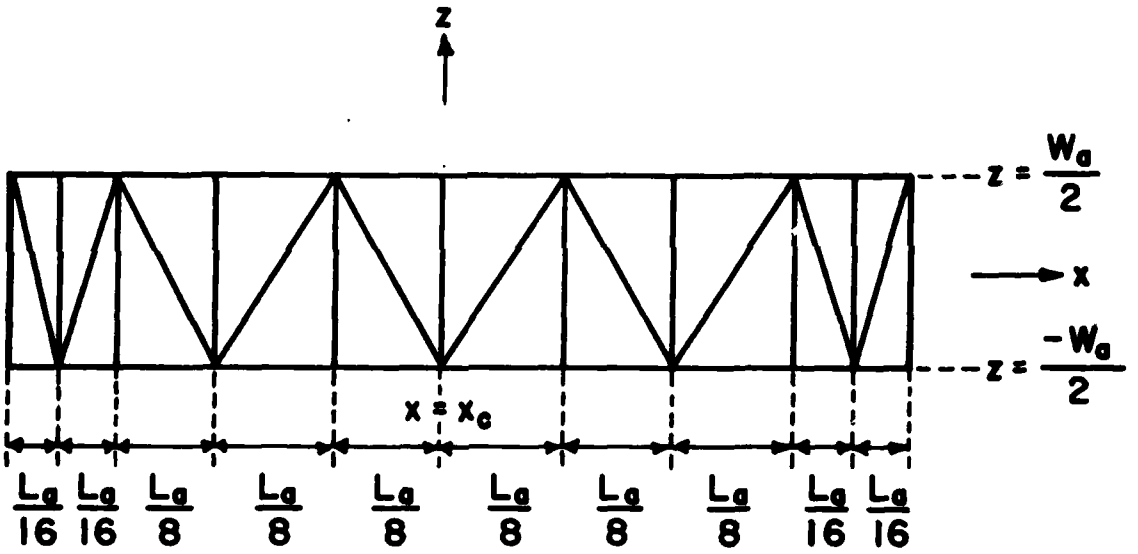

Fig. 3.7. Triangulation of a slot centered at $(x_c,0,0)$ for NA=19, NNODE=22, NEDGE=41, and NFACE=20.

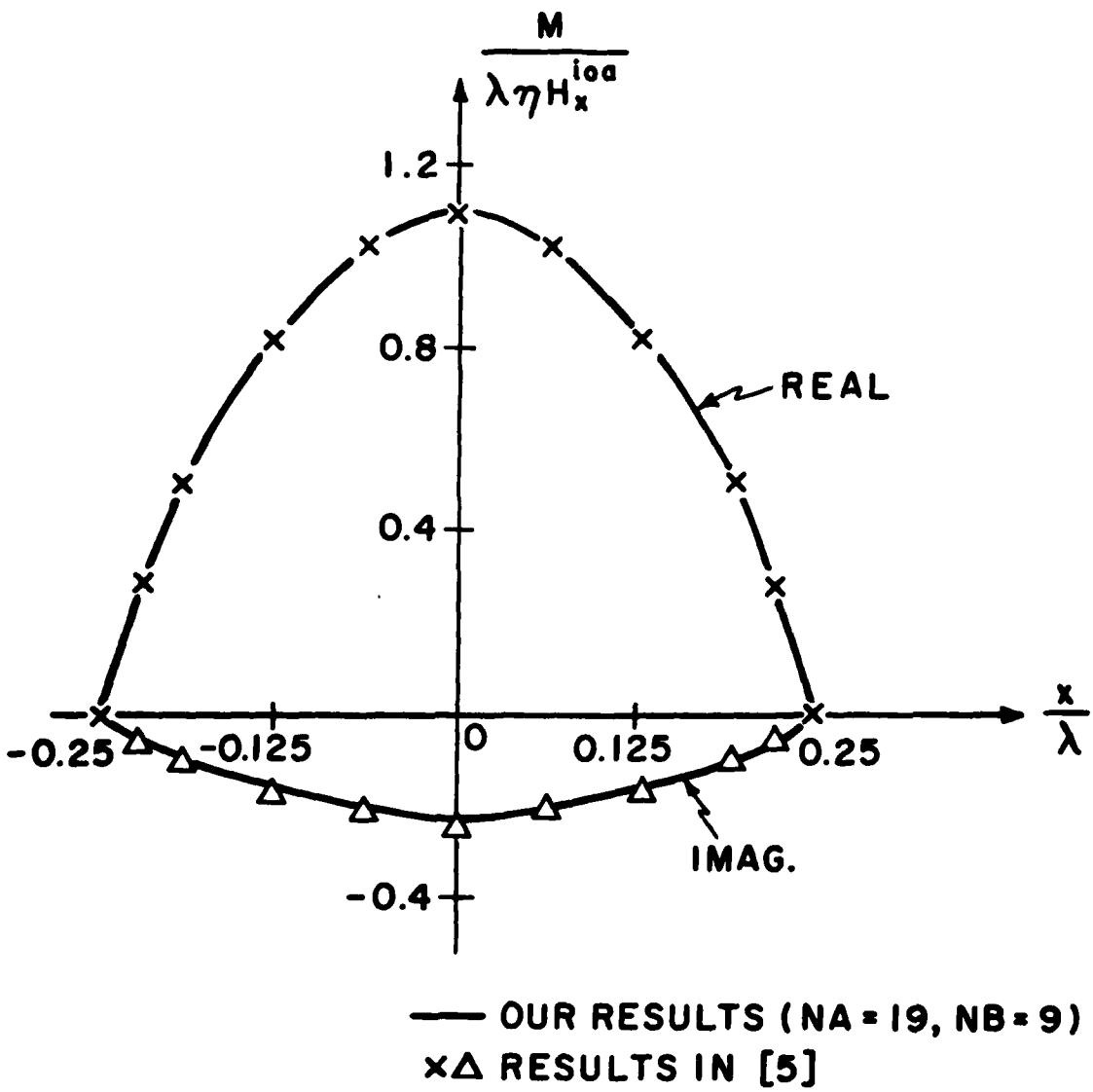

Fig. 3.8. The total x-directed magnetic current in a slot backed by an unloaded wire of finite length with normal plane wave incidence. $L_a/\lambda=0.5$, $W_a/\lambda=0.05$, $x_c=0.$, $d/\lambda=0.25$, $r_B/\lambda=0.001$, $L/\lambda=0.5$, and $H_x^{ioa}=1$ ampere/meter. (λ =1 meter)

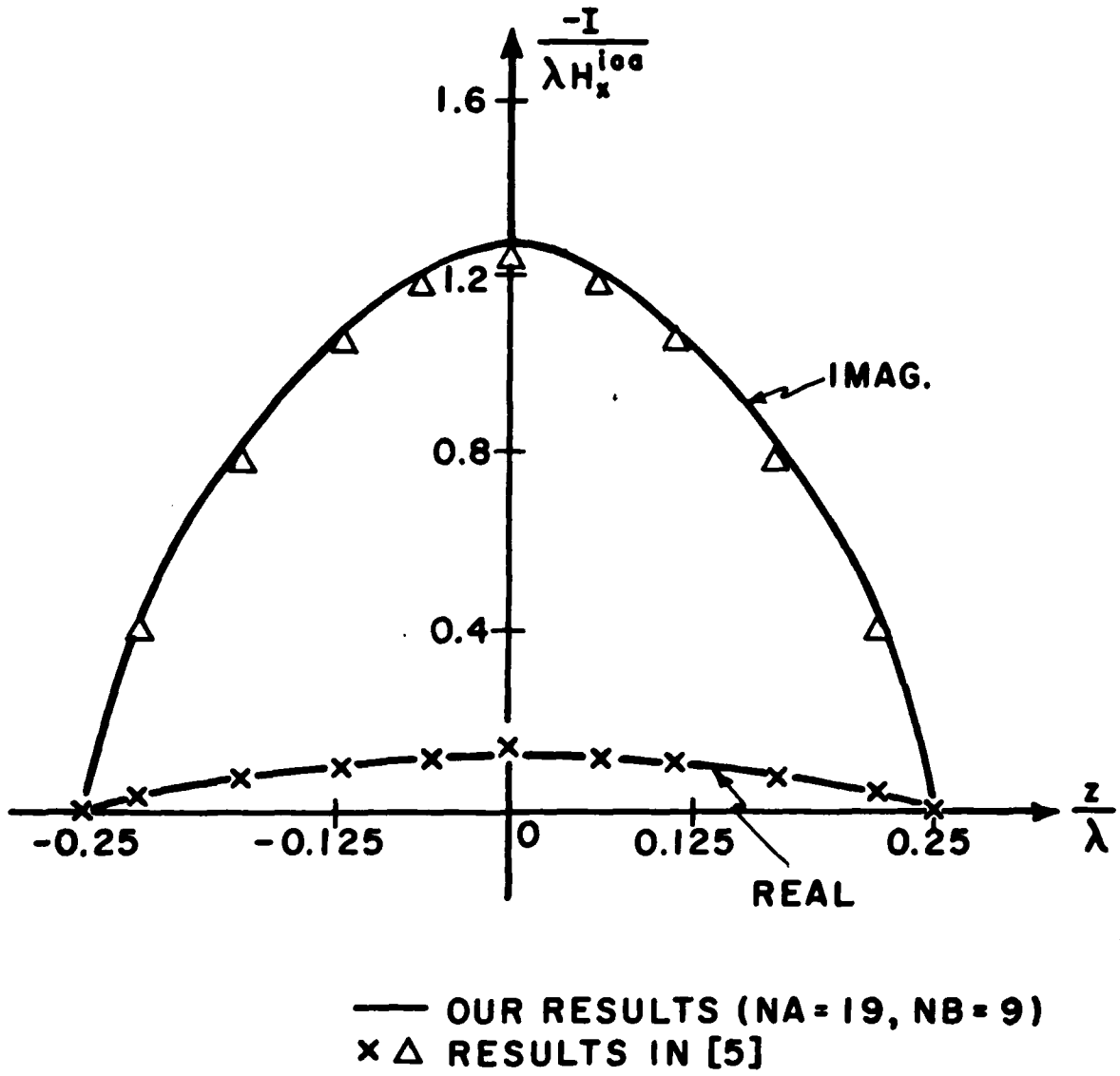

Fig. 3.9. The electric current on an unloaded wire of finite length passing by a slot with normal plane wave incidence. L_a/λ=0.5, W_a/λ=0.05, x_c=0., d/λ=0.25, r_B/λ=0.001, L/λ=0.5, and H_x^{ioa}=1 ampere/meter. (λ =1 meter)

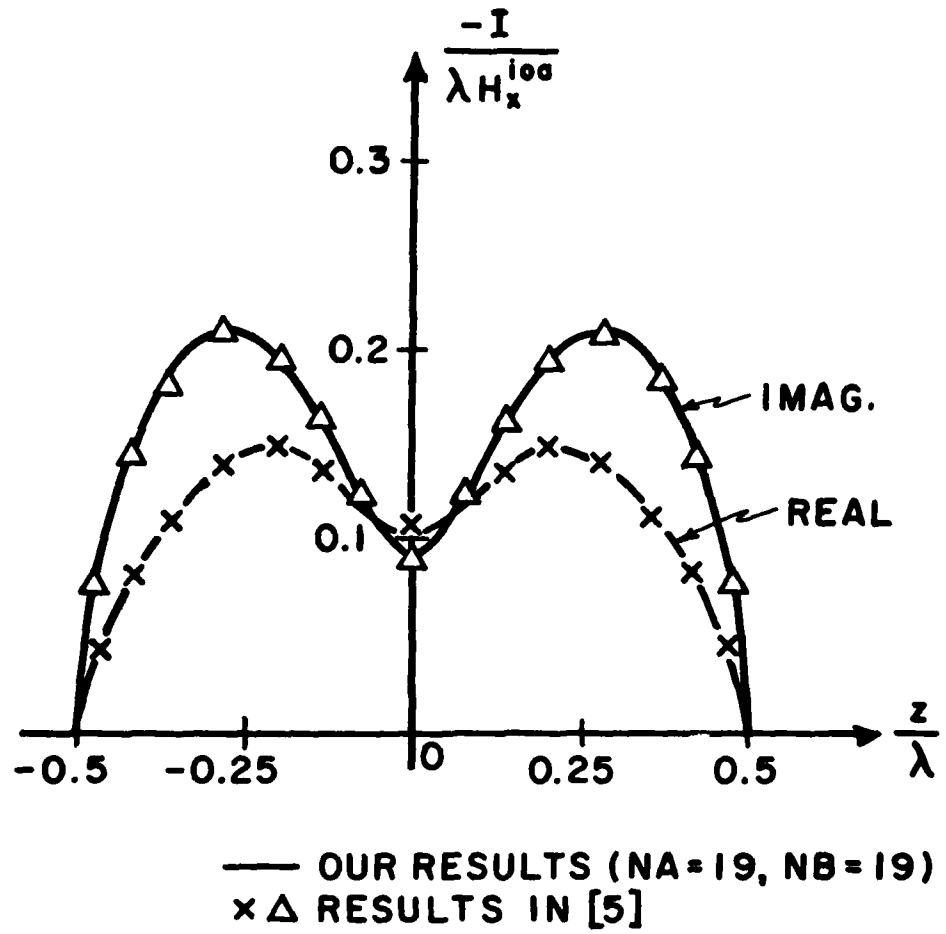

Fig. 3.10. The electric current on an unloaded wire of finite length passing by a slot with normal plane wave incidence. L_a/λ=0.5, W_a/λ=0.05, x_c=0., d/λ=0.125, r_B/λ=0.001, L/λ=1.0, and H_x^{ioa}=1 ampere/meter. (λ =1 meter)

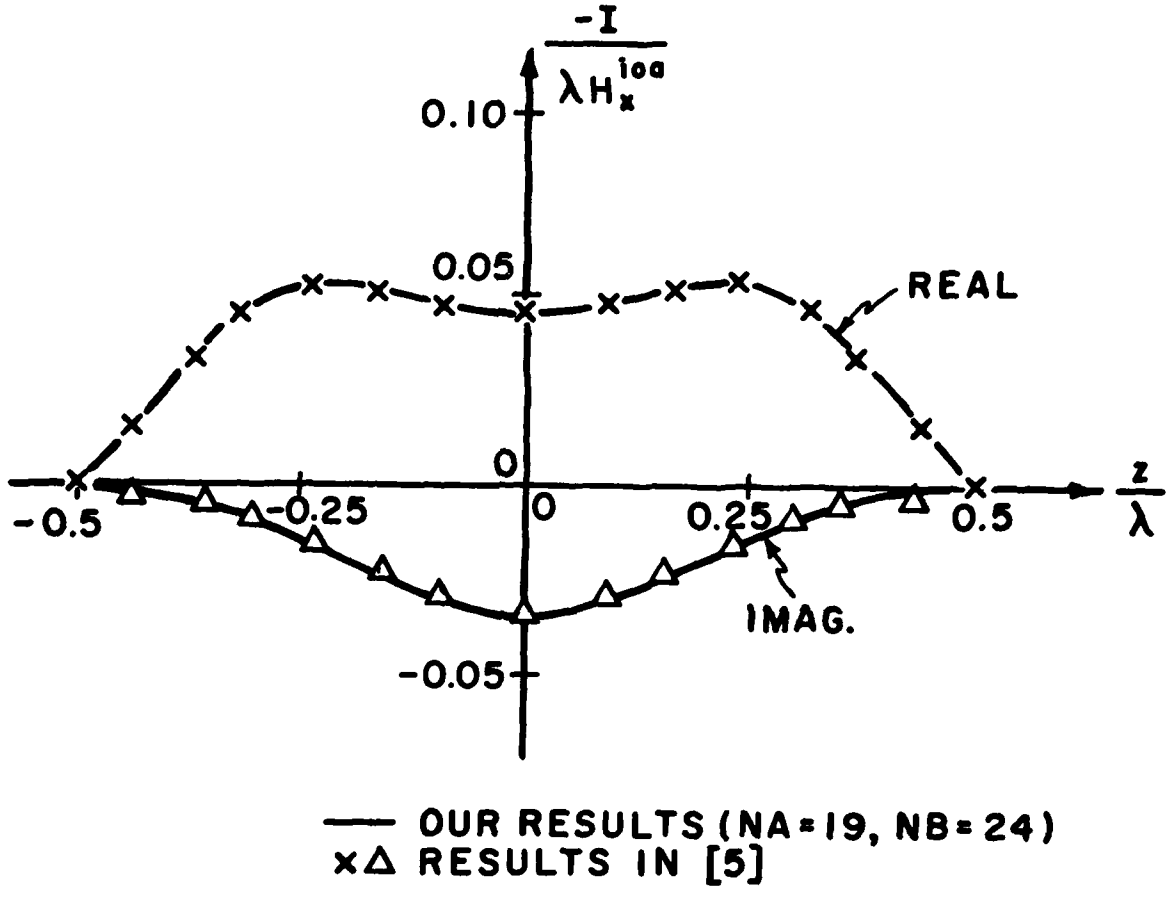

Fig. 3.11. The electric current on an unloaded wire of finite length passing by a slot with normal plane wave incidence. L_a/λ=1.0, W_a/λ=0.05, x_c/λ=0.25, d/λ=0.25, r_B/λ=0.001, L/λ=1.0, and H_x^{ioa}=1 ampere/meter. (λ =1 meter)

Chapter 4

APPLICATION TO THE PROBLEM OF AN INFINITELY LONG WIRE BEHIND AN APERTURE OF ARBITRARY SIZE AND SHAPE

4.1. Problem Specification

In this chapter, the wire considered in Chapter 3 is extended to an infinitely long wire. The geometry of the wire and an aperture of arbitrary size and shape is shown in Fig. 4.1. The excitation is a plane wave incident from region a of Fig. 4.1, and is defined in (3-1). The expansion functions and the matrices developed in Chapter 3 are modified to include the effect of the infinitely long wire. For this, two exponential wave functions, in addition to the pulse functions, are added to the expansion functions on the wire. The objective is to obtain the current distributions in the aperture and on the wire.

4.2. Expansion Functions

Since the aperture is arbitrarily sized and shaped, the expansion functions for the aperture remain the same as those developed in Chapter 3. It is noted that a transmission line without reflections

is formed by the presence of the infinitely long wire and the conducting plane. Therefore, the electric current on the wire consists of two outward traveling TEM currents plus evanescent currents (higher order modes) existing in a finite region near the aperture. We use pulse functions to represent the total current (evanescent currents plus outward traveling TEM currents) in this finite region. We use two exponential wave functions to represent the outward traveling TEM currents outside the finite region. This finite region must be greater than the dimension of the aperture in the z-direction. Therefore, the electric current expansion functions on the wire are

$$\underline{J}_1 = \underline{u}_z e^{jkz} \qquad -\infty < z < -\frac{L}{2} \tag{4-1}$$

$$\underline{J}_n = \underline{u}_z P(z-z_n) \qquad |z| \leq \frac{L}{2}, \; n=2,3,\ldots,NB-1 \tag{4-2}$$

$$\underline{J}_{NB} = \underline{u}_z e^{-jkz} \qquad \frac{L}{2} < z < \infty \tag{4-3}$$

Here, P is the pulse function defined in (3-7) and L is the length of the finite region. Each subsection in this finite region is of length $2\alpha_B$. Note that in order to include the outward traveling TEM currents, the indexes in (4-2) are slightly changed from those of (3-6).

4.3. MATRIX EVALUATION

It is noted that the magnetic current expansion functions for the aperture and the electric current expansion functions for the finite region of the wire are the same as those in Chapter 3. Therefore, the corresponding elements of the matrices $[Y^a+Y^b]$, $\vec{I}^{ia}$, $\vec{I}^{ib}$, and $\vec{V}^{ib}$ are identical to those in (3-8), (3-34), and (3-35). The elements Z_{mn} for m, n = 2, 3, ..., NB-1 are defined in (3-27), while the elements $T_{mn} = -\hat{T}_{nm}$ for m = 1, 2,..., NA and n = 2, 3, ..., NB-1 are defined in (3-33).

We now evaluate the matrix elements Z_{mn} associated with the outward traveling TEM currents on the wire. By (B-17) and (B-18), the z-components of electric fields due to $\underline{J}_1$ plus its image $\underline{J}'_1=-\underline{J}_1$ and $\underline{J}_{NB}$ plus its image $\underline{J}'_{NB}=-\underline{J}_{NB}$ are

$$E_z(\underline{J}_1,\underline{J}'_1) = -\frac{e^{-jk\frac{L}{2}}}{4\pi j\omega\epsilon}\{[\frac{jk}{r_0^-}-\frac{jk(z+\frac{L}{2})}{(r_0^-)^2}-\frac{z+\frac{L}{2}}{(r_0^-)^3}]e^{-jkr_0^-}$$

$$-[\frac{jk}{r'^-_0}-\frac{jk(z+\frac{L}{2})}{(r'^-_0)^2}-\frac{z+\frac{L}{2}}{(r'^-_0)^3}]e^{-jkr'^-_0}\} \qquad (4\text{-}4)$$

$$E_z(\underline{J}_{NB},\underline{J}'_{NB}) = -\frac{e^{-jk\frac{L}{2}}}{4\pi j\omega\epsilon}\{[\frac{jk}{r_0^+}+\frac{jk(z-\frac{L}{2})}{(r_0^+)^2}+\frac{z-\frac{L}{2}}{(r_0^+)^3}]e^{-jkr_0^+}$$

$$-[\frac{jk}{r'^+_0}+\frac{jk(z-\frac{L}{2})}{(r'^+_0)^2}+\frac{z-\frac{L}{2}}{(r'^+_0)^3}]e^{-jkr'^+_0}\} \qquad (4\text{-}5)$$

where

$$r_0^{\pm} = \sqrt{(z \mp \frac{L}{2})^2 + r_B^2} \tag{4-6}$$

$$r'^{\pm}_0 = \sqrt{(z \mp \frac{L}{2})^2 + (2d)^2} \tag{4-7}$$

However it is noted that the charge densities associated with $\underline{J}_1$ and $\underline{J}_{NB}$ are

$$\frac{dJ_1}{-j\omega dz} = \frac{1}{-j\omega}[jke^{jkz} - \delta(z + \frac{L}{2})e^{-jk\frac{L}{2}}] \tag{4-8}$$

$$\frac{dJ_{NB}}{-j\omega dz} = \frac{1}{-j\omega}[-jke^{-jkz} + \delta(z - \frac{L}{2})e^{-jk\frac{L}{2}}] \tag{4-9}$$

The z-components of electric fields due to point charges $[\pm\delta(z \mp L/2)e^{-jkL/2}]/(-j\omega)$ plus their images are the terms involving $(r_0^{\pm})^{-2}$, $(r_0^{\pm})^{-3}$, $(r'^{\pm}_0)^{-2}$, and $(r'^{\pm}_0)^{-3}$ in (4-4) and (4-5). To assure the continuity of the total current on the wire, we first replace delta functions $\delta(z \pm L/2)$ in (4-8) and (4-9) by pulse functions $P(z \pm L/2)/\Delta l_0$ over a small region Δl_0. Then we replace the E_z due to the point charges by the E_z due to these pulse functions. Δl_0 is chosen, for simplicity, to be equal to $2\alpha_B$. Thus, (4-4) and (4-5) become

$$E_z(\underline{J}_1, \underline{J}'_1) = \frac{-ke^{-jk\frac{L}{2}}}{4\pi\omega\varepsilon}\left(\frac{e^{-jkr_0^-}}{r_0^-} - \frac{e^{-jkr'^-_0}}{r'^-_0}\right) + E_z(P^-) \tag{4-10}$$

$$E_z(\underline{J}_{NB}, \underline{J}'_{NB}) = \frac{-ke^{-jk\frac{L}{2}}}{4\pi\omega\varepsilon}\left(\frac{e^{-jkr_0^+}}{r_0^+} - \frac{e^{-jkr'^+_0}}{r'^+_0}\right) + E_z(P^+) \tag{4-11}$$

Here,

$$E_z(P^{\pm}) = \frac{\pm e^{-jk\frac{L}{2}}}{4\pi j\omega\varepsilon\Delta l_0}\frac{\partial}{\partial z}\int P(z'\mp\frac{L}{2})(\frac{e^{-jkR}}{R}-\frac{e^{-jkR'}}{R'})dz'$$

$$= \frac{\pm e^{-jk\frac{L}{2}}}{4\pi j\omega\varepsilon\Delta l_0}\frac{\partial}{\partial z}\int P(z')(\frac{e^{-jkr^{\pm}}}{r^{\pm}}-\frac{e^{-jkr'^{\pm}}}{r'^{\pm}})dz' \qquad (4\text{-}12)$$

is obtained from the second term of (3-24). R and R' are defined in (3-25) and (3-26), and

$$r^{\pm} = \sqrt{(z\mp\frac{L}{2}-z')^2+r_B^2} \qquad (4\text{-}13)$$

$$r'^{\pm} = \sqrt{(z\mp\frac{L}{2}-z')^2+(2d)^2} \qquad (4\text{-}14)$$

By (2-42), (4-1), (4-10), (4-12), (C-3), and (C-4), we have

$$Z_{11} = \frac{e^{-jkL}}{j\omega\varepsilon}[\underline{\psi}(0,0,r_B) - \underline{\psi}(0,0,2d)] \qquad (4\text{-}15)$$

where $\underline{\psi}$ is defined in (3-28). By (2-42), (4-3), (4-11), (4-12), (C-3), and (C-4), we have

$$Z_{NB,NB} = Z_{11} \qquad (4\text{-}16)$$

By (2-42), (4-3), (4-10), (4-12), (C-5), and (C-6), we obtain

$$Z_{NB,1} = \frac{-e^{-jkL}}{j\omega\varepsilon}[\underline{\Psi}(L,0,r_B) - \underline{\psi}(L,0,2d)]$$

$$+ \frac{k}{2\pi\omega\varepsilon}\{-Ci(ku_2)+Ci(ku'_2)+j[Si(ku_2)-Si(ku'_2)]\} \qquad (4\text{-}17)$$

where Ci and Si are defined in (C-7) and (C-8), and

$$u_2 = L + \sqrt{L^2 + r_B^2} \tag{4-18}$$

$$u'_2 = L + \sqrt{L^2 + (2d)^2} \tag{4-19}$$

By (2-42), (4-1), (4-11), (4-12), (C-5), and (C-6), we obtain

$$Z_{1,NB} = Z_{NB,1} \tag{4-20}$$

Substituting (4-2), (4-10), and (4-12) into (2-42), we have

$$\begin{aligned} Z_{m1} = \frac{e^{-jk\frac{L}{2}}}{j\omega\epsilon}\{ & jk\Delta l_m [\underline{\psi}(z_m + \tfrac{L}{2},0,r_B) - \underline{\psi}(z_m + \tfrac{L}{2},0,2d)] \\ & + \underline{\psi}(z_{m+} + \tfrac{L}{2},0,r_B) - \underline{\psi}(z_{m+} + \tfrac{L}{2},0,2d) \\ & - \underline{\psi}(z_{m-} + \tfrac{L}{2},0,r_B) + \underline{\psi}(z_{m-} + \tfrac{L}{2},0,2d)\} \qquad m=2,3,\ldots,NB-1 \end{aligned} \tag{4-21}$$

Substitution of (4-2), (4-11), and (4-12) into (2-42) gives

$$\begin{aligned} Z_{m,NB} = \frac{e^{-jk\frac{L}{2}}}{j\omega\epsilon}\{ & jk\Delta l_m [\underline{\psi}(z_m - \tfrac{L}{2},0,r_B) - \underline{\psi}(z_m - \tfrac{L}{2},0,2d)] \\ & - \underline{\psi}(z_{m+} - \tfrac{L}{2},0,r_B) + \underline{\psi}(z_{m+} - \tfrac{L}{2},0,2d) \\ & + \underline{\psi}(z_{m-} - \tfrac{L}{2},0,r_B) - \underline{\psi}(z_{m-} - \tfrac{L}{2},0,2d)\} \qquad m=2,3,\ldots,NB-1 \end{aligned} \tag{4-22}$$

By (2-37), we have

$$Z_{1m} = Z_{m1} \qquad m=2,3,\ldots,NB-1 \tag{4-23}$$

$$Z_{NB,m} = Z_{m,NB} \qquad m=2,3,\ldots, NB-1 \tag{4-24}$$

The evaluation of the matrix [Z] is now complete.

Finally, we evaluate T_{m1}, $T_{m,NB}$, $\hat{T}_{1m}$, and $\hat{T}_{NB,m}$ for $m = 1, 2, \ldots, NA$ as follows.

Substitution of (B-14) with $z_2=L/2$ and $\underline{J}^-=\underline{J}_1$ into (3-30) gives

$$T_{m1} \approx \frac{dl_m e^{-jk\frac{L}{2}}}{4\pi} \left\{ \frac{\hat{x}_m^{c+}}{(x_m^{c+})^2+d^2}\left[1 - \frac{z_m^{c+}+\frac{L}{2}}{\sqrt{(x_m^{c+})^2+d^2+(z_m^{c+}+\frac{L}{2})^2}}\right] \right.$$

$$e^{-jk\sqrt{(x_m^{c+})^2+d^2+(z_m^{c+}+\frac{L}{2})^2}} + \frac{x_m^{c-}}{(x_m^{c-})^2+d^2}$$

$$\left[1 - \frac{z_m^{c-}+\frac{L}{2}}{\sqrt{(x_m^{c-})^2+d^2+(z_m^{c-}+\frac{L}{2})^2}}\right] e^{-jk\sqrt{(x_m^{c-})^2+d^2+(z_m^{c-}+\frac{L}{2})^2}} \left. \right\}$$

$$m = 1, 2, \ldots, NA \tag{4-25}$$

where $\hat{x}_m^{c\pm}$, $x_m^{c\pm}$, and $z_m^{c\pm}$ are defined in (3-30) and (3-32).

Similarly, substituting (B-4) with $z_1=L/2$ and $\underline{J}^+=\underline{J}_{NB}$ into (3-30), we obtain

$$T_{m,NB} \approx \frac{dl_m e^{-jk\frac{L}{2}}}{4\pi} \left\{ \frac{\hat{x}_m^{c+}}{(x_m^{c+})^2+d^2}\left[1 + \frac{z_m^{c+}-\frac{L}{2}}{\sqrt{(x_m^{c+})^2+d^2+(z_m^{c+}-\frac{L}{2})^2}}\right] \right.$$

$$e^{-jk\sqrt{(x_m^{c+})^2+d^2+(z_m^{c+}-\frac{L}{2})^2}} + \frac{\hat{x}_m^{c-}}{(x_m^{c-})^2+d^2}$$

$$\left[1 + \frac{z_m^{c-}-\frac{L}{2}}{\sqrt{(x_m^{c-})^2+d^2+(z_m^{c-}-\frac{L}{2})^2}}\right] e^{-jk\sqrt{(x_m^{c-})^2+d^2+(z_m^{c-}-\frac{L}{2})^2}} \Big\}$$

$$m = 1, 2, \ldots, NA \qquad (4\text{-}26)$$

$\hat{T}_{1m}$ and $\hat{T}_{NB,m}$, for m = 1,2,...,NA, can be obtained by (2-38).

By solving (2-14) and (2-15) with matrices evaluated above, we can obtain the current distributions in the aperture and on the wire.

4.4. Numerical Results

In this section, numerical results for the magnetic current in the aperture and the electric current on the wire are presented. To ensure the validity of our formulation, we compare our numerical results with those available in the literature for several examples. Very good agreement is obtained.

The aperture of the first example is an electrically small ellipse with major axis of length $L_a=0.02\lambda$ and minor axis of length $W_a=0.002\lambda$. An infinitely long wire of radius $r_B=0.001\lambda$ is located at y=d, where d=0.15λ, 0.10λ, or 0.05λ. A plane wave with $H_x^{ioa} = -e^{-jkz}/\eta$ ampere/meter is incident from region a of Fig. 4.1. Here, $\eta=\sqrt{\mu/\varepsilon}$. We use two kinds of triangulations to model the aperture. Figure 4.2(a) shows a triangulation with greater patch densities at the extremities of both major and minor axes than in the center of the aperture.

Figure 4.2(b) shows the other triangulation which has greater patch density only at the extremities of the major axis. In both figures, NA, NNODE, NEDGE, and NFACE are the numbers of unkowns, nodes, edges, and faces of the aperture, respectively. About the triangulations, there are two things to be noticed. First, to compensate for the loss in the total area, we should put the boundary nodes outside the aperture so that we get the correct total aperture area. Second, to take care of the edge effect, we need a higher patch density around the boundary than in the center. In Fig. 4.2, the boundary nodes are placed on the boundary of an ellipse that is 1.01044 times larger than the actual one. That is, $2l=1.01044\ L_a$. We compare our results from the two triangulations in Fig. 4.2 to illustrate the edge effect. Table 4.1 shows that the amplitudes of outward traveling TEM currents on the wire agree very well with those obtained by using the formula in [1]. It also shows that the results (NA=41) using the triangulation of Fig. 4.2(a) have better agreement than those (NA=17) using that of Fig. 4.2(b).

The second example is for an electrically small circular aperture of radius $r_A=0.01\lambda$, backed by an infinitely long wire of radius $r_B=0.001\lambda$. The wire is at $y=d=0.03\lambda$, 0.04λ, 0.05λ, or 0.06λ. The excitation is a plane wave with $H_x^{ioa}= -e^{-jkz}/\eta$ ampere/meter. Figure 4.3 shows the triangulation used for the circular aperture. There is a higher patch density around the boundary than in the center. In order to get the correct total aperture area, we use $r=1.0539r_A$ as the radius for the triangulation. Table 4.2 shows that the amplitudes of the outward traveling TEM currents agree very well with those obtained by using the formula in [1]. For examples 1 and 2, our results also

agree with those of the formulas in [2] and [3].

The third example is for a narrow slot which has length $L_a=0.5\lambda$ and width $W_a=0.05\lambda$ and is centered at (0,0,0). An infinitely long wire of radius $r_B=0.001\lambda$ is located at $y=d=0.1\lambda$. A plane wave is normally incident with $H_x^{ioa}=1$ ampere/meter. Figure 3.7 shows the triangulation used for the slot. Figures 4.4, 4.5, and 4.6, respectively, show that the total x-directed magnetic current M in the slot and the real and imaginary parts of the electric current on the wire agree very well with those in [4]. Figures 4.5 and 4.6 show that the evanescent current on the wire is concentrated in the region for which $|z|<0.25\lambda$. Beyond this region, the currents are two outward traveling TEM waves. Therefore, the choice of $L=2.0\lambda$ used in our calculation should be adequate.

Finally, we consider a circular aperture of radius $r_A=0.1\lambda$ backed by an infinitely long wire. The wire has radius $r_B=0.001\lambda$ and is located at $y=d=0.05\lambda$. The excitation is a plane wave with $H_x^{ioa}=-e^{-jkz}/\eta$ ampere/meter. We use the triangulation shown in Fig. 4.3 for the aperture, where $r=1.0539r_A$ is the radius in the patching. Figure 4.7 shows that the evanescent current on the wire drops to zero rapidly, and can be neglected beyond a small region of $z=-0.25\lambda$ to 0.25λ. Note that both the evanescent current and the outward traveling TEM currents are discontinuous at $z=0$. The total current is continuous everywhere along the wire. This implies that pulses must begin and end at $z=0$. The replacement of delta functions by pulse functions in Section 4.3 has assured continuity of the total current on the wire. Figure 4.8 shows the radial component of the

magnetic current per unit length V crossing a circle of radius 5/6 r_A in the aperture. When V is positive, the current flows away from the center of the aperture. When V is negative, the current flows toward the center. It is seen that V is antisymmetric about the z-axis (θ=0.). There is no available data to compare with for this example. In Figs. 4.7 and 4.8, $H_x^{ioa}(0)$ denotes H_x^{ioa} at z=0.

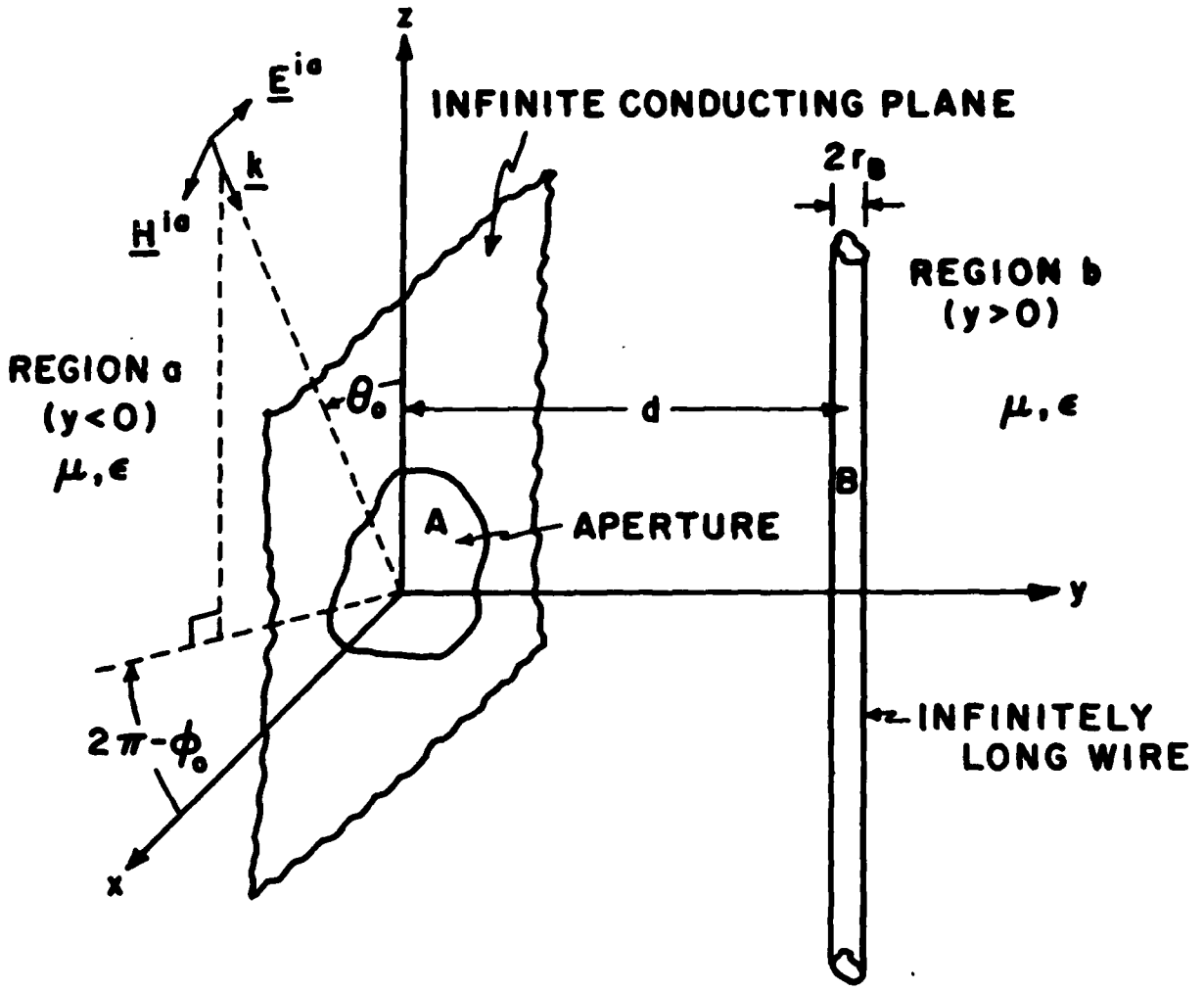

Fig. 4.1. An infinitely long wire behind an aperture.

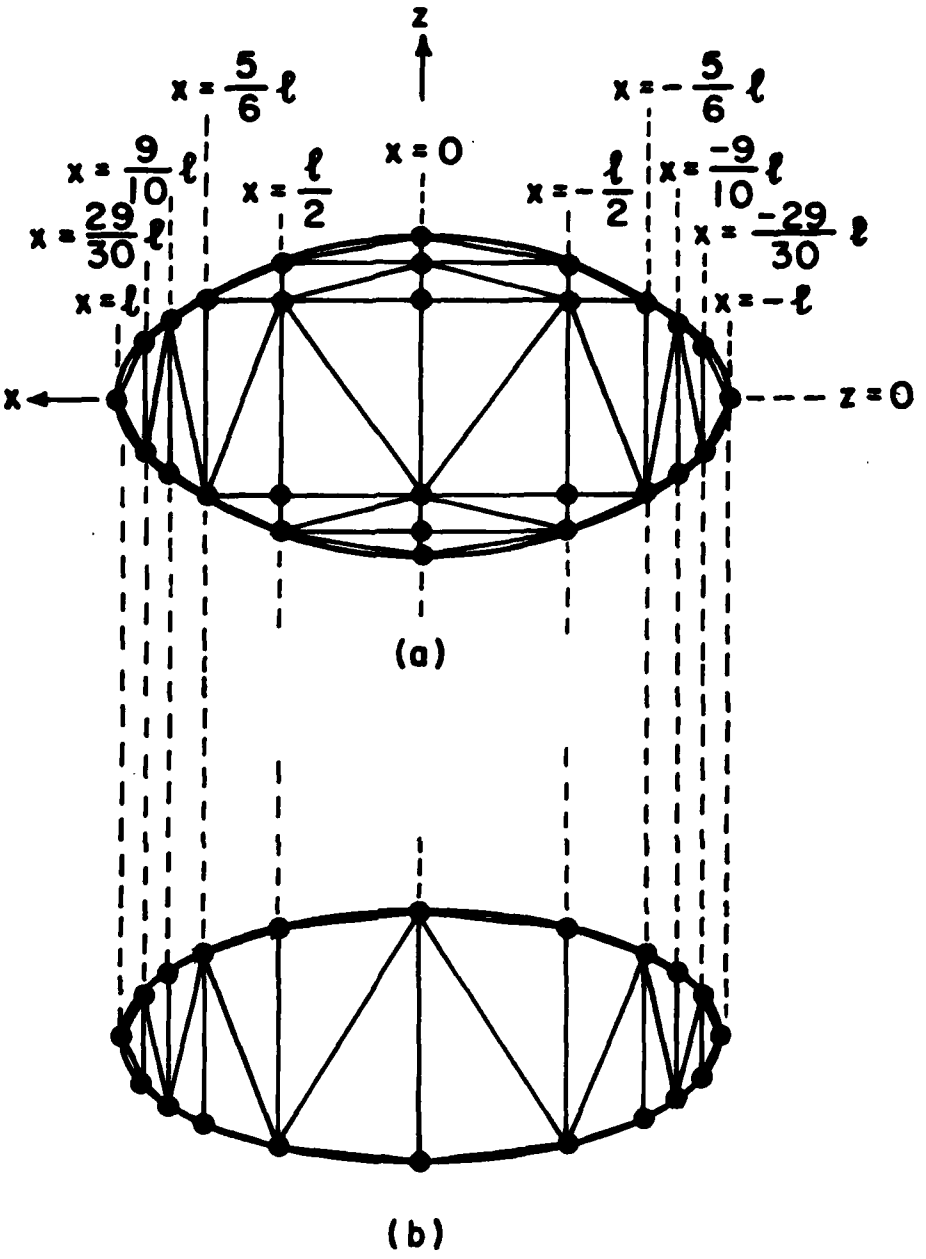

Fig. 4.2. Triangulations of an elliptical aperture. (a) NA=41, NNODE=28, NEDGE=61, and NFACE=34. (b) NA=17, NNODE=20, NEDGE=37, and NFACE=18.

Table 4.1. Amplitudes I_1 and I_{NB} of outward traveling TEM currents on an infinitely long wire passing by a small elliptical aperture. $L_a/\lambda=0.02$, $W_a/\lambda=0.002$, $r_B/\lambda=0.001$, and $H_x^{ioa}= -e^{-jkz}/\eta$ ampere/meter. (λ=1 meter)

d/λ	Our Solution					Solution of [1]*	
	NA	NB	L/λ	$I_1/10^{-7}$	$I_{NB}/10^{-7}$	$I_1/10^{-7}$	$I_{NB}/10^{-7}$
0.15	41	62	1.5	-0.0091-j0.1457	-0.0086-j0.1393	-j0.1554	-j0.1474
	17	62	1.5	-0.0086-j0.1391	-0.0087-j0.1391		
0.10	41	62	1.5	-0.0077-j0.2358	-0.0072-j0.2254	-j0.2509	-j0.2380
	17	62	1.5	-0.0072-j0.2251	-0.0072-j0.2251		
0.05	41	62	1.5	-0.0078-j0.5401	-0.0069-j0.5162	-j0.5763	-j0.5476
	17	62	1.5	-0.0072-j0.5153	-0.0072-j0.5153		

* Nearly the same as the solutions by the formulas in [2] and [3].

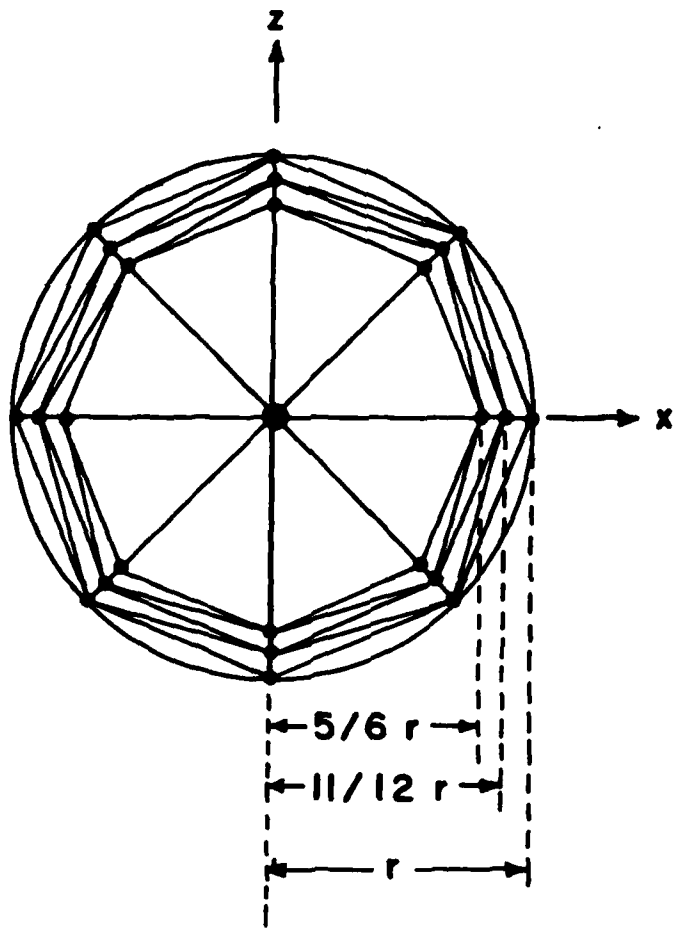

Fig. 4.3. Triangulation of a circular aperture. NA=56, NNODE=25, NEDGE=64, and NFACE=40.

Table 4.2. Amplitudes I_1 and I_{NB} of outward traveling TEM currents on an infinitely long wire passing by a small circular aperture. $r_A/\lambda=0.01$, $r_B/\lambda=0.001$, and $H_x^{ioa}= -e^{-jkz}/\eta$ ampere/meter. (λ=1 meter)

d/λ	Our Solution					Solution of [1]	
	NA	NB	L/λ	$I_1/10^{-6}$	$I_{NB}/10^{-6}$	$I_1/10^{-6}$	$I_{NB}/10^{-6}$
0.03	56	22	0.3	-0.0070-j0.4943	-0.0024-j0.1682	-j0.5427	-j0.1809
0.04	56	22	0.4	-0.0067-j0.3498	-0.0009-j0.1191	-j0.3803	-j0.1267
0.05	56	22	0.5	-0.0067-j0.2682	-0.0003-j0.0929	-j0.2895	-j0.0965
0.06	56	22	0.6	-0.0069-j0.2163	-0.0007-j0.0758	-j0.2321	-j0.0774

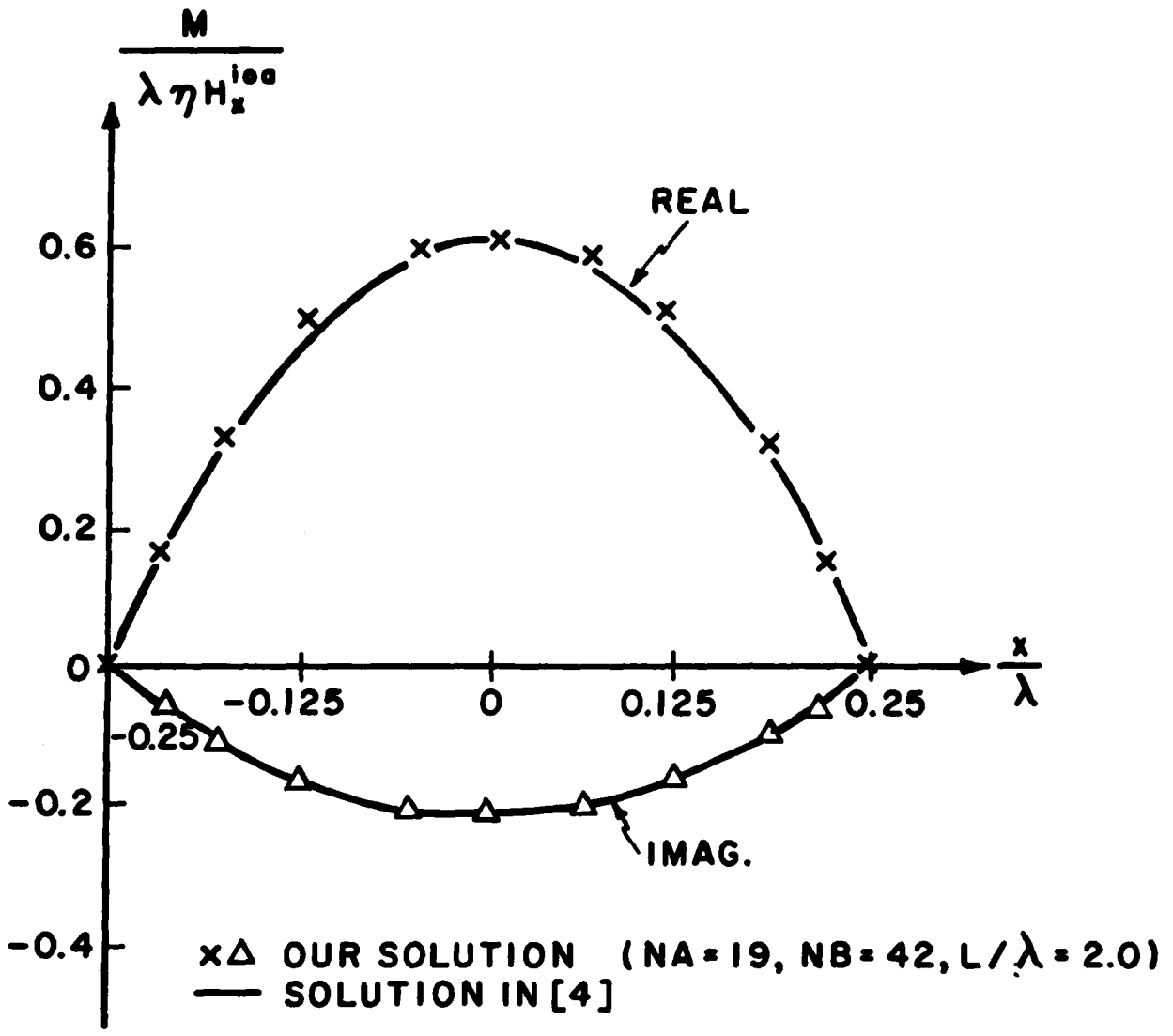

Fig. 4.4. The total x-directed magnetic current in a slot backed by an infinitely long wire for L_a/λ=0.5, W_a/λ=0.05, x_c=0., r_B/λ=0.001, d/λ=0.1, and normal plane wave incidence. (λ=1 meter)

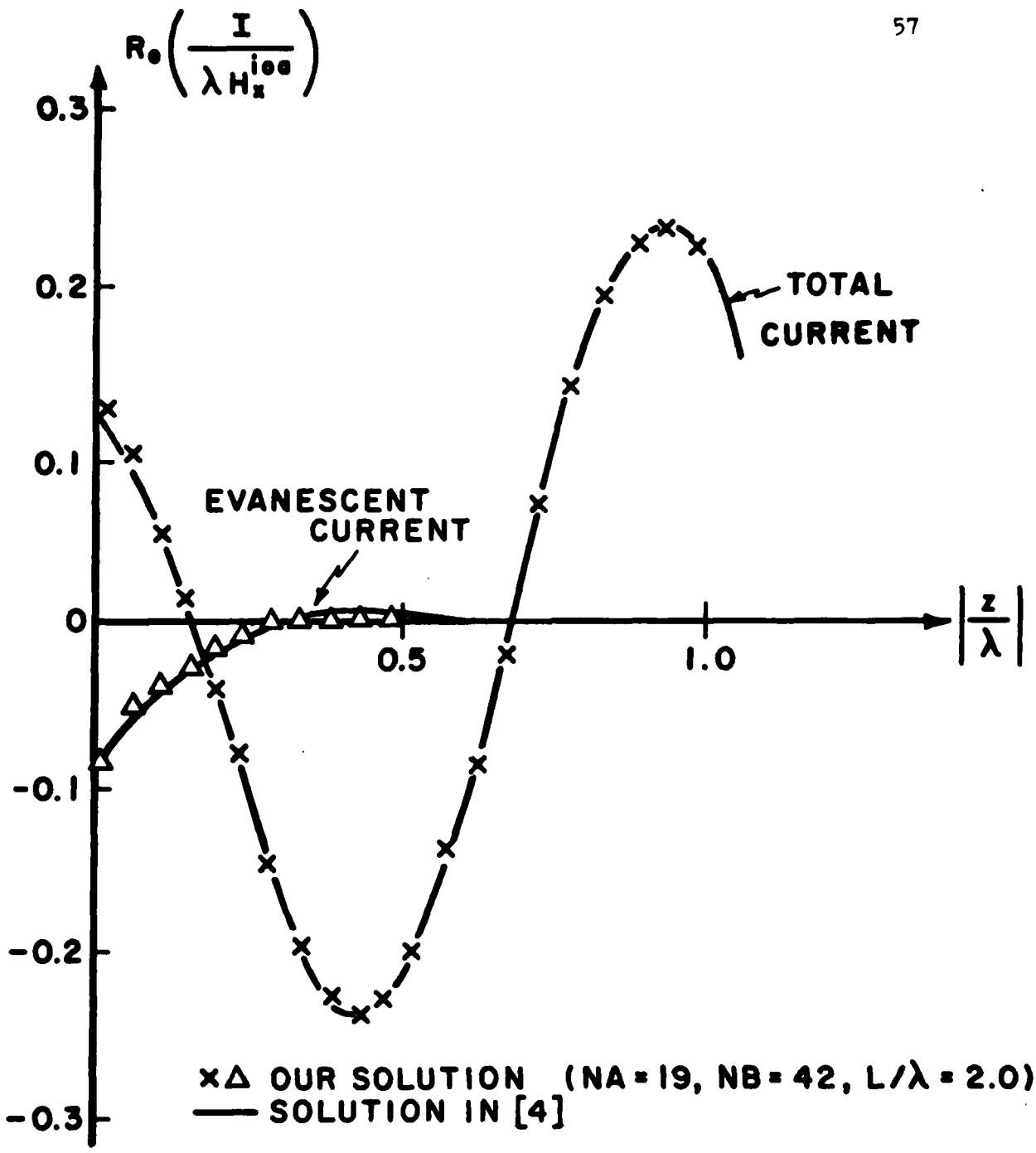

Fig. 4.5. The real part of the current on an infinitely long wire passing by a slot for L_a/λ=0.5, W_a/λ=0.05, x_c=0., r_B/λ=0.001, d/λ=0.1, and normal plane wave incidence. (λ=1 meter)

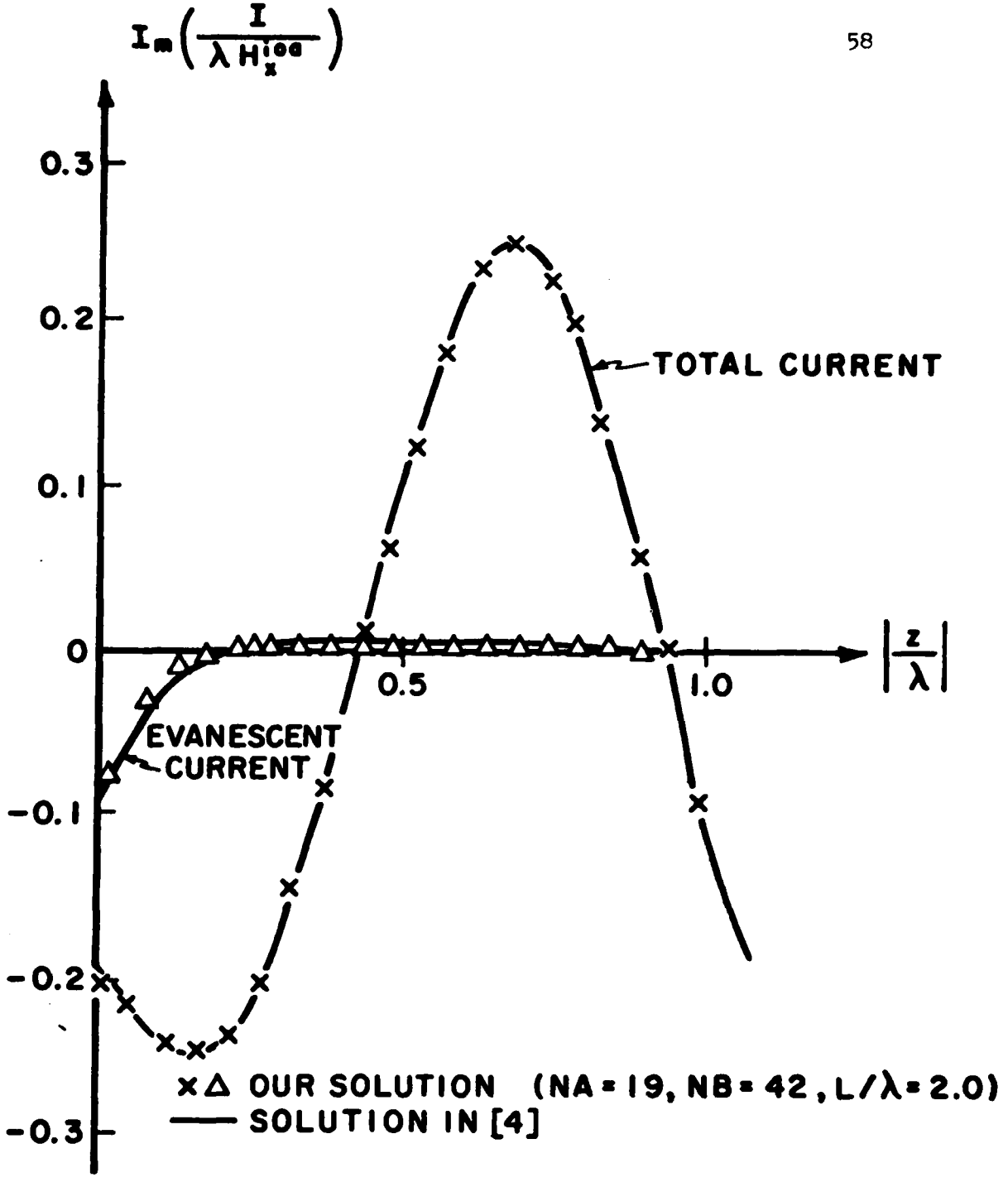

Fig. 4.6. The imaginary part of the current on an infinitely long wire passing by a slot for L_a/λ=0.5, W_a/λ=0.05, x_c=0., r_B/λ=0.001, d/λ=0.1, and normal plane wave incidence. (λ =1 meter)

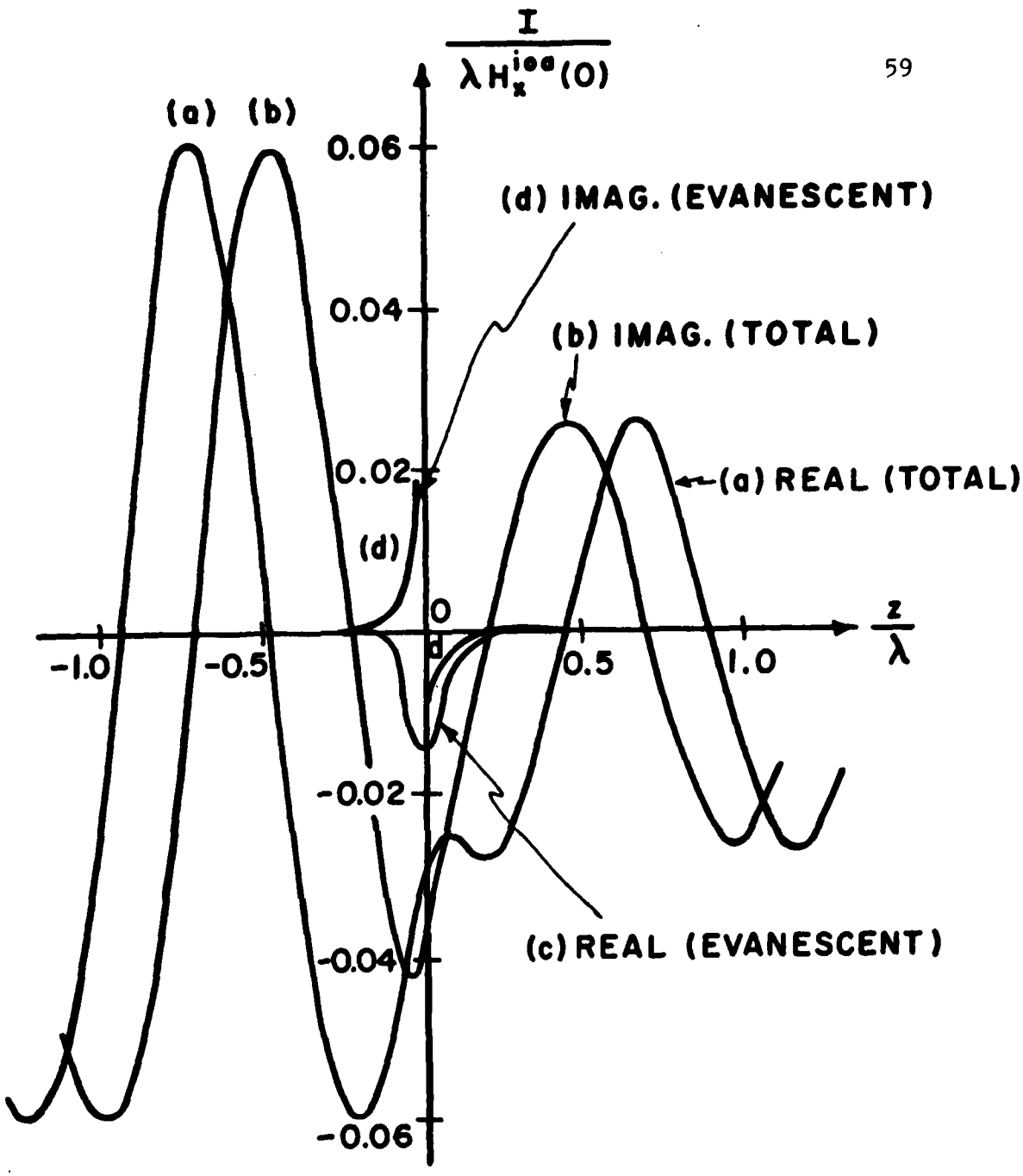

Fig. 4.7. The electric current on an infinitely long wire passing by a circular aperture with plane wave incidence. $r_A/\lambda=0.1$, $d/\lambda=0.05$, $r_B/\lambda=0.001$, and $H_x^{ioa}= -e^{-jkz}/\eta$ ampere/meter. (a) Real part of total current. (b) Imaginary part of total current. (c) Real part of evanescent current. (d) Imaginary part of evanescent current. (NA=56, NB=62, $L/\lambda=2.$, and $\lambda=1$ meter)

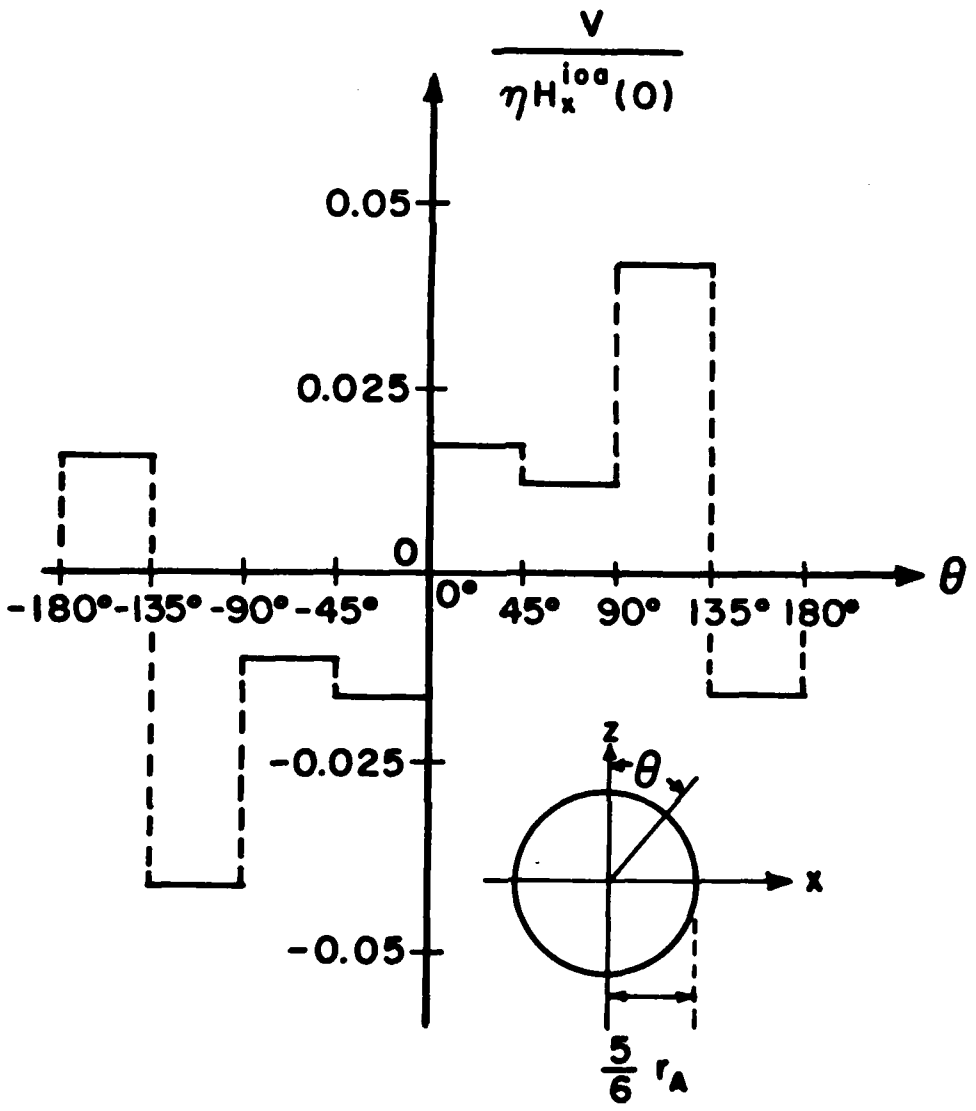

Fig. 4.8. The radial component of the magnetic current per unit length crossing a circle of radius 5/6 r_A in a circular aperture backed by an infinitely long wire with plane wave incidence. r_A/λ=0.1, d/λ=0.05, r_B/λ=0.001, and $H_x^{ioa} = -e^{-jkz}/\eta$ ampere/meter. (NA=56, NB=62, L/λ=2.0, and λ =1 meter)

Chapter 5

APPLICATION TO THE PROBLEM OF AN ARBITRARILY LOADED WIRE BEHIND AN APERTURE OF ARBITRARY SIZE AND SHAPE

5.1. Problem Specification

In this chapter, the problem is generalized to that of an arbitrarily loaded wire passing by an aperture with excitations coming from either one or both sides of the conducting plane. Figure 5.1 shows the geometric configuration of the problem to be considered. An aperture-perforated infinite conducting plane of zero thickness covers the entire x-z plane and separates regions a and b. In region a ($y < 0$), the plane wave defined in (3-1) is incident at an angle (θ_o, ϕ_o). In region b ($y > 0$), a z-directed thin wire of radius r_B is terminated by loads Z_{L1} and Z_{L2} at $z = -L_w/2$ and $L_w/2$, respectively, and is parallel to the conducting plane at a distance of d. There are TEM voltage sources V_1^i and V_2^i applied across both ends of the wire. The space is filled with a loss-free homogeneous medium of permeability μ and permittivity ϵ.

The generalization is to include the reflection effect caused by the terminations of the wire into the moment method solution developed in Chapter 4. The objective is to find the current distributions in the aperture and on the wire. We then evaluate the power transmitted through the aperture. In addition, an equivalent circuit of the aperture for the transmission line mode on the wire is obtained. The derivation of such an equivalent circuit is detailed in Appendix D. Utilizing the circuit and transmission line equations, currents and voltages of the TEM mode along an arbitrarily loaded wire can be calculated.

5.2. Solution Development

As in Chapter 4, the presence of the aperture excites two outward traveling TEM currents plus evanescent current on the wire. In addition, there are reflections of these currents due to the terminations of the wire. The wire is assumed long enough that the evanescent currents do not reach the terminations. Thus, the reflections can be represented by two pure TEM current waves. The situations at the terminations are shown in Fig. 5.2, where $(I_1 e^{jkz}\underline{u}_z, I_{NB} e^{-jkz}\underline{u}_z)$ and $(I^- e^{jkz}\underline{u}_z, I^+ e^{-jkz}\underline{u}_z)$ are the outward traveling TEM currents and the pure TEM currents, respectively, and the arrow denotes the direction of the propagation. The original problem in Fig. 5.1 is then equivalent to that in Fig. 5.3, where the loads and the voltage sources are replaced by the pure TEM currents $\underline{J}^+ = I^+ e^{-jkz}\underline{u}_z$ and $\underline{J}^- = I^- e^{jkz}\underline{u}_z$ traveling on an infinitely long wire.

Here, I^+ and I^- are related to the voltage sources, the loads, and the outward traveling TEM currents. The relationships are derived as follows.

Referring to Fig. 5.2, the voltages at the terminations are

$$Z_0(I^+e^{-jkz}-I^-e^{jkz}-I_1e^{jkz}) = V_1^i - Z_{L1}(I^+e^{-jkz}+I^-e^{jkz}+I_1e^{jkz}) \quad (5\text{-}1)$$

$$Z_0(I^+e^{-jkz}-I^-e^{jkz}+I_{NB}e^{-jkz}) = V_2^i + Z_{L2}(I^+e^{-jkz}+I^-e^{jkz}+I_{NB}e^{-jkz}) \quad (5\text{-}2)$$

where Z_0 is the characteristic impedance of the transmission line formed by the wire and the ground plane.

At z=0, (5-1) and (5-2) become

$$Z_0(I^+ - I^- - I_1) = V_1 - Z_1(I^+ + I^- + I_1) \quad (5\text{-}3)$$

$$Z_0(I^+ - I^- + I_{NB}) = V_2 + Z_2(I^+ + I^- + I_{NB}) \quad (5\text{-}4)$$

Here, V_1 and V_2 are V_1^i and V_2^i referred to z=0, respectively. Z_1 and Z_2 are the impedances Z_{L1} and Z_{L2} referred to z=0, respectively.

By solving (5-3) and (5-4) for I^+ and I^-, we obtain

$$I^+ = I_0^+ + C_1I_1 + C_2I_{NB} \quad (5\text{-}5)$$

$$I^- = I_0^- + C_2I_1 + C_3I_{NB} \quad (5\text{-}6)$$

where

$$I_0^+ = \frac{(1-\Gamma_1)V_1+\Gamma_1(1-\Gamma_2)V_2}{2Z_0(1-\Gamma_1\Gamma_2)} \tag{5-7}$$

$$I_0^- = \frac{-\Gamma_2(1-\Gamma_1)V_1-(1-\Gamma_2)V_2}{2Z_0(1-\Gamma_1\Gamma_2)} \tag{5-8}$$

$$C_1 = \frac{-\Gamma_1}{1-\Gamma_1\Gamma_2} \tag{5-9}$$

$$C_2 = \frac{\Gamma_1\Gamma_2}{1-\Gamma_1\Gamma_2} \tag{5-10}$$

$$C_3 = \frac{-\Gamma_2}{1-\Gamma_1\Gamma_2} \tag{5-11}$$

$$\Gamma_1 = \frac{Z_1-Z_0}{Z_1+Z_0} \tag{5-12}$$

$$\Gamma_2 = \frac{Z_2-Z_0}{Z_2+Z_0} \tag{5-13}$$

Γ_1 and Γ_2 are the reflection coefficients at $z=0^-$ and 0^+, respectively. Note, I^+ and I^- are infinite only when $Z_1=Z_2=\infty$ or $Z_1=-Z_2$. The first case ($Z_1=Z_2=\infty$) does not exist for the loaded wire. The second case ($Z_1=-Z_2$) occurs when the resistance of one of the loads is negative or the resistances of both loads are zero. However, usually the loads are passive and the sources are lossy. Thus, this case does not arise. Therefore, I^+ and I^- are finite .

By (5-5) and (5-6), we have

$$\underline{J}^{+} = \underline{J}_0^{+} + I_1\underline{J}_1^{+} + I_{NB}\underline{J}_{NB}^{+} \qquad |z| < \infty \tag{5-14}$$

$$\underline{J}^{-} = \underline{J}_0^{-} + I_1\underline{J}_1^{-} + I_{NB}\underline{J}_{NB}^{-} \qquad |z| < \infty \tag{5-15}$$

where

$$\underline{J}_0^{+} = I_0^{+}e^{-jkz}\underline{u}_z \qquad |z| < \infty \tag{5-16}$$

$$\underline{J}_1^{+} = C_1 e^{-jkz}\underline{u}_z \qquad |z| < \infty \tag{5-17}$$

$$\underline{J}_{NB}^{+} = C_2 e^{-jkz}\underline{u}_z \qquad |z| < \infty \tag{5-18}$$

$$\underline{J}_0^{-} = I_0^{-}e^{jkz}\underline{u}_z \qquad |z| < \infty \tag{5-19}$$

$$\underline{J}_1^{-} = C_2 e^{jkz}\underline{u}_z \qquad |z| < \infty \tag{5-20}$$

$$\underline{J}_{NB}^{-} = C_3 e^{jkz}\underline{u}_z \qquad |z| < \infty \tag{5-21}$$

We now consider the problem in Fig. 5.3. There are an equivalent magnetic current sheet $\underline{M}$ over the aperture, the pure TEM currents, and an induced electric current $\underline{J}$ on the wire due to $\underline{M}$. We can use the same expansion functions for $\underline{M}$ and $\underline{J}$ as those in Chapter 4. The formulations and matrices developed in Chapter 4 can also be utilized with some modifications.

We now apply the boundary conditions stated in Section 2.2 to the problem. The first condition that the tangential $\underline{E}$ is continuous at the aperture is assured by the magnetic current sheets $\underline{M}$ and $-\underline{M}$ over the two sides of the aperture region. Due to the additional pure TEM currents, the second condition, (2-9), becomes

$$-\underline{H}_t^a(\underline{M})-\underline{H}_t^b(\underline{M})+\underline{H}_t^b(\underline{J}+I_1\underline{J}_1^+ +I_1\underline{J}_1^- +I_{NB}\underline{J}_{NB}^+ +I_{NB}\underline{J}_{NB}^-) = \underline{H}_t^{ia}-\underline{H}_t^b(\underline{J}_0^+ +\underline{J}_0^-)$$

$$\text{on A} \qquad (5\text{-}22)$$

Here, $\underline{J}$ consists of two outward traveling TEM currents plus evanescent current. The condition (2-10) remains the same because the tangential $\underline{E}$ from a pure TEM current vanishes on the wire.

Therefore, the matrices $[Y^a+Y^b]$, $[Z]$, $[\hat{T}]$, $\vec{I}^{ia}$, and $\vec{V}^{ib}$ remain the same as those in Chapter 4 while $[T]$ and $\vec{I}^{ib}$ must be modified. Note that here $[T]$ is defined in (2-38) or (2-40) with $\underline{J}_1$ replaced by $\underline{J}_1+\underline{J}_1^+ +\underline{J}_1^-$ and $\underline{J}_{NB}$ by $\underline{J}_{NB}+\underline{J}_{NB}^+ +\underline{J}_{NB}^-$, and $\vec{I}^{ib}$ is defined as

$$I_m^{ib} = \langle \underline{M}_m, \underline{H}_t^b(\underline{J}_0^+ +\underline{J}_0^-)\rangle_A \qquad (5\text{-}23)$$

We now modify the $[T]$ matrix. By (2-40) and (5-22), the modified matrix is the sum of the $[T]$ due to $\underline{J}$ (same $[T]$ developed in Chapter 4) plus additional terms T_{m1}^a and $T_{m,NB}^a$ due to $\underline{J}_1^+$, $\underline{J}_1^-$, $\underline{J}_{NB}^+$, and $\underline{J}_{NB}^-$, for m=1,2,...,NA. The additional terms are

$$T_{m1}^a = \langle \underline{M}_m, \underline{H}_t(\underline{J}_1^+, \underline{J}_1^-, \underline{J'}_1^+, \underline{J'}_1^-)\rangle_A \qquad (5\text{-}24)$$

$$T^a_{m,NB} = \langle \underline{M}_m, \underline{H}_t(\underline{J}^+_{NB}, \underline{J}^-_{NB}, \underline{J}'^+_{NB}, \underline{J}'^-_{NB}) \rangle_A \tag{5-25}$$

where $\underline{J}'^{\pm}_1$ and $\underline{J}'^{\pm}_{NB}$ are the images of $\underline{J}^{\pm}_1$ and $\underline{J}^{\pm}_{NB}$, respectively.

By [4, Eqs. (80), (83)] and (3-29), the tangential magnetic field in the aperture due to a pure TEM current $e^{\pm jkz}\underline{u}_z$ on the wire is

$$\underline{H}^{\pm}_0 = \frac{de^{\pm jkz}}{2\pi(x^2+d^2)}\underline{u}_x \tag{5-26}$$

By (5-17), (5-18), (5-20), (5-21), and (5-26), we have

$$\underline{H}_t(\underline{J}^+_1, \underline{J}^-_1, \underline{J}'^+_1, \underline{J}'^-_1) = 2(C_1\underline{H}^-_0 + C_2\underline{H}^+_0) \tag{5-27}$$

$$\underline{H}_t(\underline{J}^+_{NB}, \underline{J}^-_{NB}, \underline{J}'^+_{NB}, \underline{J}'^-_{NB}) = 2(C_2\underline{H}^-_0 + C_3\underline{H}^+_0) \tag{5-28}$$

Substitution of (3-4), (5-27), and (5-28) into (5-24) and (5-25) gives

$$T^a_{m1} = C_1T^-_m + C_2T^+_m \qquad m = 1, 2, \ldots, NA \tag{5-29}$$

$$T^a_{m,NB} = C_2T^-_m + C_3T^+_m \qquad m=1,2,\ldots, NA \tag{5-30}$$

where

$$T^{\pm}_m = \frac{dl_m}{2\pi}\left[\frac{\hat{x}^{c+}_m e^{\pm jkz^{c+}_m}}{(x^{c+}_m)^2+d^2} + \frac{\hat{x}^{c-}_m e^{\pm jkz^{c-}_m}}{(x^{c-}_m)^2+d^2}\right] \tag{5-31}$$

$\hat{x}^{c\pm}_m$, $x^{c\pm}_m$ and $z^{c\pm}_m$ are defined in (3-30) and (3-32).

By (3-4), (5-16), (5-19), and (5-23), the mth element of the source vector $\vec{I}^{ib}$ due to $\underline{J}_0^+$ and $\underline{J}_0^-$ is

$$I_m^{ib} = I_0^+ T_m^- + I_0^- T_m^+ \qquad m=1,2,\ldots,NA \tag{5-32}$$

The evaluation of the matrices is now complete. By solving (2-14) and (2-15) with the matrices evaluated above, the currents in the aperture and on the loaded wire can be obtained.

The total current on the wire is

$$\underline{J}^t = \underline{J} + \underline{J}^+ + \underline{J}^- \tag{5-33}$$

Thus, the total TEM currents at $z=0^-$ and 0^+ are

$$I_{TEM}^- = (1+C_1+C_2)I_1 + (C_2+C_3)I_{NB} + I_0^+ + I_0^- \tag{5-34}$$

$$I_{TEM}^+ = (C_1+C_2)I_1 + (1+C_2+C_3)I_{NB} + I_0^+ + I_0^- \tag{5-35}$$

It is noteworthy to verify that the problem considered in Chapter 4 is a special case here. The infinitely long wire considered in Chapter 4 is equivalent to a loaded wire with $Z_1=Z_2=Z_0$ and $V_1=V_2=0$. Thus, (5-5) - (5-13) give $I^+=I^-=0$. The current on the wire is then reduced to that of Chapter 4.

Finally, for a loaded wire whose length is very short, the solution developed here may not apply. For this case, the method of Chapter 3 can be utilized. However, the pulse functions on the wire must be extended to the terminations. In addition, the impedance matrix [Z] must be modified by adding a diagonal matrix with loads as its diagonal elements corresponding to the terminations.

5.3. Power Transmitted through the Aperture

In this section, we derive the power transmitted through the aperture into region a of Fig. 5.1 when the excitation is incident from region b.

By [7, Eq.(1-57)], the complex power transmitted through the aperture into region a is

$$P_f^a = -\iint_A (\underline{E}^a \times \underline{H}^{a*}) \cdot \underline{u}_y \, dS$$

$$= -\iint_A (\underline{u}_y \times \underline{E}^a) \cdot \underline{H}^{a*} \, dS$$

$$= -\iint_A \underline{M} \cdot \underline{H}^{a*}(\underline{M}) dS$$

$$= -\sum_{m=1}^{NA} \sum_{n=1}^{NA} V_m V_n^* \iint_A \underline{M}_m \cdot \underline{H}^{a*}(\underline{M}_n) dS$$

$$= \sum_{m=1}^{NA} \sum_{n=1}^{NA} V_m V_n^* Y_{mn}^{a*}$$

$$= \tilde{\vec{V}}[Y^a]^{*}\vec{V}^{*} \qquad (5\text{-}36)$$

where " * " denotes complex conjugate. In (5-36), the vector identity $(\underline{A}x\underline{B})\cdot\underline{C} = (\underline{C}x\underline{A})\cdot\underline{B}$, (2-1) with $\underline{n}=\underline{u}_y$, (2-11), and (2-16) are used. The time-average power P_t transmitted through the aperture is given by the real part of P_f^a.

5.4. Evaluation of an Equivalent Circuit

In this section, an equivalent circuit at z=0 of the aperture for the transmission line mode on the wire is presented. For simplicity, a plane wave incident from region a of Fig. 5.1 is the only excitation. Using this circuit, we can obtain the TEM currents and voltages on the wire.

The derivation of the equivalent circuit is detailed in Appendix D. In Appendix D, the solution for the current on a wire with matched loads (or infinitely long wire) is utilized to evaluate the impedances and sources of the circuit. We therefore consider the wire as infinitely long.

The general T network is shown in Fig. D.5. The impedances Z_1^e, Z_2^e, and Z_3^e defined in (D-21) - (D-23) depend on Z_0, $\hat{I}_1$, $\hat{I}_{NB}$, $\hat{\hat{I}}_1$, and $\hat{\hat{I}}_{NB}$. Here, $(\hat{I}_1,\hat{I}_{NB})$ and $(\hat{\hat{I}}_1,\hat{\hat{I}}_{NB})$ are the amplitudes of outward traveling TEM currents in the -z and the +z directions on the wire when the original incidence is replaced by TEM current excitations $e^{-jkz}\underline{u}_z$ and $e^{jkz}\underline{u}_z$ applied to the wire, respectively. The sources V_1^e

and V_2^e in (D-24) and (D-25) depend on Z_0, Z_1^e, Z_2^e, Z_3^e, I_1, and I_{NB}. I_1 and I_{NB} are the amplitudes of outward traveling TEM currents in the -z and the +z directions on the wire, respectively, when the excitation is the original incident field.

If the aperture is symmetric about z=0 or is small, the network in Fig. D.7 is used. The impedances Z_1^s and Z_2^s and sources V_1^s and V_2^s defined in (D-28) - (D-31) depend on Z_0, $\hat{I}_1$, $\hat{I}_{NB}$, I_1, and I_{NB}.

If the aperture induces symmetric outward traveling TEM currents on the wire, the network in Fig. D.8 with impedance Z^e in (D-32) and source V^e in (D-33) is utilized. The network depends on Z_0, $\hat{I}_1$, and I_1.

If the aperture induces antisymmetric outward traveling TEM currents on the wire, the network in Fig. D.9 with impedance Z^a in (D-34) and source V^a in (D-35) is used. The network depends on Z_0, $\hat{I}_1$, and I_1.

To obtain the network, we first calculate the amplitudes of the outward traveling TEM currents as follows.

To calculate $(\hat{I}_1,\hat{I}_{NB})$, $(\hat{\hat{I}}_1,\hat{\hat{I}}_{NB})$, and (I_1,I_{NB}), we solve (2-14) and (2-15) with the matrices $[Y^a+Y^b]$, $[Z]$, $[T]$, and $[\hat{T}]$ evaluated in Chapter 4 and with $\vec{V}^{ib}=0$ for the current on the wire. For $(\hat{I}_1,\hat{I}_{NB})$, the source vectors $\vec{I}^{ia}=0$ and $\vec{I}^{ib}$ defined in (5-32) with $I_0^+=1$ and $I_0^-=0$ are used. For $(\hat{\hat{I}}_1,\hat{\hat{I}}_{NB})$, $\vec{I}^{ia}=0$ and $\vec{I}^{ib}$ defined in (5-32) with $I_0^+=0$ and

$I_0^-=1$ are used. For (I_1, I_{NB}), $\vec{I}^{ia}$ defined in (3-35) and $\vec{I}^{ib}=0$ are used.

Next, we substitute these amplitudes and Z_0 into the expressions for the sources and impedances of the network.

5.5. Numerical Results

Numerical results for the current distributions in the aperture and on the wire are presented in this section. Numerical results for the power transmitted through the aperture are also given here. In addition, we calculate the impedances and sources of the equivalent circuit. The TEM current on the wire is then computed from this circuit and compared with that obtained from the solution of Section 5.2.

The first example is for a slot of width $W_a=0.05\lambda$ and length L_a varying from 0.2λ to 1.0λ. A matched wire of radius $r_B=0.001\lambda$ is located at $y=d=0.1\lambda$. A TEM voltage excitation with $V_1=2Z_0$ volts and $V_2=0$ is applied on the wire. Figure 5.4 shows that our solution for the time-average power transmitted through the slot agrees very well with that in [6]. It is seen that the maximum of the power occurs when the length of the slot is about 0.46λ, which is its resonant length.

Next, we consider a slot of length $L_a=0.5\lambda$ and width $W_a=0.05\lambda$ backed by a wire of radius $r_B=0.001\lambda$. The wire is located at various positions from $y=d=0.1\lambda$ to 0.4λ. A plane wave is normally incident from region a of Fig. 5.1. Figure 3.7 with $x_c=0.$ is used for the triangulation of the slot. Figures 5.5 and 5.6 show the source and impedance of the equivalent circuit (in Fig. D.8) of the transmission line mode on the wire. Our solution agrees very well with that in [4]. From this circuit, we can also calculate the TEM current at z=0 on the wire, by terminating the two ports of the circuit with Z_1 and Z_2. This is shown in Fig. 5.7. The TEM current at z=0 is equal to the loop current I in Fig. 5.7. Table 5.1 gives the results for $d=0.1\lambda$ and various loads. It shows that the results are (almost) identical to those obtained by the solution in Section 5.2. They also agree well with those in [6]. In addition, the results of the last three cases show that the total TEM current at z=0 is unchanged if the sum of loads Z_1 and Z_2 remains unchanged.

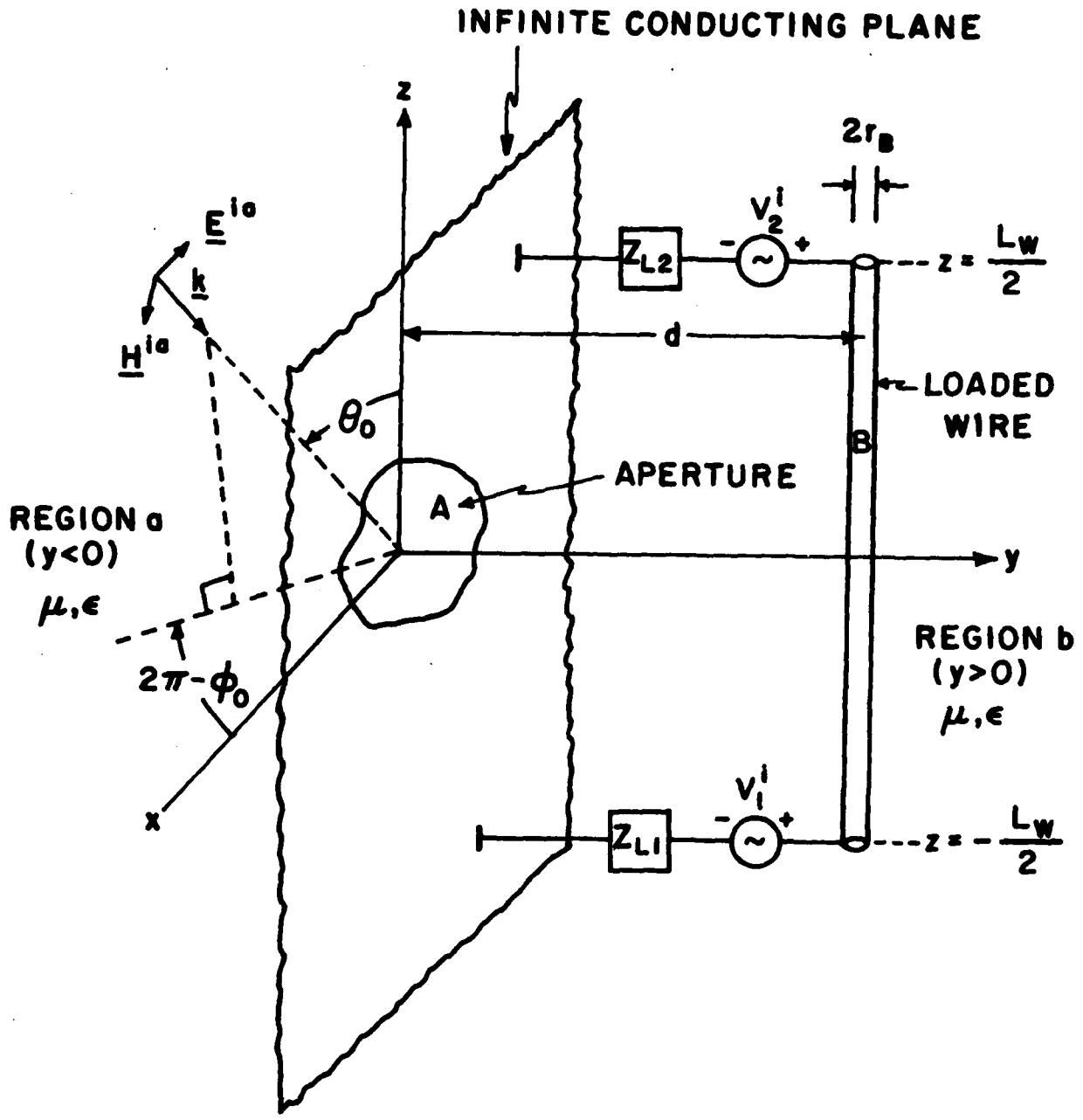

Fig. 5.1. A loaded wire passing by an aperture.

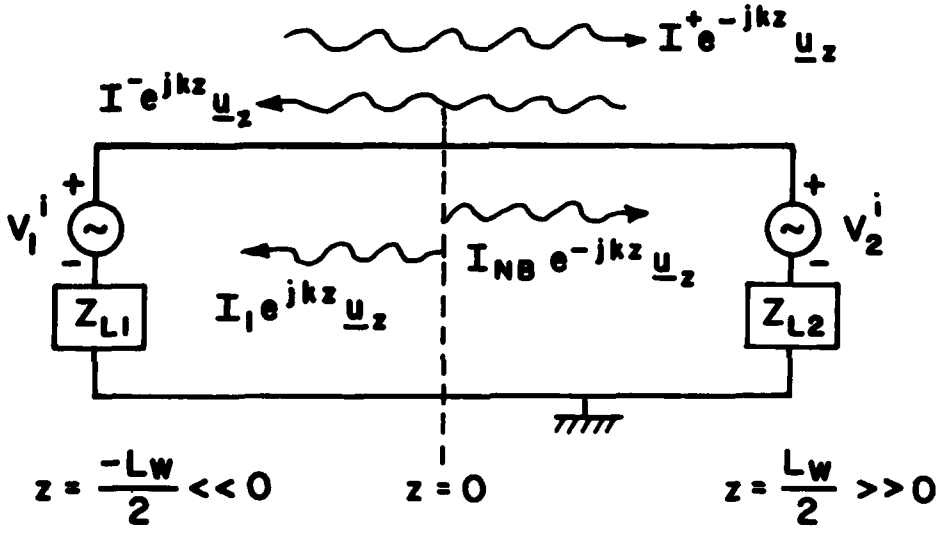

Fig. 5.2. A circuit for the terminations of the wire.

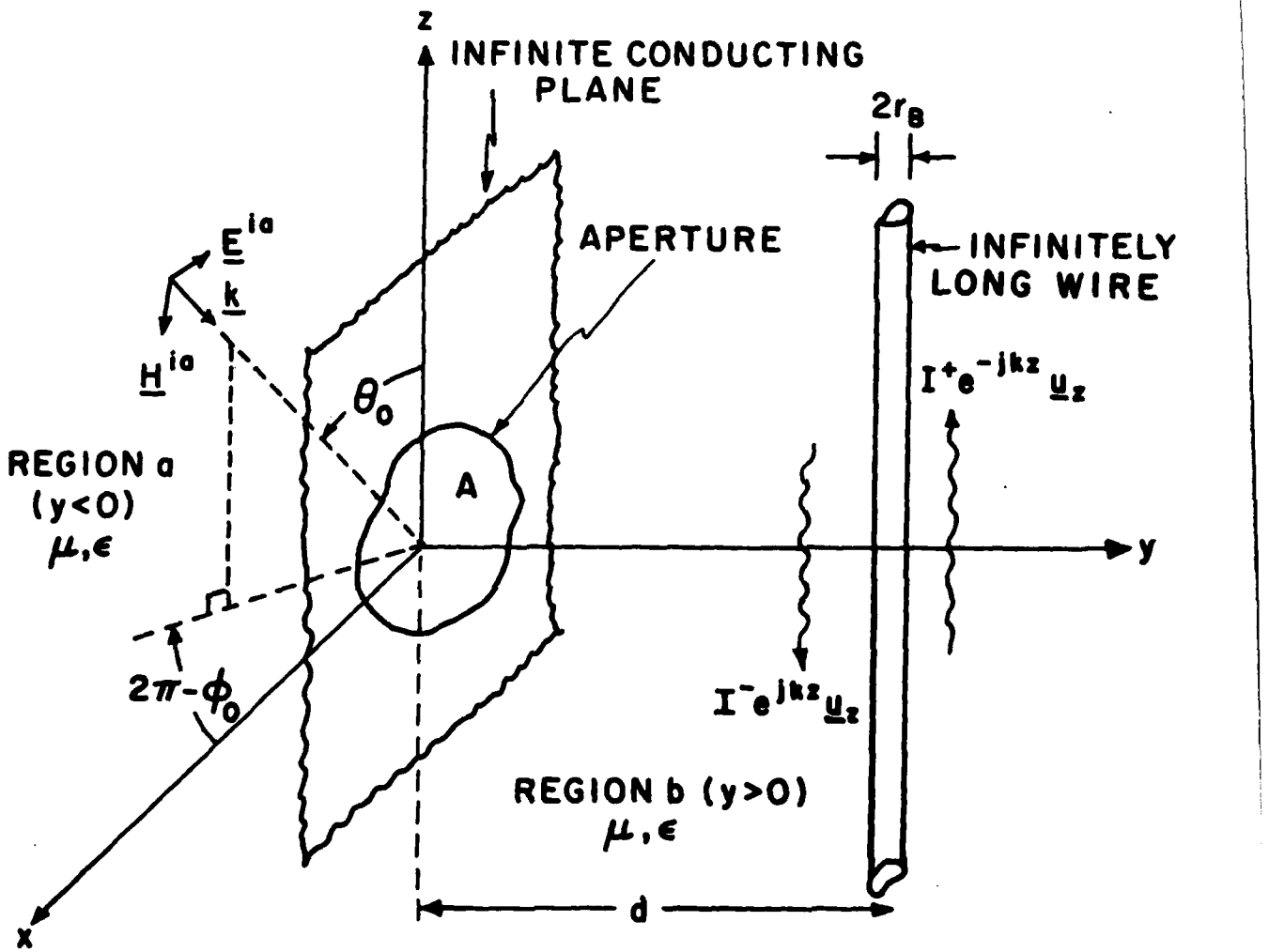

Fig. 5.3. The equivalence of the problem in Fig. 5.1. Arrows denote the propagation directions.

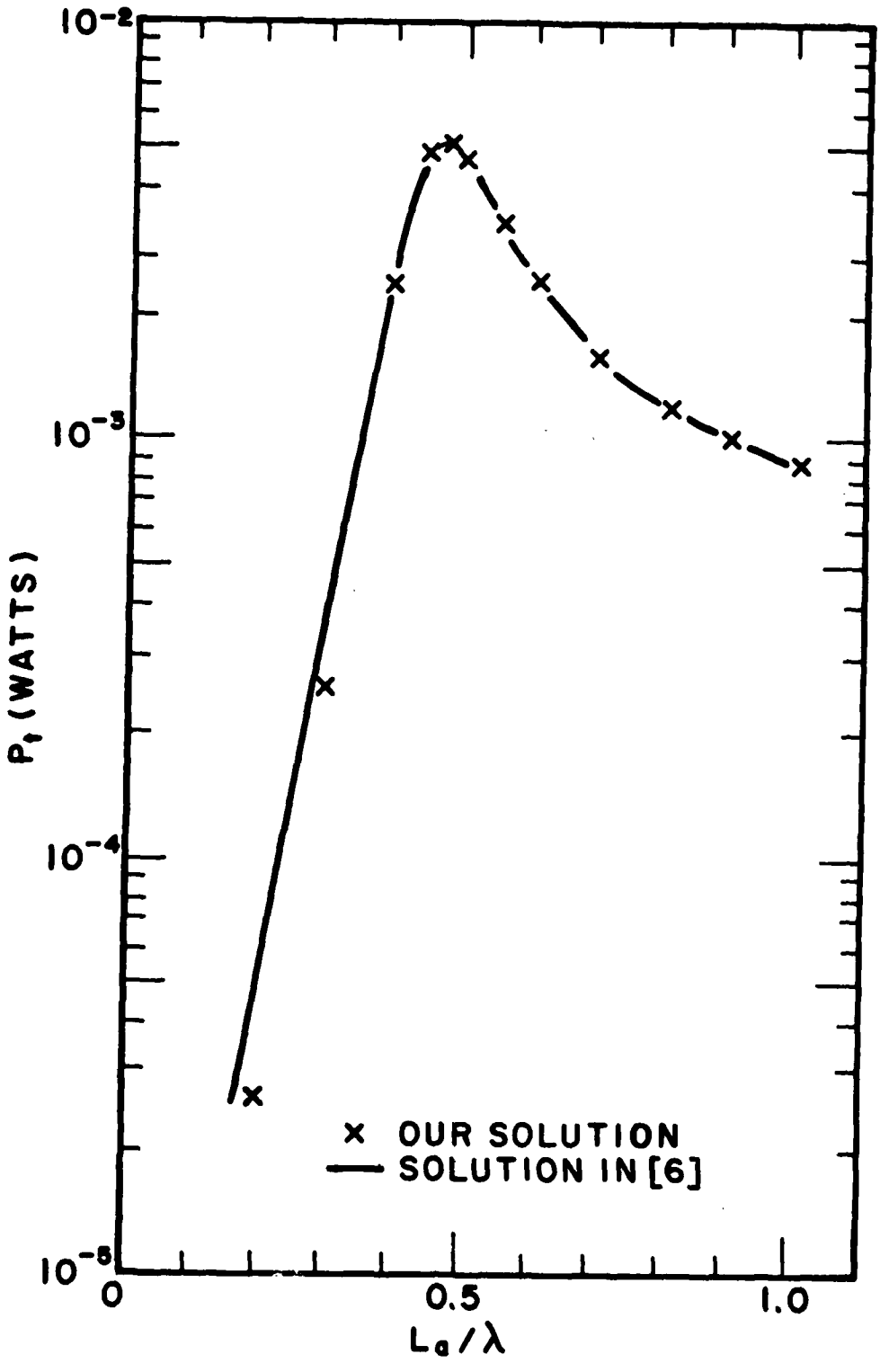

Fig.5.4. The time-average power transmitted through a slot backed by a loaded wire with a TEM voltage applied on the wire. W_a/λ=0.05, r_B/λ=0.001, d/λ=0.1, $V_1=2Z_0$, and V_2=0. (λ=1 meter)

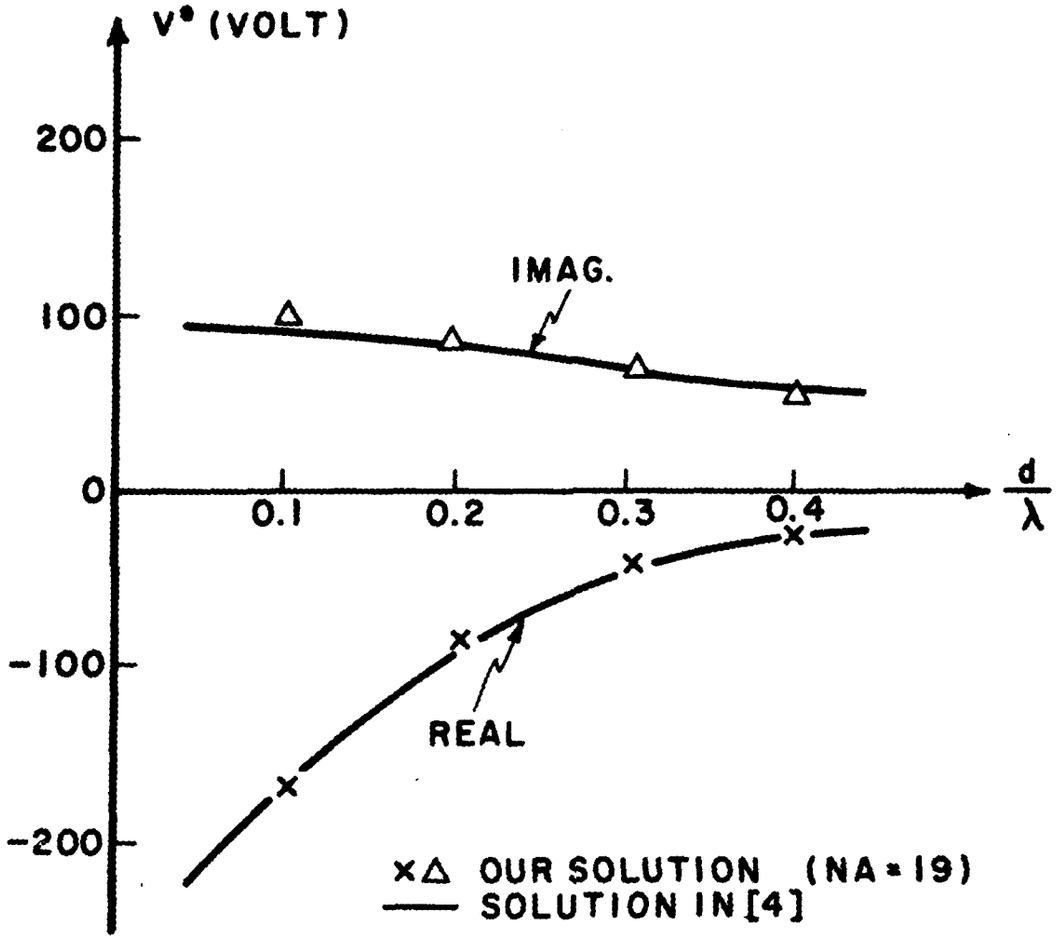

Fig. 5.5. Equivalent source for the TEM mode at z=0 on an arbitrarily loaded wire passing by a slot with normal plane wave incidence. $L_a/\lambda = 0.5$, $W_a/\lambda = 0.05$, $r_B/\lambda = 0.001$, and $H_x^{ioa} = 1$ ampere/meter. (λ=1 meter)

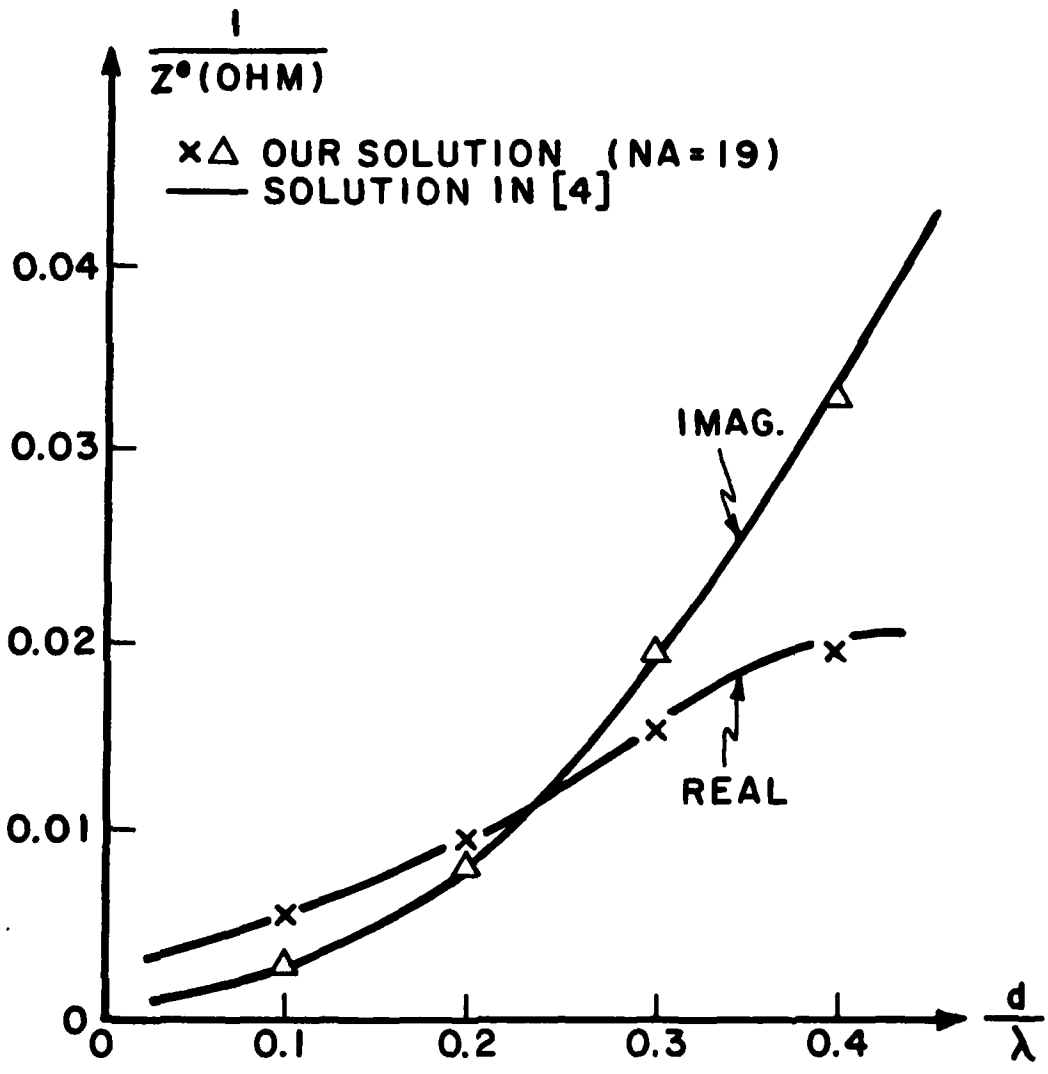

Fig. 5.6. Equivalent impedance for the TEM mode at z=0 on an arbitrarily loaded wire passing by a slot with normal plane wave incidence. $L_a/\lambda=0.5$, $W_a/\lambda=0.05$, $r_B/\lambda=0.001$, and $H_x^{ioa}=1$ ampere/meter. ($\lambda=1$ meter)

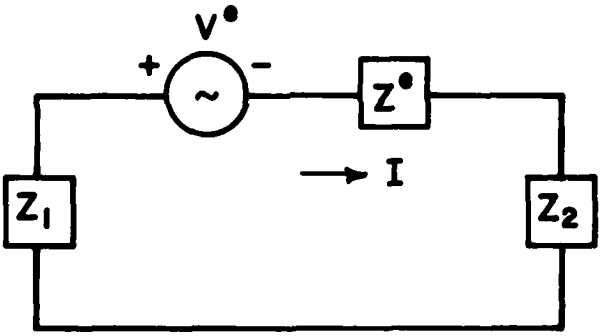

Fig. 5.7. The circuit used to calculate the TEM current at z=0 on a wire terminated with loads Z_1 and Z_2 and passing by a slot.

Table 5.1. Total TEM current at z=0 on a loaded wire passing by a slot with normal plane wave incidence. $L_a/\lambda = 0.5$, $W_a/\lambda = 0.05$, $d/\lambda = 0.1$, $r_B/\lambda = 0.001$, and $H_x^{ioa} = 1$ ampere/meter. ($\lambda = 1$ meter, NA=19, NB=62, and $L_w/\lambda = 1.5$)

Reflections		Solution of (5-34) or (5-35)	Calculated from Fig. 5.7	Solution in [6]
Γ_1	Γ_2			
0.1	0	0.2191-j0.0792	0.2192-j0.0792	0.2062-j0.0861
1.0	0	0	0	0
0.9	0	0.0287-j0.0129	0.0287-j0.0129	0.0264-j0.0136
0.8182	0.8182	0.0287-j0.0129	0.0287-j0.0129	0.0264-j0.0136
0.8750	0.6667	0.0287-j0.0129	0.0287-j0.0129	0.0264-j0.0136

Chapter 6

CONCLUSION

A moment method solution for the problem of electromagnetic coupling between an aperture and a conducting body is developed. Both the aperture and the conducting body are arbitrarily sized and shaped. This method is then implemented in specific cases whereby the conducting body is a wire. The wire is finite-length unloaded, infinitely long, or arbitrarily loaded. The aperture is modeled by triangular patches, which can conform closely to any geometry and permit greater patch densities on those portions where more resolution is desired. Local position vectors are used as the expansion functions in the aperture. There are two outward traveling TEM currents and evanescent current on the infinitely long wire. The evanescent current is found to exist in a small finite region near the aperture. Numerical results show very good agreement with available data in the literature.

Further work is recommended for more general problems as follows. First, consider the problem of a set of arbitrary apertures with a set of parallel wires. Each wire can be finite-length unloaded, infinitely long, or arbitrarily loaded and can be in different media. One can use the same expansion functions as those developed in this

work for each aperture and each wire. The matrices in (2-14) and (2-15) must be modified to include the coupling among apertures and wires. In addition, different permeabilities and permittivities must be included in the matrices. By solving (2-14) and (2-15), the currents in the apertures and on the wires can be obtained.

The problem of a set of arbitrary apertures with a set of arbitrary conducting bodies can also be done. To solve this problem, one can use the formulation developed in Chapter 2 and the matrix equations (2-14) and (2-15). Triangular patching is recommended to model apertures and conducting bodies. Local position vectors can be used as expansion functions . The work may be complicated, but it can be done without too much difficulty.

APPENDIX A

SURFACE INTEGRATIONS FOR FIELD PROBLEM

In this appendix, we evaluate the following surface integrals:

$$I \triangleq \int_{\eta=0}^{1} \int_{\xi=0}^{1-\eta} \frac{e^{-jkR}}{R} d\xi d\eta \tag{A-1}$$

$$I_\xi \triangleq \int_{\eta=0}^{1} \int_{\xi=0}^{1-\eta} \xi \frac{e^{-jkR}}{R} d\xi d\eta \tag{A-2}$$

$$I_\eta \triangleq \int_{\eta=0}^{1} \int_{\xi=0}^{1-\eta} \eta \frac{e^{-jkR}}{R} d\xi d\eta \tag{A-3}$$

Here, $R=|\underline{r}-\underline{r}'|$ is the distance between a source point at $\underline{r}'$ in triangle T and an observation point at $\underline{r}$. The area coordinates of triangle T are ξ and η defined in (3-11) and (3-12).

To avoid the singularity of these integrals at $\underline{r}=\underline{r}'$, we rewrite (A-1) - (A-3) as

$$I = \int_{\eta=0}^{1} \int_{\xi=0}^{1-\eta} \frac{e^{-jkR}-1}{R} d\xi d\eta + \int_{\eta=0}^{1} \int_{\xi=0}^{1-\eta} \frac{1}{R} d\xi d\eta \tag{A-4}$$

$$I_\xi = \int_{\eta=0}^{1} \int_{\xi=0}^{1-\eta} \xi \frac{e^{-jkR}-1}{R} d\xi d\eta + \int_{\eta=0}^{1} \int_{\xi=0}^{1-\eta} \frac{\xi}{R} d\xi d\eta \qquad \text{(A-5)}$$

$$I_\eta = \int_{\eta=0}^{1} \int_{\xi=0}^{1-\eta} \eta \frac{e^{-jkR}-1}{R} d\xi d\eta + \int_{\eta=0}^{1} \int_{\xi=0}^{1-\eta} \frac{\eta}{R} d\xi d\eta \qquad \text{(A-6)}$$

The first terms of (A-4) - (A-6) can be approximated by using a seven-point Gaussian quadrature formula developed for a triangular region [16]. The formula is

$$\int_{\eta=0}^{1} \int_{\xi=0}^{1-\eta} g(\underline{r},\xi,\eta) d\xi d\eta \simeq \sum_{i=1}^{7} w_i a_i g(\underline{r},\xi_i,\eta_i) \qquad \text{(A-7)}$$

Here, g is the integrand, (ξ_i, η_i) is a point in triangle T, w_i is the weight, and a_i is the coefficient. They are

$$\begin{cases} w_i = 0.5 & i=1,2,\ldots,7 \\ a_1 = 0.225 \\ a_2 = a_3 = a_4 = 0.1323942 \\ a_5 = a_6 = a_7 = 0.1259392 \\ \xi_1 = \eta_1 = 0.333333 \\ \xi_2 = \eta_3 = 0.0597\,1587 \end{cases} \qquad \text{(A-8)}$$

$$\xi_3=\xi_4=\eta_2=\eta_4=0.47014206$$

$$\xi_5=\eta_6=0.7974269$$

$$\xi_6=\xi_7=\eta_5=\eta_7=0.1012865$$

To evaluate the second terms of (A-4) - (A-6), we first introduce some vectors and variables as shown in Fig. A.1. O denotes the origin of the global coordinates. $\underline{\rho}$ is the projection of $\underline{r}'-\underline{r}$ onto the plane of the triangle T. The distance between the observation point and the plane of the triangle T is d. The contour along the boundary of T is defined as C, which is the sum of three straight lines C_1, C_2, and C_3 along the edges of the triangle. $\underline{u}_1$, $\underline{u}_2$, and $\underline{u}_3$ are the outward unit vectors normal to each edge. Point P denotes the projection of the observation point onto T. For edge i (i=1,2,3), $\underline{\rho}_i$ and $\underline{\rho}_{oi}$ are the vectors from point P to a point on C_i and to the projection of the observation point onto line C_i, respectively. The unit vectors of $\underline{\rho}_i$ and $\underline{\rho}_{oi}$ are $\underline{u}_{\rho i}$ and $\underline{u}_{\rho oi}$. Point Q denotes the projection of point O onto line C_i. Variable l_i is the length measured from point Q to a point on C_i and is in the direction of a unit vector $\underline{u}_{li}$. This unit vector is in the direction of the boundary contour of triangle T along edge C_i. The end points of C_i and the projection of the observation point onto C_i are at $l_i=l_i^-$, l_i^+, and l_{oi}, respectively.

We now evaluate the second term of (A-4), which can be written by using (3-16) as

$$I_1 = \frac{1}{2A_o} \iint_T \frac{dS'}{|\underline{r}-\underline{r}'|} \qquad \text{(A-9)}$$

where A_o is the area of the triangle T. (A-9) has been evaluated in [17] and is summarized as follows.

We use the surface divergence theorem [18]

$$\iint_S \nabla_s \cdot \underline{f} dS = \oint_C \underline{f} \cdot \underline{u} dl \tag{A-10}$$

to transform the integral in (A-9) into a line integral. In (A-10), S is the area of integration, C the boundary, and $\underline{u}$ the unit outward vector normal to C. It is found that a function

$$\underline{f}(\rho) = \frac{|\underline{r}-\underline{r}'|}{\rho} \underline{u}_\rho \tag{A-11}$$

satisfies

$$\nabla'_s \cdot \underline{f}(\rho) = \frac{1}{|\underline{r}-\underline{r}'|} \tag{A-12}$$

where $\underline{u}_\rho$ is the unit vector in the ρ direction, and ∇'_s is the surface divergence with respect to the coordinates of $\underline{r}'$.

By (A-11) and (A-12), we can evaluate (A-9) using the formula in (A-10). However, note that application of (A-10) requires the continuous differentiability of the integrand on the domain of integration, S. This is not the case when P is in S or on C. Therefore, a region T_ε, defined as the intersection with T of an infinitesimal sphere with radius ε centered at P, is isolated for separate treatment. The boundary of T_ε is defined as C_ε, and $\alpha(\underline{r})$ is

the angular extent of C_ε about P. The region of T excluding T_ε is $T-T_\varepsilon$, and the corresponding contour is defined as $C-C_\varepsilon$. Thus, (A-9) is rewritten as

$$I_1 = \lim_{\varepsilon\to 0} \frac{1}{2A_o}\left[\iint_{T-T_\varepsilon} \frac{dS'}{|\underline{r}-\underline{r}'|} + \iint_{T_\varepsilon} \frac{dS'}{|\underline{r}-\underline{r}'|}\right] \tag{A-13}$$

The second integral in (A-13) is

$$\lim_{\varepsilon\to 0} \alpha(r)(\sqrt{\varepsilon^2+d^2}-|d|) = 0 \tag{A-14}$$

By (A-10) - (A-14), we have

$$I_1 = \lim_{\varepsilon\to 0} \frac{1}{2A_o} \iint_{T-T_\varepsilon} \nabla'_s \cdot \left(\frac{|\underline{r}-\underline{r}'|}{\rho}\,\underline{u}_\rho\right) dS'$$

$$= \lim_{\varepsilon\to 0} \frac{1}{2A_o} \int_{C-C_\varepsilon} \frac{|\underline{r}-\underline{r}'|}{\rho}\underline{u}_\rho \cdot \underline{u}\, dl$$

$$= \lim_{\varepsilon\to 0} \frac{1}{2A_o}\left[\int_C \frac{|\underline{r}-\underline{r}'|}{\rho}\underline{u}_\rho \cdot \underline{u}\, dl - \int_{C_\varepsilon} \frac{\sqrt{\varepsilon^2+d^2}}{\varepsilon}\varepsilon\, d\phi\right]$$

$$= \frac{1}{2A_o}\left[\sum_{i=1}^{3} \int_{C_i} \frac{|\underline{r}-\underline{r}'|}{\rho_i}\underline{u}_{\rho i} \cdot \underline{u}_i\, dl_i - \alpha(r)|d|\right] \tag{A-15}$$

Here, $\alpha(\underline{r})$ can be written as

$$\alpha(\underline{r}) = \sum_{i=1}^{3} \underline{u}_{\rho oi} \cdot \underline{u}_i \left(\tan^{-1}\frac{\Delta l_i^+}{\rho_{oi}} - \tan^{-1}\frac{\Delta l_i^-}{\rho_{oi}}\right) \tag{A-16}$$

where

$$\Delta l_i^{\pm} = l_i^{\pm} - l_{oi} \qquad i=1,2,3 \tag{A-17}$$

This can be verified by the values of $\alpha(\underline{r})$,

$$\alpha(\underline{r}) = \begin{cases} 0, \text{ if P is exterior to triangle T.} \\ 2\pi, \text{ if P is interior to T.} \\ \pi, \text{ if P is on C but not at a node of T.} \\ \alpha_i, \text{ if P is at node i with interior angle } \alpha_i \text{ of T.} \end{cases} \tag{A-18}$$

When the source point in Fig. A.1 is on line C_i, we have

$$\frac{|\underline{r}-\underline{r}'|}{\rho_i^2} = \frac{1}{\sqrt{\rho_i^2+d^2}} + \frac{d^2}{\rho_i^2\sqrt{\rho_i^2+d^2}} \tag{A-19}$$

$$\underline{u}_{\rho i}\cdot\underline{u}_i = \frac{\rho_{oi}}{\rho_i}\,\underline{u}_{\rho oi}\cdot\underline{u}_i \tag{A-20}$$

$$\rho_i^2 = (\rho_{oi})^2 + (l_i - l_{oi})^2 \tag{A-21}$$

By (A-19) - (A-21) and [19, Eqs. (200.01), (387)], we have

$$\int_{C_i} \frac{|\underline{r}-\underline{r}'|}{\rho_i}\underline{u}_{\rho i}\cdot\underline{u}_i\,dl_i = \rho_{oi}\underline{u}_{\rho oi}\cdot\underline{u}_i\left[\ln\left|\frac{R_i^+ + \Delta l_i^+}{R_i^- + \Delta l_i^-}\right| + \frac{|d|}{\rho_{oi}}\left(\tan^{-1}\frac{\Delta l_i^+|d|}{\rho_{oi}R_i^+} - \tan^{-1}\frac{\Delta l_i^-|d|}{\rho_{oi}R_i^-}\right)\right] \tag{A-22}$$

where

$$R_i^{\pm} = \sqrt{d^2+(\rho_{oi})^2+(\Delta l_i^{\pm})^2} \tag{A-23}$$

Substitution of (A-16) and (A-22) into (A-15) gives

$$I_1 = \frac{1}{2A_o} \sum_{i=1}^{3} \underline{u}_{\rho oi} \cdot \underline{u}_i \left[\rho_{oi} \ln\left|\frac{R_i^+ + \Delta l_i^+}{R_i^- + \Delta l_i^-}\right| - |d|\left(\tan^{-1} \frac{\rho_{oi}\Delta l_i^+}{d^2+\rho_{oi}^2+|d|R_i^+} - \tan^{-1} \frac{\rho_{oi}\Delta l_i^-}{d^2+\rho_{oi}^2+|d|R_i^-}\right)\right] \tag{A-24}$$

In (A-24),

$$\tan(A-B) = \frac{\tan A - \tan B}{1+\tan A \tan B} \tag{A-25}$$

is used.

There are four things to be noted about (A-24): (1) when $\rho_{oi}=0$, the ln term vanishes, (2) when $\rho_{oi} \neq 0$, the arguments $R_i^{\pm}+\Delta l_i^{\pm}$ of the ln term are positive, (3) when $d=0$, the $\tan^{-1}$ terms vanish, and (4) when $d \neq 0$, the arguments of $\tan^{-1}$ are finite (i.e., $d^2+\rho_{oi}^2+|d|R_i^{\pm} > 0$). In addition, (A-24) can be applied to any surface with multiple edges. If there are N edges, the summation index i is up to N.

Finally, we consider the second terms of (A-5) and (A-6). They have been evaluated in [12, Appendix C] in terms of the value of I_1 defined in (A-9) by using [19, Eqs. (380.011), (380.201)]. The results are

$$\int_{\eta=0}^{1}\int_{\xi=0}^{1-\eta}\frac{\xi}{R}\,d\xi\,d\eta = \frac{4B(J_1-J_2)-2E(J_3-J_4)-(2BC-ED)I_1}{4AB-E^2} \tag{A-26}$$

$$\int_{\eta=0}^{1}\int_{\xi=0}^{1-\eta}\frac{\eta}{R}\,d\xi\,d\eta = \frac{4A(J_3-J_4)-2E(J_1-J_2)-(2AD-EC)I_1}{4AB-E^2} \tag{A-27}$$

where

$$\begin{cases}
A = |\underline{r}_2-\underline{r}_1|^2 \\
B = |\underline{r}_3-\underline{r}_1|^2 \\
C = -2(\underline{r}-\underline{r}_1)\cdot(\underline{r}_2-\underline{r}_1) \\
D = -2(\underline{r}-\underline{r}_1)\cdot(\underline{r}_3-\underline{r}_1) \\
E = 2(\underline{r}_2-\underline{r}_1)\cdot(\underline{r}_3-\underline{r}_1) \\
F = |\underline{r}-\underline{r}_1|^2 \\
J_1 = \dfrac{(2B-C+D-E)\sqrt{B+D+F}+(2A+C-D-E)\sqrt{A+C+F}}{4(A+B-E)} \\
\qquad + \dfrac{4(A+C)(B+D+F)+4F(B-C-E)-(C+D+E)^2}{8(A+B-E)^{3/2}} \\
\qquad\qquad \ln\left|\dfrac{2\sqrt{(A+B-E)(B+D+F)}+(2B-C+D-E)}{2\sqrt{(A+B-E)(A+C+F)}-(2A+C-D-E)}\right| \\
J_2 = \dfrac{(2B+D)\sqrt{B+D+F}-D\sqrt{F}}{4B} + \dfrac{4BF-D^2}{8B\sqrt{B}}\ln\left|\dfrac{2\sqrt{B(B+D+F)}+2B+D}{2\sqrt{BF}+D}\right| \\
J_3 = \dfrac{(2A+C-D-E)\sqrt{A+C+F}+(2B-C+D-E)\sqrt{B+D+F}}{4(A+B-E)}
\end{cases} \tag{A-28}$$

AD-A138 394 ELECTROMAGNETIC COUPLING BETWEEN A CONDUCTING BODY AND AN APERTURE IN AN..(U) SYRACUSE UNIV NY DEPT OF ELECTRICAL AND COMPUTER ENGINEERING.. S W HSI ET AL. 2/2

UNCLASSIFIED DEC 83 SYRU/DECE/TR-83/19 N00014-76-C-0225 F/G 20/3 NL

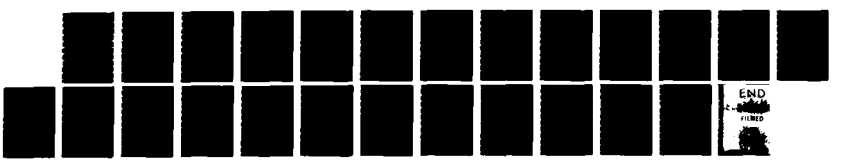

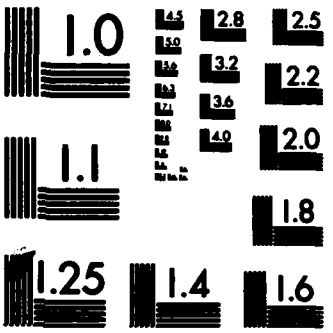

MICROCOPY RESOLUTION TEST CHART
NATIONAL BUREAU OF STANDARDS-1963-A

$$+\frac{4(A+C)(B+D+F)+4F(B-C-E)-(C+D+E)^2}{8(A+B-E)^{3/2}}$$

$$\ln\left|\frac{2\sqrt{(A+B-E)(A+C+F)}+(2A+C-D-E)}{2\sqrt{(A+B-E)(B+D+F)}-(2B-C+D-E)}\right|$$

$$J_4=\frac{(2A+C)\sqrt{A+C+F}-C\sqrt{F}}{4A}+\frac{4AF-C^2}{8A\sqrt{A}}\ln\left|\frac{2\sqrt{A(A+C+F)}+2A+C}{2\sqrt{AF}+C}\right|$$

Here, $\underline{r}_1$, $\underline{r}_2$, and $\underline{r}_3$ are defined in Fig. 3.6.

The evaluations of the integrals in (A-1) - (A-3) are now complete.

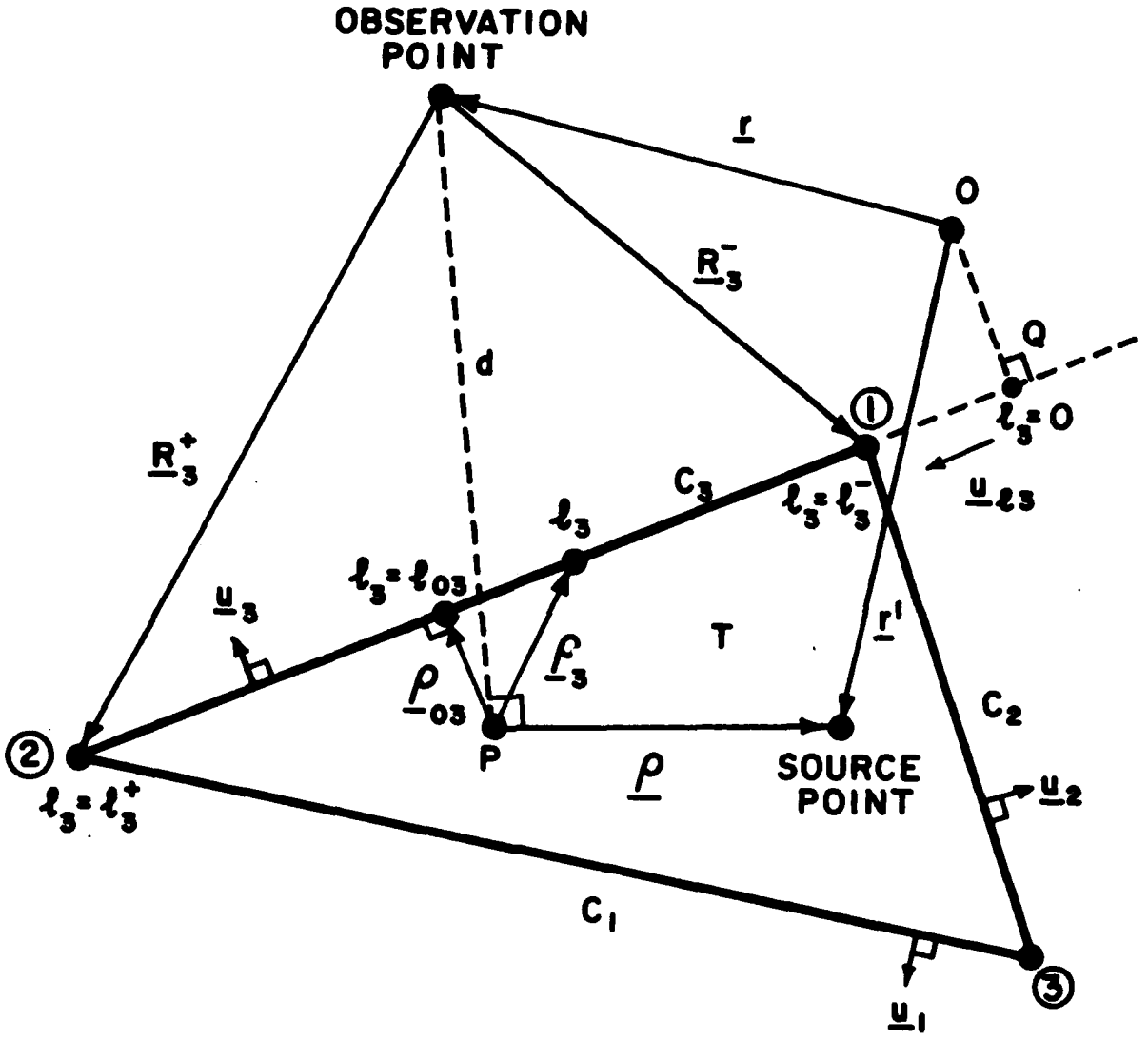

Fig. A.1. Geometrical quantities associated with an observation point, a source point, and edges of source triangle T.

APPENDIX B

ELECTRIC AND MAGNETIC FIELDS DUE TO OUTWARD TRAVELING TEM CURRENTS

Here, we derive fields due to two outward traveling TEM currents starting from $z=z_1$ and $-z_2$ and traveling to infinity in the z and the -z directions, respectively. The currents are defined as

$$\underline{J}^+ = e^{-jkz}\underline{u}_z \qquad 0 \leq z_1 < z < \infty \tag{B-1}$$

$$\underline{J}^- = e^{jkz}\underline{u}_z \qquad -\infty < z < -z_2 \leq 0 \tag{B-2}$$

We first evaluate the ϕ-component of the magnetic field due to $\underline{J}^+$ at a point (ρ,ϕ,z) as follows.

$$H_\phi(\underline{J}^+) = -\frac{\partial A_z(\underline{J}^+)}{\mu\,\partial\rho}$$

$$= -\frac{1}{4\pi}\int_{z_1}^{\infty}\frac{\partial}{\partial\rho}\left(\frac{e^{-jk(r+z')}}{r}\right)dz'$$

$$= -\frac{e^{-jkz_1}}{4\pi}\int_0^{\infty}\frac{\partial}{\partial\rho}\left(\frac{e^{-jk(r+z'')}}{r}\right)dz'' \tag{B-3}$$

$$= -\frac{e^{-jkz_1}}{4\pi}\lim_{L\to\infty}\int_0^{L}\left(\frac{-jk\rho}{r^2}-\frac{\rho}{r^3}\right)e^{-jk(r+z'')}dz''$$

$$= -\frac{e^{-jkz_1}}{4\pi} \lim_{L\to\infty}\left[\frac{\rho e^{-jk(r+z")}}{r(r+z"+z_1-z)}\right]_{z"=0}^{z"=L}$$

$$= -\frac{\rho e^{-jkz_1}}{4\pi} \lim_{L\to\infty}\left[\frac{e^{-jk(r_L+L)}}{r_L(r_L+L+z_1-z)} - \frac{e^{-jkr_0^+}}{r_0^+(r_0^++z_1-z)}\right]$$

$$= -\frac{\rho e^{-jkz_1}}{4\pi} \lim_{L\to\infty}\left\{\frac{(r_L-L+z-z_1)e^{-jk(r_L+L)}}{r_L[r_L^2-(L-z+z_1)^2]} - \frac{(r_0^++z-z_1)e^{-jkr_0^+}}{r_0^+[(r_0^+)^2-(z-z_1)^2]}\right\}$$

$$= \frac{e^{-jkz_1}}{4\pi\rho}\left(1+\frac{z-z_1}{r_0^+}\right)e^{-jkr_0^+} \qquad \text{(B-4)}$$

Here,

$$r = \sqrt{\rho^2+(z-z')^2} = \sqrt{\rho^2+(z-z_1-z")^2} \qquad \text{(B-5)}$$

$$z" = z' - z_1 \qquad \text{(B-6)}$$

$$r_L = \sqrt{\rho^2+(z-z_1-L)^2} \qquad \text{(B-7)}$$

$$r_0^+ = \sqrt{\rho^2+(z-z_1)^2} \qquad \text{(B-8)}$$

(B-5) is used on the third step, and the relationship

$$r_L^2 - (L-z+z_1)^2 = (r_0^+)^2 - (z-z_1)^2 = \rho^2 \qquad \text{(B-9)}$$

and

$$\lim_{L\to\infty} \frac{r_L-L+z-z_1}{r_L} = 0 \qquad \text{(B-10)}$$

are used on the last step.

Similarly, the ϕ-component of the magnetic field due to $\underline{J}^-$ can be obtained as follows.

$$H_\phi(\underline{J}^-) = -\frac{\partial A_z(\underline{J}^-)}{\mu\,\partial\rho}$$

$$= -\frac{1}{4\pi}\int_{-\infty}^{-z_2}\frac{\partial}{\partial\rho}\left(\frac{e^{-jk(r^- - z')}}{r^-}\right)dz'$$

$$= -\frac{e^{-jkz_2}}{4\pi}\int_0^{\infty}\frac{\partial}{\partial\rho}\left(\frac{e^{-jk(r^- + z'')}}{r^-}\right)dz'' \qquad \text{(B-11)}$$

where

$$z'' = -(z' + z_2) \qquad \text{(B-12)}$$

$$r^- = \sqrt{\rho^2 + (z - z')^2} = \sqrt{\rho^2 + [-(z + z_2) - z'']^2} \qquad \text{(B-13)}$$

Comparing (B-11) with (B-3) and (B-13) with (B-5), we can obtain $H_\phi(\underline{J}^-)$ by substituting e^{-jkz_2} for e^{-jkz_1} and $-(z+z_2)$ for $(z-z_1)$ into (B-4). The field is

$$H_\phi(\underline{J}^-) = \frac{e^{-jkz_2}}{4\pi\rho}\left(1 - \frac{z+z_2}{r_0^-}\right)e^{-jkr_0^-} \qquad \text{(B-14)}$$

where

$$r_0^- = \sqrt{\rho^2 + (z+z_2)^2} \qquad \text{(B-15)}$$

The z-components of electric fields due to $\underline{J}^+$ and $\underline{J}^-$ are then obtained by the equation

$$E_z = \frac{1}{j\omega\varepsilon\rho}\left[\frac{\partial}{\partial\rho}(\rho H_\phi)\right] \tag{B-16}$$

Substituting (B-4) and (B-14), respectively, into (B-16), we obtain

$$E_z(\underline{J}^+) = -\frac{e^{-jkz_1}}{4\pi j\omega\varepsilon}\left[\frac{jk}{r_0^+} + \frac{jk(z-z_1)}{(r_0^+)^2} + \frac{z-z_1}{(r_0^+)^3}\right]e^{-jkr_0^+} \tag{B-17}$$

$$E_z(\underline{J}^-) = -\frac{e^{-jkz_2}}{4\pi j\omega\varepsilon}\left[\frac{jk}{r_0^-} - \frac{jk(z+z_2)}{(r_0^-)^2} - \frac{z+z_2}{(r_0^-)^3}\right]e^{-jkr_0^-} \tag{B-18}$$

APPENDIX C

DERIVATIONS OF INTEGRAL FORMULATIONS USED IN CHAPTER 4

The integral formulations used in Chapter 4 are listed as follows and proved later in this appendix.

$$\int_0^{\infty} \frac{e^{-jk(\sqrt{z^2+\rho^2}+z)}}{\sqrt{z^2+\rho^2}}\,dz = \int_{-\infty}^{0} \frac{e^{-jk(\sqrt{z^2+\rho^2}-z)}}{\sqrt{z^2+\rho^2}}\,dz$$

$$= -Ci(k\rho)-j\left[\frac{\pi}{2}-Si(k\rho)\right] \qquad (C\text{-}1)$$

$$\int_0^{a} \frac{e^{-jk(\sqrt{z^2+\rho^2}+z)}}{\sqrt{z^2+\rho^2}}\,dz = \int_{-a}^{0} \frac{e^{-jk(\sqrt{z^2+\rho^2}-z)}}{\sqrt{z^2+\rho^2}}\,dz$$

$$= Ci(ku_1)-Ci(k\rho)-j[Si(ku_1)-Si(k\rho)] \qquad (C\text{-}2)$$

$$\int_a^{\infty} \frac{e^{-jk(\sqrt{(z-a)^2+\rho^2}+z)}}{\sqrt{(z-a)^2+\rho^2}}\,dz = \int_{-\infty}^{-a} \frac{e^{-jk(\sqrt{(z+a)^2+\rho^2}-z)}}{\sqrt{(z+a)^2+\rho^2}}\,dz$$

$$= e^{-jka}\{-Ci(k\rho)-j[\frac{\pi}{2}-Si(k\rho)]\} \qquad (C\text{-}3)$$

$$\int_a^{\infty} e^{-jkz}\frac{\partial}{\partial z}\Big[\int_{\Delta l_0} P(z')\frac{e^{-jk\sqrt{(z-a-z')^2+\rho^2}}}{\sqrt{(z-a-z')^2+\rho^2}}\,dz'\Big]dz$$

$$= -\int_{-\infty}^{-a} e^{jkz}\frac{\partial}{\partial z}\Big[\int_{\Delta l_0} P(z')\frac{e^{-jk\sqrt{(z+a-z')^2+\rho^2}}}{\sqrt{(z+a-z')^2+\rho^2}}\,dz'\Big]dz$$

$$\approx -4\pi\Delta l_0 e^{-jka}\underline{\psi}(0,0,\rho)+jk\Delta l_0 e^{-jka}\{-Ci(k\rho)-j[\tfrac{\pi}{2}-Si(k\rho)]\} \qquad (C\text{-}4)$$

$$\int_a^{\infty}\frac{e^{-jk(\sqrt{(z+a)^2+\rho^2}+z)}}{\sqrt{(z+a)^2+\rho^2}}dz = \int_{-\infty}^{-a}\frac{e^{-jk(\sqrt{(z-a)^2+\rho^2}-z)}}{\sqrt{(z-a)^2+\rho^2}}dz$$

$$= e^{jka}\{-Ci(ku_2)+j[Si(ku_2)-\tfrac{\pi}{2}]\} \qquad (C\text{-}5)$$

$$\int_a^{\infty} e^{-jkz}\frac{\partial}{\partial z}\Big[\int_{\Delta l_0} P(z')\frac{e^{-jk\sqrt{(z+a-z')^2+\rho^2}}}{\sqrt{(z+a-z')^2+\rho^2}}\,dz'\Big]dz$$

$$= -\int_{-\infty}^{-a} e^{jkz}\frac{\partial}{\partial z}\Big[\int_{\Delta l_0} P(z')\frac{e^{-jk\sqrt{(z-a-z')^2+\rho^2}}}{\sqrt{(z-a-z')^2+\rho^2}}\,dz'\Big]dz$$

$$\approx -4\pi\Delta l_0 e^{-jka}\underline{\psi}(2a,0,\rho)+jk\Delta l_0 e^{jka}\{-Ci(ku_2)+j[Si(ku_2)-\tfrac{\pi}{2}]\} \qquad (C\text{-}6)$$

Here,

$$Ci(x) = -\int_x^{\infty}\frac{\cos u}{u}du \qquad (C\text{-}7)$$

$$Si(x) = \int_0^x \frac{\sin u}{u} du \tag{C-8}$$

$$u_1 = a + \sqrt{a^2 + \rho^2} \tag{C-9}$$

$$u_2 = 2a + \sqrt{(2a)^2 + \rho^2} \tag{C-10}$$

$$\underline{\psi}(z_1, 0, \rho) = \frac{1}{4\pi\Delta l_0} \int P(z') \frac{e^{-jk\sqrt{(z_1 - z')^2 + \rho^2}}}{\sqrt{(z_1 - z')^2 + \rho^2}} dz' \tag{C-11}$$

P is a pulse function over a very small region Δl_0, and $\rho > 0$.

We now start to prove (C-1). Letting

$$u = k(\sqrt{z^2 + \rho^2} + z) \tag{C-12}$$

, we have

$$du = k\left(\frac{z + \sqrt{z^2 + \rho^2}}{\sqrt{z^2 + \rho^2}}\right) dz \tag{C-13}$$

Substitution of (C-12) and (C-13) into the left-hand side of (C-1) gives

$$\int_{k\rho}^{\infty} \frac{e^{-ju}}{u} du = \int_{k\rho}^{\infty} \frac{\cos u}{u} du - j\left[\int_0^{\infty} \frac{\sin u}{u} du - \int_0^{k\rho} \frac{\sin u}{u} du\right]$$

$$= -Ci(k\rho) - j\left[\frac{\pi}{2} - Si(k\rho)\right]$$

Thus, (C-1) is proved.

The left-hand side of (C-2) can be rewritten as

$$\int_0^\infty \frac{e^{-jk(\sqrt{z^2+\rho^2}+z)}}{\sqrt{z^2+\rho^2}}dz - \int_a^\infty \frac{e^{-jk(\sqrt{z^2+\rho^2}+z)}}{\sqrt{z^2+\rho^2}}dz \qquad (C-14)$$

By (C-12) and (C-13), we have

$$\int_a^\infty \frac{e^{-jk(\sqrt{z^2+\rho^2}+z)}}{\sqrt{z^2+\rho^2}}dz = \int_{ku_1}^\infty \frac{\cos u}{u}du - j\Big[\int_0^\infty \frac{\sin u}{u}du$$

$$- \int_0^{ku_1} \frac{\sin u}{u}du\Big]$$

$$= - Ci(ku_1) - j\Big[\frac{\pi}{2} - Si(ku_1)\Big] \qquad (C-15)$$

Using (C-1), (C-14), and (C-15), we obtain the right-hand side of (C-2).

Replacing z by z'+a in the left-hand side of (C-3) and using (C-1), we obtain the right-hand side of (C-3).

The left-hand side of (C-4) is equal to

$$\Big[e^{-jkz} \int_{\Delta l_0} \frac{e^{-jk\sqrt{(z-a-z')^2+\rho^2}}}{\sqrt{(z-a-z')^2+\rho^2}}dz'\Big]_{z=a}^{z=\infty}$$

$$+ jk \int_a^\infty e^{-jkz} \int_{\Delta l_0} \frac{e^{-jk\sqrt{(z-a-z')^2+\rho^2}}}{\sqrt{(z-a-z')^2+\rho^2}}dz'dz$$

The first term equals

$$-4\pi\Delta l_0 e^{-jka}\underline{\psi}(0,0,\rho)$$

Approximating the integral with respect to z' in the second term by the product of Δl_0 and the integrand at z'=0, and then using (C-3), we have the second term equal to

$$jk\Delta l_0 e^{-jka}\{-Ci(k\rho)-j[\frac{\pi}{2}-Si(k\rho)]\}$$

We thus complete the derivation of (C-4).

Replacing z by z'-a in the left-hand side of (C-5) and using (C-1) and (C-2) with a replaced by 2a, we obtain the right-hand side of (C-5).

Finally, using the same procedures as those in deriving (C-4) and (C-5), we obtain (C-6).

APPENDIX D

EQUIVALENT CIRCUIT OF THE APERTURE FOR THE TRANSMISSION LINE MODE ON A LOADED WIRE

In this appendix, we derive formulations for an equivalent circuit of the aperture for the transmission line mode at z=0 on a wire. The wire is in the z-direction, terminated with arbitrary loads, and parallel to an aperture-perforated infinite conducting plane. The aperture is arbitrarily sized and shaped and is centered at z=0. Incident fields come from either one or both sides of the conducting plane. This circuit can be utilized to calculate the TEM currents and voltages on the wire.

It is known that an equivalent circuit of a wire passing by an aperture is a two-port network as shown in Fig. D.1. The parameters $[Z^e]$ depend only on the geometry of the problem. They can be obtained by removing the incident fields from the system and applying mathematically arbitrary excitations to the transmission line formed by the wire and the conducting plane. The sources V_1^e and V_2^e can be obtained from the incident fields and $[Z^e]$. In order to find the equivalent circuit, the solution for the current on an infinitely long wire (or a matched wire with the characteristic impedance Z_0) is needed. Therefore, we now consider the wire as infinitely long.

(A) Network Parameters $[Z^e]$

To obtain the elements of $[Z^e]$, we use the definitions

$$v_1 = Z^e_{11}\, i_1 + Z^e_{12}\, i_2 \tag{D-1}$$

$$v_2 = Z^e_{21}\, i_1 + Z^e_{22}\, i_2 \tag{D-2}$$

where i_1, i_2, v_1, and v_2 are port currents and voltages at port 1 ($z=0^-$) and port 2 ($z=0^+$), respectively, with reference directions shown in Fig. D.2.

To represent an excitation, we mathematically apply a TEM current wave $I^+ e^{-jkz} \underline{u}_z$ to the transmission line. I^+ is an arbitrary constant. This excitation will induce an equivalent magnetic current sheet in the aperture. The magnetic current sheet then excites two outward traveling TEM currents $\hat{I}_1 e^{jkz} \underline{u}_z$ and $\hat{I}_{NB} e^{-jkz} \underline{u}_z$ traveling on both semi-infinite halves of the wire . It also excites evanescent current on the wire in the vicinity of the aperture. Figure D.3 shows the propagation directions of the excitation and the outward traveling TEM currents.

Combining Figs. D.2 and D.3, we obtain port currents $\hat{i}_1$ and $\hat{i}_2$ and port voltages $\hat{v}_1$ and $\hat{v}_2$. They are

$$\hat{i}_1 = I^+ + \hat{I}_1 \tag{D-3}$$

$$\hat{i}_2 = -(I^+ + \hat{I}_{NB}) \tag{D-4}$$

$$\hat{v}_1 = Z_0(I^+ - \hat{I}_1) \tag{D-5}$$

$$\hat{v}_2 = Z_0(I^+ + \hat{I}_{NB}) \tag{D-6}$$

Here, $Z_0 = 60\ln(2d/r_B)$ is the characteristic impedance of the transmission line, d is the distance of the wire to the conducting plane, and r_B is the radius of the wire. Since $[Z^e]$ is independent of the excitation, (D-1) and (D-2) hold for the port currents and voltages defined in (D-3) - (D-6). That is,

$$\hat{v}_1 = Z^e_{11}\hat{i}_1 + Z^e_{12}\hat{i}_2 \tag{D-7}$$

$$\hat{v}_2 = Z^e_{21}\hat{i}_1 + Z^e_{22}\hat{i}_2 \tag{D-8}$$

To solve for $[Z^e]$, two more equations relating the port currents and voltages to $[Z^e]$ are needed, in addition to (D-7) and (D-8). One can apply a TEM current excitation $I^- e^{jkz}\underline{u}_z$ to the wire. Again, the aperture excites two outward traveling currents $\hat{\hat{I}}_1 e^{jkz}\underline{u}_z$ and $\hat{I}_{NB} e^{-jkz}\underline{u}_z$ traveling on both semi-infinite halves of the wire, as shown in Fig. D.4. The port currents and voltages for this case can be obtained by combining Figs. D.2 and D.4, giving

$$\hat{\hat{i}}_1 = I^- + \hat{\hat{I}}_1 \tag{D-9}$$

$$\hat{\hat{i}}_2 = -(I^- + \hat{I}_{NB}) \tag{D-10}$$

$$\hat{\hat{v}}_1 = -Z_0(I^- + \hat{\hat{I}}_1) \tag{D-11}$$

$$\hat{\hat{v}}_2 = Z_0(\hat{\hat{I}}_{NB} - I^-) \tag{D-12}$$

Similar to (D-7) and (D-8), we have a pair of equations relating these port currents and voltages to $[Z^e]$. They are

$$\hat{\hat{v}}_1 = Z^e_{11}\hat{\hat{i}}_1 + Z^e_{12}\hat{\hat{i}}_2 \tag{D-13}$$

$$\hat{v}_2 = Z^e_{21}\hat{\hat{i}}_1 + Z^e_{22}\hat{i}_2 \tag{D-14}$$

For simplicity, I^+ and I^- are chosen to be the constant 1. Thus, (D-3) - (D-14) give

$$Z^e_{11} = [(1+\hat{I}_{NB})(1+\hat{\hat{I}}_1)+(1-\hat{I}_1)(1+\hat{\hat{I}}_{NB})]F \tag{D-15}$$

$$Z^e_{12} = 2(1+\hat{\hat{I}}_1)F \tag{D-16}$$

$$Z^e_{21} = 2(1+\hat{I}_{NB})F \tag{D-17}$$

$$Z^e_{22} = [(1+\hat{I}_{NB})(1+\hat{\hat{I}}_1)+(1+\hat{I}_1)(1-\hat{\hat{I}}_{NB})]F \tag{D-18}$$

where

$$F = \frac{Z_0}{(1+\hat{I}_1)(1+\hat{\hat{I}}_{NB})-(1+\hat{I}_{NB})(1+\hat{\hat{I}}_1)} \tag{D-19}$$

By the reciprocity theorem [7, Sec. 3-8], we have

$$Z^e_{12} = Z^e_{21} \tag{D-20}$$

The network is then equivalent to a T network as shown in Fig. D.5, where the impedances are, as obtained by using (D-15) - (D-20),

$$Z^e_1 = Z^e_{11}-Z^e_{12} = [(1-\hat{I}_1)(1+\hat{\hat{I}}_{NB})-(1-\hat{I}_{NB})(1+\hat{\hat{I}}_1)]F \tag{D-21}$$

$$Z^e_2 = Z^e_{12} = Z^e_{21} = 2(1+\hat{I}_{NB})F \tag{D-22}$$

$$Z^e_3 = Z^e_{22}-Z^e_{21} = [(1+\hat{I}_1)(1-\hat{\hat{I}}_{NB})-(1+\hat{I}_{NB})(1-\hat{\hat{I}}_1)]F \tag{D-23}$$

(B) Sources $\underline{V}^e_1$ and $\underline{V}^e_2$

If both ports of Fig. D.5 are terminated with matched loads, as shown in Fig. D.6, the network corresponds to our original problem. The original incident fields induce two outward traveling TEM currents $I_1 e^{jkz}\underline{u}_z$ and $I_{NB} e^{-jkz}\underline{u}_z$ on the wire. The loop currents i_1 and i_2 in Fig. D.6 are equal to I_1 and $-I_{NB}$, respectively. Thus, Fig. D.6 gives

the sources,

$$V_1^e = -(Z_0+Z_1^e+Z_2^e)I_1+Z_2^eI_{NB} \tag{D-24}$$

$$V_2^e = (Z_0+Z_2^e+Z_3^e)I_{NB}-Z_2^eI_1 \tag{D-25}$$

Note that Z_1^e, Z_2^e, Z_3^e, V_1^e, and V_2^e are proportional to Z_0. Hence, they can be normalized by Z_0. The equivalent network is now obtained.

If the aperture is symmetric about z=0 or is small, then

$$\hat{\hat{I}}_1 = \hat{I}_{NB} \tag{D-26}$$

$$\hat{\hat{I}}_{NB} = \hat{I}_1 \tag{D-27}$$

By (D-21) - (D-27), the network is reduced to the symmetric T network shown in Fig. D.7 where the impedances and sources are

$$Z_1^s = \frac{-(\hat{I}_1+\hat{I}_{NB})Z_0}{2+\hat{I}_1+\hat{I}_{NB}} \tag{D-28}$$

$$Z_2^s = \frac{2(1+\hat{I}_{NB})Z_0}{(\hat{I}_1-\hat{I}_{NB})(2+\hat{I}_1+\hat{I}_{NB})} \tag{D-29}$$

$$V_1^s = -(Z_0+Z_1^s+Z_2^s)I_1+Z_2^sI_{NB} \tag{D-30}$$

$$V_2^s = (Z_0+Z_1^s+Z_2^s)I_{NB}-Z_2^sI_1 \tag{D-31}$$

For the case when the outward traveling TEM currents are symmetric about z=0 ($\hat{I}_1=\hat{I}_{NB}$, $I_1=I_{NB}$), Z_2^s in (D-29) is infinite and the equivalent network in Fig. D.7 can be reduced to that in Fig. D.8 with the impedance and source defined as

$$Z^e = \frac{-2\hat{I}_1 Z_0}{1+\hat{I}_1} \tag{D-32}$$

$$V^e = -I_1(2Z_0 + Z^e) \tag{D-33}$$

They agree with those in [4] where the symmetric case was considered. An example of this case is a narrow slot whose axis is perpendicular to the wire. This is expected because the magnetic current in the slot is equivalent to a superposition of magnetic dipoles which produce symmetric currents on the wire.

For the case when the outward traveling TEM currents are antisymmetric about z=0 ($\hat{I}_1=-\hat{I}_{NB}$, $I_1=-I_{NB}$), Z_1^s in (D-28) vanishes and the network in Fig. D.7 is reduced to that in Fig. D.9, where the impedance and the source are

$$Z^a = \frac{(1-\hat{I}_1)Z_0}{2\hat{I}_1} \tag{D-34}$$

$$V^a = -(Z_0+2Z^a)I_1 \tag{D-35}$$

An example of this case is a small loop aperture. The magnetic current in the aperture is equivalent to an electric dipole which points normal to the wire and produces antisymmetric currents on the wire.

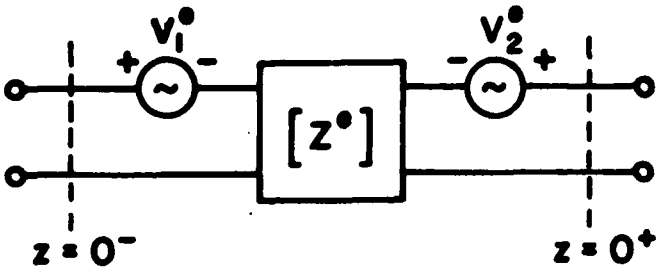

Fig. D.1. A two-port equivalent circuit.

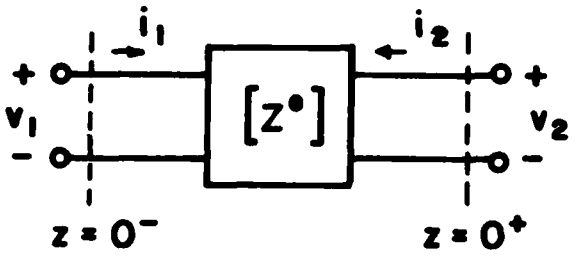

Fig. D.2. Reference directions for i and v.

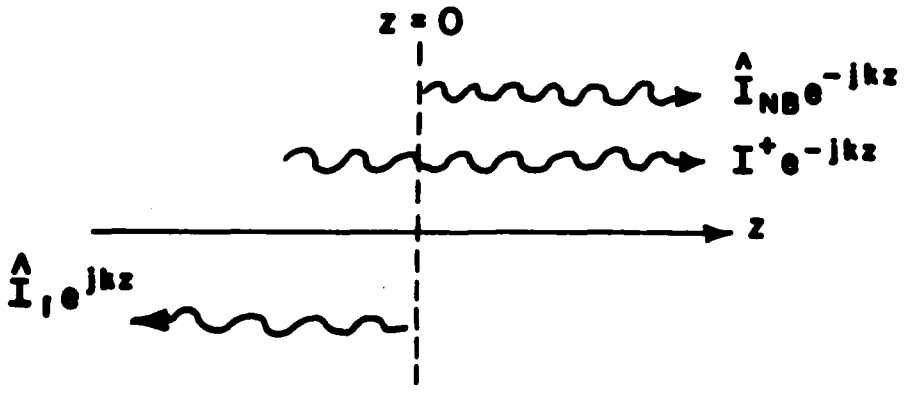

Fig. D.3. A TEM current excitation $I^+e^{-jkz}\underline{u}_z$ produces outward traveling TEM currents $\hat{I}_1 e^{jkz}\underline{u}_z$ and $\hat{I}_{NB}e^{-jkz}\underline{u}_z$.

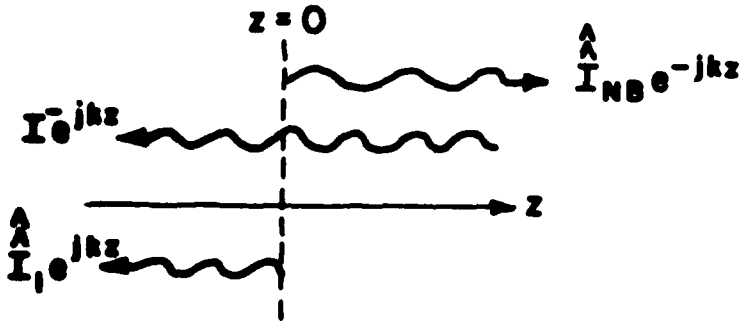

Fig. D.4. A TEM current excitation $I^-e^{jkz}\underline{u}_z$ produces outward traveling TEM currents $\hat{I}_1e^{jkz}\underline{u}_z$ and $\hat{I}_{NB}e^{-jkz}\underline{u}_z$.

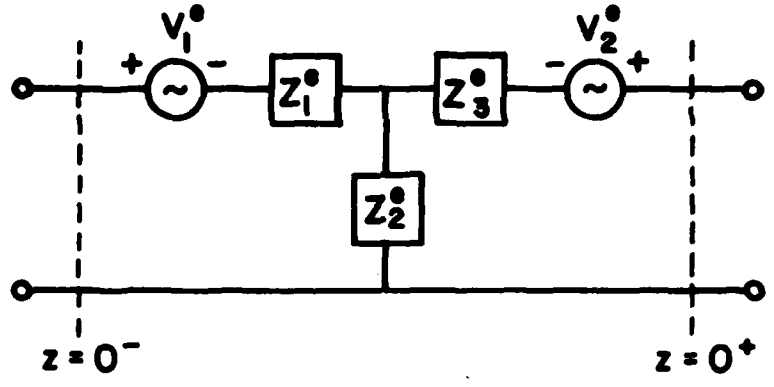

Fig. D.5. An equivalent T network.

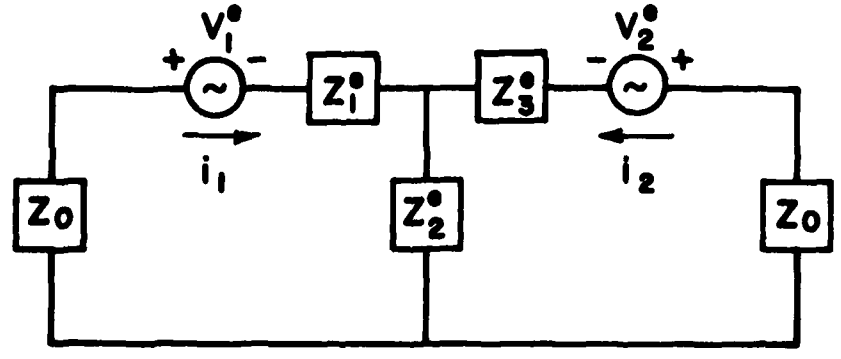

Fig. D.6. Equivalent circuit for the calculation of V_1^e and V_2^e.

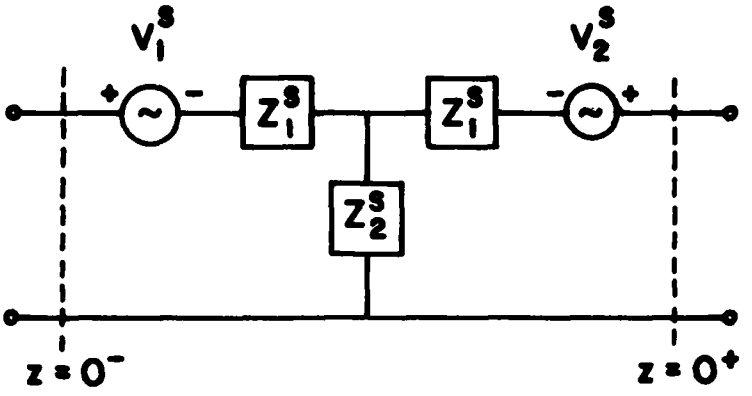

Fig. D.7. An equivalent symmetric T network for the case when the aperture is symmetric about z=0 or is small.

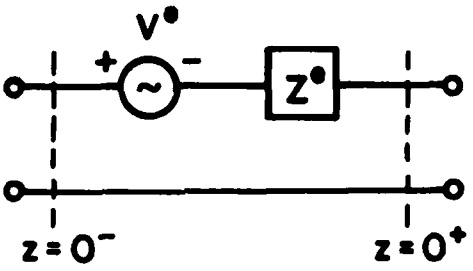

Fig. D.8. Equivalent circuit for the case when the aperture induces symmetric outward traveling TEM currents on the wire.

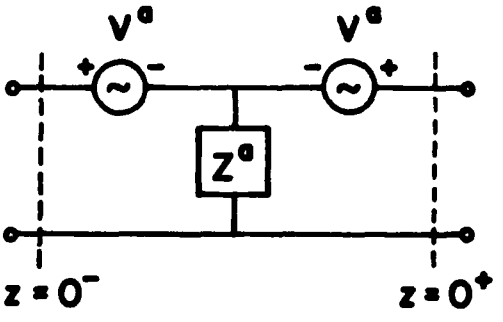

Fig. D.9. Equivalent circuit for the case when the aperture induces antisymmetric outward traveling TEM currents on the wire.

REFERENCES

[1] D. Kajfez, "Excitation of a Terminated TEM Transmission Line through a Small Aperture," AFWL Interaction Note 215, July 1974.

[2] K. S. H. Lee and F. C. Yang, "A Wire Passing by a Circular Aperture in an Infinite Ground Plane," AFWL Interaction Note 317, Feb. 1977.

[3] S. W. Hsi and R. F. Harrington, "Electromagnetic Coupling to an Infinite Wire through a Small Aperture of Arbitrary Shape," Technical Report No. 19 on Contract No. N00014-76-C-0225, Department of Electrical and Computer Engineering, Syracuse University, Syracuse, N. Y., Feb. 1983.

[4] Yang Naiheng and R. F. Harrington, "Electromagnetic Coupling to an Infinite Wire through a Slot in a Conducting Plane," Technical Report No. 15 on Contract No. N00014-76-C-0225, Department of Electrical and Computer Engineering, Syracuse University, March 1982.

[5] C. M. Butler and K. R. Umashankar, "Electromagnetic Excitation of a Wire through an Aperture-Perforated Conducting Screen," IEEE Trans. Antennas Propagat., Vol. AP-24, No. 4, pp. 456-462, July 1976.

[6] Yang Naiheng and R. F. Harrington, "Electromagnetic Coupling to and from a Terminated Wire through a Rectangular Slot in a Conducting Screen," Report No. TR-82-7, Department of Electrical and Computer Engineering, Syracuse University, June 1982.

[7] R. F. Harrington, Time-Harmonic Electromagnetic Fields, McGraw-Hill Book Co., New York, 1961.

[8] R. F. Harrington, Field Computation by Moment Methods, The Macmillan Co., New York, 1968.

[9] A. Sankar and T. C. Tong, "Current Computation on Complex Structures by Finite-Element Method," Electronics Letters, Vol. 11, No. 20, pp. 481-482, Oct. 1975.

[10] J. J. H. Wang, "Numerical Analysis of Three-Dimensional Arbitrarily-Shaped Conducting Scatterers by Trilateral Surface Cell Modelling," Radio Science, Vol. 13, No. 6, pp. 947-952, Nov. -Dec. 1978.

[11] J. J. H. Wang and C. Papanicolopulos, "Surface Patch Modeling of Scatterers of Arbitrary Shapes," AP-S Int. Symp. Digest, University of Washington, Seattle, pp. 159-162, June 1979.

[12] S. M. Rao, "Electromagnetic Scattering and Radiation of Arbitrarily-Shaped Surfaces by Triangular Patch Modeling," Ph. D. Dissertation, University of Mississippi, August 1980.

[13] C. L. I and R. F. Harrington, "Electromagnetic Transmission through an Aperture of Arbitrary Shape in a Conducting Screen," Technical Report No. 16 on Contract No. N0001 4-76-C-0225, Department of Electrical and Computer Engineering, Syracuse University, April 1982.

[14] A. W. Glisson, "On the Development of Numerical Techniques for treating Arbitrarily-shaped Surfaces, " Ph. D. dissertation, University of Mississippi, 1978.

[15] R. F. Harrington, "Matrix Methods for Field Problems," Proc. IEEE, Vol. 55, No. 2, pp. 136-149, Feb. 1967.

[16] P. C. Hammer, O. J. Marlowe and A. H. Stroud, "Numerical Integration over Simplexes and Cones," Math. Tables Aids Comp. , Vol. 10, pp. 130-137, 1956.

[17] D. R. Wilton, Private Communication, 1983.

[18] J. Van Bladel, Electromagnetic Fields, McGraw-Hill Book Co., New York, 1964.

[19] H. B. Dwight, Tables of Integrals and Other Mathematical Data, The Macmillan Co., New York, 1961.

[20] R. E. Collin, Foundations for Microwave Engineering, McGraw-Hill Book Co., New York, 1966.


FILME